

Development of a novel *in-vitro* vascular model for
determination of physiological and pathophysiological
mechanobiology

Inaugural Dissertation

zur

Erlangung des Doktorgrades
Dr. nat. med.

der Medizinischen Fakultät
und
der Mathematisch-Naturwissenschaftlichen Fakultät
der Universität zu Köln

vorgelegt von

Robin Bayer

aus Neuss

Prost Druck GmbH, Jülich

2021

Betreuer Prof. Dr. Jürgen Hescheler
Prof. Dr. Dr. Aysegül T. Artmann

Referenten Prof. Dr. Stephan Baldus
Prof. Dr. Günter Schwarz

Datum der mündlichen Prüfung: 15.01.2021

Table of Contents

1.	Abstract.....	1
2.	Introduction	5
3.	Working Hypothesis.....	7
4.	Background	8
4.1.	Vascular Wall	8
4.2.	Blood pressure regulation	9
4.3.	Hypertension	12
4.4.	Mechanical Cellular Stimulation	14
4.5.	Biomechanics.....	14
4.5.1.	Cellular Force Measurement	15
4.6.	<i>In-vitro</i> Model	16
4.6.1.	CellDrum Technology.....	17
5.	Material & Methods.....	18
5.1.	Technology Overview	20
5.2.	CellDrum	20
5.2.1.	Membrane Characterization.....	21
5.2.2.	Membrane Functionalization	21
5.3.	Tissue Tension Analyzer.....	22
5.3.1.	Development	22
5.3.1.1.	Mechanical Construction.....	23
5.3.1.2.	Electronic Components	23
5.3.1.3.	Proximity Measuring.....	25
5.3.1.4.	Calibration	25
5.3.1.5.	Programming	26
5.4.	Physical Model.....	28
5.5.	General Biomechanics	29
5.6.	Cell Culture	29
5.6.1.	Human Aortic Smooth Muscle Cells	29
5.6.2.	Human Aortic Endothelial Cells	30
5.6.3.	Co-Cultures	30
5.6.3.1.	Conditioned Co-Culture	31
5.6.3.2.	Direct Co-Culture	31
5.6.3.3.	3D Co-Culture	32
5.6.4.	Vitality Test.....	33
5.6.5.	Microscopic Analysis.....	33

5.7.	Pharmacological Testing	34
5.8.	Blood Sera Screening	38
5.8.1.	Blood Collection and Sera Extraction	38
5.8.2.	Blood Sera Analysis.....	38
5.9.	PuSElect	38
5.10.	Stimulation Protocol	40
5.11.	Cell Morphology Index (CMI).....	41
5.12.	Gene Analysis.....	42
5.12.1.	Microarray Analysis	42
5.12.1.1.	Microarray Analysis Evaluation	42
5.12.2.	Quantitative PCR.....	42
5.12.2.1.	RNA Isolation	44
5.12.2.2.	Reverse Transcription.....	44
5.12.2.3.	qPCR Analysis.....	45
5.12.3.	Endothelin-1 ELISA.....	45
6.	Results.....	46
6.1.	Biomechanics – Proof of Principle	46
6.2.	Pharmacology	47
6.2.1.	Ca ² Channel Modulators.....	47
6.2.2.	K ⁺ Channel Modulators.....	48
6.2.3.	NO.....	50
6.2.4.	Vasoactive Mediators	51
6.2.5.	PDE5 Inhibitor.....	52
6.2.6.	Stimulants & Toxins	53
6.2.7.	Dose-Response Model.....	55
6.3.	Mechanical Stimulation	56
6.3.1.	Microarray Analysis	60
6.3.2.	qPCR.....	63
6.4.	Co-Culture.....	65
6.5.	Blood Sera.....	68
7.	Discussion	69
7.1.	Mechanobiological Vascular <i>in-vitro</i> Model	69
7.2.	Hypertension Disease Model Induced by Mechanical Stimulation	74
7.3.	Co-Cultivation and Arrangement of haSMC and haEC.....	80
7.4.	Application for Medical Laboratory Screening.....	82
7.5.	Methodical Discussion	83
8.	Conclusion.....	85

9.	References	87
10.	Appendix	102
10.1.	List of Abbreviations	102
10.2.	List of Figures	103
10.3.	List of Tables	109
10.4.	Constructions	110
10.5.	Electronics.....	113
10.6.	Coding.....	114

1. Abstract

Background/Aims

The aim of the study was to develop a biological and technological method to investigate *in-vitro* the physiology and pathophysiology biomechanical phenomena of a vascular wall. In particular, cellular contraction and relaxation as a biomechanical response to vasoactive substances and different mechanical stimulation intervals were studied to provide data for basic research and pharmacological developments in cardiovascular diseases such as arterial hypertension.

Methods:

Methodologically, the study is based on CellDrum technology, which is a method to determine cellular stress changes of a few kilo Pascal(kPa). Especially for this study, a new approach was developed to characterize the cell stresses of monolayers and multilayer tissue equivalents in a standardized way.

A monolayer model consisting of human aortic smooth muscle cells (haSMC) was primarily developed for CellDrum as a vascular *in-vitro* cell culture model. Also, a model of human aortic endothelial cells (haEC) was established, and an approach for a 3D co-culture model of both cell types was developed.

Vasoactive substances with different mechanisms of action and concentrations were tested to represent the physiological properties of the model. For the first time, the biomechanical influence of blood sera was analyzed on the CellDrum models to test the potential possibility of a laboratory screening procedure.

The PulSElect system was developed, which exposes the CellDrum models to a defined, cyclical, mechanical stress by stretching, to simulate the symptoms of mechanically induced hypertension. The influence of the mechanical stress was observed by cytoskeletal alignment quantification, transcriptome analysis, gene expression of mechanosensitive as well as biomechanically relevant genes and biomechanical stress evaluation to elucidate cellular stiffening and cellular stress management.

Results

The haSMC cell models showed significant physiological and biomechanical changes in cell tone after application of the vasoactive substances, sera and conditioned media (~6-10% relative to initial tension).

Mechanical stimulation of the cells allowed quantification of both mechanical and transcriptomic changes as well as morphological adaptation. Furthermore, it was possible to present the obtained results in a time-dependent manner. Also, mechanical stimulation has been shown to induce the development of the contractile phenotype of haSMC and improve its cellular integrity, resulting in increased basal tension and overall contractility.

As an extension of a well-established haSMC CellDrum model, an approach for direct co-cultivation of human aortic smooth muscle cells and endothelial cells was elaborated.

Conclusion

Different CellDrum models have been established to replicate biomechanical processes of the vascular system. The study showed that the CellDrum technology is a suitable method to analyze biomechanical stress changes caused by different stimuli using haSMC. The analysis of blood sera using CellDrums allows for possible future use as a screening method for pharmacological and medical laboratory research.

Since the CellDrum technology is not limited to the use of monolayers, it is possible to think about an extension of cell models with additional cell types and cell layers. Although we have already been able

to show partial co-cultivation of smooth muscle cells and endothelial cells, further research is needed to establish this sufficiently.

Increased expression levels of mechanosensitive genes have been shown to correlate with literature data on the pathogenesis of hypertension, using microarray analysis (Affymetrix) and qPCR. Nevertheless, it remains a speculative reflection of the cellular changes due to induced hypertension.

The data and findings obtained to provide the promising potential supporting research and development of personalized medication, sports medicine, cell biology and stem cell research using CellDrum technology.

Hintergrund /Ziele:

Das Ziel der Studie ist es, ein biologisches und technologisches Verfahren zu entwickeln, um *in-vitro* Physiologie und Pathophysiologie biomechanischer Phänomene einer vaskulären Gefäßwand zu untersuchen. Insbesondere wird die zelluläre Kontraktion und Relaxation als biomechanische Antwort auf vasoaktive Substanzen und verschiedener Intervalle mechanischer Stimulationen untersucht, um Daten für die Grundlagenforschung und pharmakologische Entwicklungen kardiovaskuläre Erkrankungen wie Bluthochdruck zu erhalten.

Methoden:

Methodisch basiert die Studie auf der CellDrum-Technologie, welche ein Verfahren ist, um zelluläre Spannungsänderungen von wenigen Kilopascal (kPa) zu erfassen. Speziell für diese Studie wurde ein neues Analyseverfahren entwickelt, um die Zellspannungen von Zellmonolayern und mehrschichtigen Gewebeäquivalenten standardisiert zu charakterisieren und zu analysieren.

Ein Monolayer-Modell, bestehend aus glatten Muskelzellen der menschlichen Aorta (haSMC), wurde primär für CellDrum als vaskuläres *in-vitro*-Zellkulturmodell entwickelt. Außerdem wurde ein Modell aus humanen Aortenendothelzellen (haEC) etabliert und ein Ansatz für ein 3D-Co-Kulturmodell beider Zelltypen entwickelt.

Um die physiologischen Eigenschaften des Modells darzustellen, wurden Substanzen mit unterschiedlichen Wirkmechanismen und Konzentrationen getestet. Erstmals wurde der biomechanische Einfluss von Blutseren an den CellDrum-Modellen untersucht, um die potentielle Verwendung der CellDrum, als eines labortechnischen Screeningsverfahrens zu testen.

Das PulSElect-System wurde entwickelt, um die CellDrum-Modelle durch Dehnung einer definierten, zyklischen, mechanischen Belastung auszusetzen. Dies soll die Symptome einer mechanisch induzierten Hypertonie simulieren. Der Einfluss des mechanischen Stresses wurde mittels Quantifizierung der zytoskelettalen Ausrichtung, Transkriptomanalyse, Genexpression mechanosensitiver sowie biomechanisch relevanter Gene und biomechanischer Analyse ausgewertet, um die zelluläre Verfestigung und das zelluläre Stressmanagement zu verdeutlichen.

Ergebnisse:

Die haSMC Zellmodelle zeigen nach Zugabe der vasoaktiven Substanzen, Seren und konditionierten Medien signifikante physiologisch-biomechanische Änderung der Zellspannung (~6-10% relativ zur mechanischen Grundspannung).

Die mechanische Stimulation der Zellen ließ sich, sowohl mechanisch als auch durch Änderungen des Transkriptoms sowie anhand morphologischer Anpassung quantifizieren. Darüber hinaus war es möglich die gewonnenen Ergebnisse zeitabhängig zueinander darzustellen. Außerdem hat sich gezeigt, dass die mechanische Stimulation die Ausprägungen des kontraktiven Phänotyps der haSMC verstärkt und deren zelluläre Integrität verbessert, was zu einer Erhöhung der Basalspannung und der Gesamtkontraktilität geführt hat.

Als Erweiterung eines etablierten haSMC CellDrum-Modells wurde ein Ansatz zu einer direkten Co-Kultivierung von humanen glatten Aortenmuskelzellen und Endothelzellen ausgearbeitet.

Zusammenfassung:

Verschiedene CellDrum-Zellmodelle konnten etabliert werden, um biomechanische Prozesse des vaskulären Systems nachzubilden. Die Studie zeigt, dass die CellDrum Technologie eine geeignete Methode ist, um biomechanische Spannungsänderungen durch verschiedene Stimuli anhand von haSMC zu analysieren. Die Auswertung der Blutseren mittels CellDrums lässt über eine zukünftige Nutzung als Screeningverfahren für pharmakologische und labortechnische Forschung spekulieren.

Da die CellDrum nicht auf die Nutzung von Monolayern limitiert ist kann man über eine Erweiterung des Zellmodells, mit weiteren Zelltypen und Zellschichten, nachdenken. Obwohl wir bereits teilweise Co-Kultivierung von glatten Muskelzellen und Endothelzellen zeigen konnten, bedarf es weiterer Forschungsarbeit, um diese ausreichend zu etablieren.

Mittels Transkriptom-Analyse und qPCR konnten erhöhte Expressionslevel von mechanosensitiven Genen gezeigt werden, welche mit Literaturdaten der Pathogenese von Bluthochdruckerkrankungen korrelieren. Nichtsdestotrotz bleibt es stets spekulativ, die erhobenen Daten auf eine mechanisch induzierte Hypertonie zu projizieren.

Die gewonnenen Daten und Erkenntnisse liefern vielversprechendes Potential, um die Forschung und Entwicklung personalisierter Medikation, Sportmedizin, zellbiologischer Forschung und Stammzellforschung mittels CellDrum Technologie zu unterstützen.

2. Introduction

Hypertension describes the chronic and pathological increase of blood pressure, which is a major cause of premature death worldwide. According to estimations of the WHO, 1,13 billion people suffer from hypertension worldwide.

Arterial hypertension is called a “silent killer”, as there are usually no recognizable symptoms, especially in the early stages of pathogenesis. In severe cases, hypertension can cause fatigue, nausea, vomiting, confusion, anxiety, chest pain and muscle tremors. Even though medical progress has been made, there is still a lack of knowledge to fully understand the mechanism of hypertension pathogenesis and early recognition of the diagnosis.

Global epidemiological statistics from 2015 (WHO), visualize increased prevalence and grade of severity in low or middle income. Increased degree of seriousness in low and middle-income countries is still a development issue and is explainable by missing awareness, diagnostics and effective health care services.

In total, only approximately 75% of affected people are aware of their diagnosis from which less than one of five patients suffering from hypertension have the problem under control. A fatal consequence of uncontrolled hypertension can be the development of a cardiovascular disease (CVD), which is globally the number one cause of death. According to the World Health Organization (WHO), 17,9 million people, representing 31% of all global deaths, died from CVD in 2016 [CVD – WHO 17.5.2017 / checked 22.07.2019]. CVDs sum up a group of vessel and heart disorders, leading to insufficient sustenance of organs, cardiac and brain tissue, consequently having fatal consequences like heart attacks and strokes.

The increase of blood pressure is most commonly associated with the increase in vascular wall stiffness caused by increased cellular tone, vascular injury or mechanical cardiac overload. Vascular smooth muscle cell tone is the primary regulation factor of the blood pressure and can vary to regulate temporary or long-lasting blood pressure imbalances. The cellular structure can adapt to none physiological conditions, causing pathophysiological developments and cardiovascular diseases.

Due to the steady increase of medical findings, the development of medications needs methods that permit a fast, precise and personalized evaluation system for the development and testing of hypertensive regulating agents. Additionally, new combinations of applied medication need to be determined for their appropriate personalized dosages and side effects.

Due to modern medicine and nowadays pharmacology, a great variety of suitable medications and treatments are available to decrease blood pressure. The pharmacological adjustment for each patient takes a lot of effort and expenditure to find an appropriate remedy, dosage and or even multi-medication.

For drug development and validation, animal testing is an essential matter, as appropriate *in-vitro* models to avoid animal testing are currently non-existent. Current trends try to minimize the usage of animal testing. Therefore, new approaches are required to analyze biological and medical relevant characteristics, which display comparable physiological conditions.

Generally, *in-vitro* models are not capable to re-give the complexity of a living organism, including metabolism and real-live tissue. Nevertheless, *in-vitro* models offer ideal conditions to isolate cellular or tissue mechanisms, as they are easy to standardize, reproducible and ethically reasonable. Cell culture technique and tissue engineering enable to model living samples, which can be used for a broad field of experiments. Even though such models neglect great parts of the metabolic system, the specimen usually allows an excellent derivation of the cellular physiology and metabolism. Being aware

of this, this reduction of complexity allows an even better understanding of single pathway mechanisms.

As the general physiology and biochemistry of vasoconstriction and -dilation, as well as stiffening of blood vessels, is largely understood. The possibilities for mechanical evaluation of single cells and cell clusters are always limited since the challenge is usually to enable direct force transmission without a preferred mechanical direction. Also, many methods only allow for one-time measurements due to complex sample handling and a sample damaging measurement procedure. In means of the research and development of new and existing pharmacological agents, measurement methods that can evaluate the biomechanics of agent combinations and their time-dependent characteristics are highly interesting.

On the physiological level, there are also still open questions, especially regarding the adaptation to extrinsic and intrinsic changes. Thus, changes are known at both the macroscopic and transcriptomic level, but cannot be measured.

The working hypothesis of this thesis is to create a vascular model that can be used for mechanobiological and pharmacological research. Investigation of cellular adaptation caused by mechanical stimulation might be similar to mechanically induced hypertension.

For this purpose, a CellDrum approach is presented, which allows the measurement of functional cellular force generation, taking into account the cellular arrangement and composition of the extracellular matrix (ECM) as well as the anchoring of the cells within the surrounding matrix. In contrast or even better, complementary to standard *in-vitro* technologies such as microelectrode arrays (MEA), patch-clamp and high-resolution imaging. This approach is intended to provide answers to the question of the extent to which cellular and biochemical mechanisms turn into cellular force generation.

For mechanical stimulation, a system specially adapted to the CellDrum was developed, which exposes the samples to a defined cyclical mechanical stimulus. The combination of the PulSElect system and the CellDrum technology enabled a rhythmic specimen stretching due to pressure pulses. This cellular mechanical stimulation provides insights to track changes in cellular tone increase and mechanically induced stress management of the cells.

The herein presented work describes the biological and technical development of a systematical approach to elucidate the cellular effects of vasoactive substances under varying mechanical conditions, from scratch to potential medical lab applications.

3. Working Hypothesis

1. With the *in-vitro* preparation of human arterial smooth muscle cells, the biomechanical effects of vasoactive and pharmacological agents can be demonstrated physiologically and functionally.
2. Development of an *in-vitro* hypertension model. Due to cyclic mechanical stimulation of human arterial smooth muscle cells, physiological and pathological cellular adaptations on morphological, genetic and biomechanical levels can be identified and correlated.
3. The direct co-cultivation of arterial smooth muscle cells and endothelial cells allows an advanced mechanobiological investigation, including NO-mediated vasoactivity.
4. An established vascular CellDrum model can be used for clinical or laboratory examination of patient material.

4. Background

4.1. Vascular Wall

The circulatory system describes the vasculature network across the body, transporting nutrients, oxygen, carbon dioxide, hormones and blood cells throughout the organism.

There are two categories of blood vessels depending on the direction of the blood transport, whether from (veins) or towards the heart (arteries). Veins transport deoxygenated blood from the tissue back to the heart. The structure of the two types is basically the same, only the composition of the individual layers are adapted to the requirements of the respective area[1]. In comparison to arteria, venous vascular walls are most commonly thinner, especially the intima-media, as the internal pressure is usually lower[2].

Arteries transport oxygenated blood from the heart towards the tissue. In direct comparison to veins, arteria walls are more robust due to their thickness and elasticity, but also have improved contractile abilities. Great lumen vessels close to the heart have high flexibility to turn pulsatile blood flow into a laminar bloodstream. The so-called Windkessel-function stores the high energetic bloodstream pulses from the cardiac contraction to a vascular extension, which can release it in a laminar stream. Additionally, this effect decreases the mechanical load of the heart muscle by storing energy during the vascular expansion [3,4].

To have an evenly distributed blood flow and appropriate tissue supply throughout the organism, the vascular wall thickness and lumen cross-section differ from adapting the variations in blood flow, depending on the body region. These differences are classified in further subgroups, elastic, contractile and a mixed type artery.

Having a closer look at the arterial vessel wall, they consist out of three layers, the tunica intima, media and adventitia, which are composed of endothelial cells, smooth muscle cells and connective tissue[Figure 1].

The inner layer is called Intima and consists of a single endothelial cell layer, which is located on an internal elastic membrane of collagen type IV. These two layers build a direct barrier to the lumen and bloodstream. Like in other hollow organs, the lumen is lined by a single layer of endothelial cells, which primary task is to enable oxygen diffusion and prevent blood from clotting[5]. Also, endothelial cells have blood flow sensory properties to regulate blood flow and play a major role in vascular wall healing and angiogenesis [6,7]. Besides, regulation of the lumen diameter due to permanent secretion of vasoactive substances[8], the endothelium also regulates the proliferation of vascular muscles by producing a heparin-like substance to prevent lumen rejuvenation through cellular over-proliferation [9,10].

The outer layer is called tunica adventitia, which consists mainly of connective tissue and provides vascular anchorage to adjacent tissue and protects the inner layers. This protective and shaping structure accounts for a large part of the mechanical stability of the vascular wall. Under healthy physiological conditions, it is not involved in blood pressure generation.[11]. However, in the pathological case, the strength of the connective tissue structures can be linked to the development of certain hypertensive diseases[12,13].

In between, the tunica intima is situated, which mainly consists of smooth muscle cells and connective tissue. This layer provides regulation and stabilization of the blood flow by cellular contraction or relaxation. The key player for this feature is the smooth muscle cell, which mechanisms will be discussed in more detail during the next chapters.

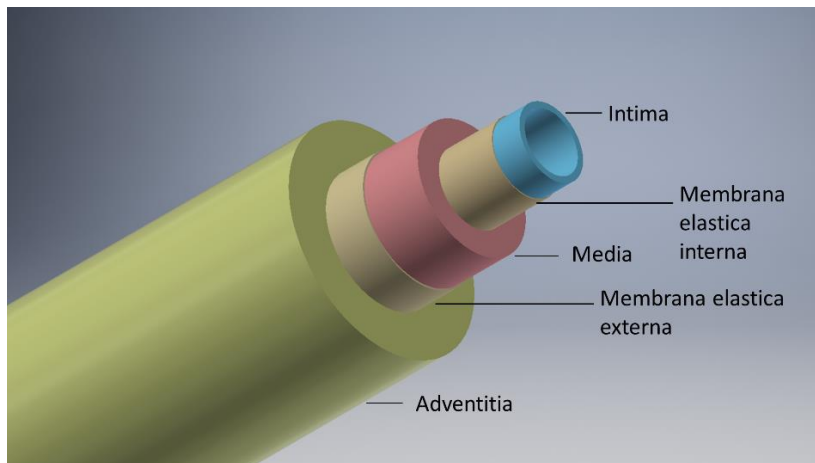


Figure 1 Schematic structure of an artery with the designation of the individual functional layers (Adventitia, Media & Intima) and the related connecting layers.

The ratio of connective tissue and cell amount varies depending on the body region and blood flow condition. Hence, arteria close to the heart is usually classified as elastic arteries, having a large lumen diameter consisting of a comparable low cell density, which is even less aligned. In contrast, peripheral arteries situated at the limbs contain higher smooth muscle cell density with higher cellular alignment, offering better contraction abilities and greater variations of the vessel volume. These features keep muscular tissue oxygenated during physical stress and provides stabilization of the body's core temperature.

4.2. Blood pressure regulation

Blood pressure regulation is a crucial player in keeping body homeostasis. Material transport, tissue nutrition, pH and body core temperature are depending on permanent and sufficient blood circulation.

The mean arterial blood pressure consists of the resulting cardiac output and the peripheral arterial flow resistance and can be temporarily adjusted. The arterial blood pressure is measured by pressoreceptors situated in the aortic arch and the carotid sinus. Sensed blood pressure deviations are transmitted to the cardiovascular center of the vegetative nervous system, which is located in the medulla oblongata and nearby areas. For bilateral blood pressure regulation, there are two vasomotor centers, the excitatory, to increase and the inhibitory, to decrease the blood pressure. An additional blood pressure regulator is the hypothalamic center, adjusting blood pressure to the overall vegetative status[14].

Moreover, blood pressure can be regulated locally due to mechanical stimuli[15], drop of CO₂ or O₂ partial pressure [16,17] or changes in pH-value. Local, as well as global blood pressure regulation, causes the vascular system to modulate the inner lumen diameter to adapt to current conditions.

The endothelium of the intima permanently secretes vasoactive substances that contribute to the homeostasis of blood flow. Thus, blood pressure is regulated by the endothelium mostly via secreted messengers such as endothelin-1 (ET1), angiotensin-2 (AT2) and endothelial nitric oxide (eNO). Since the vascular endothelium is in direct contact with the bloodstream, it can react to biochemical changes in the blood and also mechanosensory to changes in blood flow. Studies have shown that the regulatory mechanisms of the endothelial cells can be affected and amplified by mechanical stimuli, especially shear and stretch forces[18–21].

Vascular constriction and dilation are provided by the contractile properties of smooth muscle cells. With the help of the Actin-myosin apparatus, the smooth muscle cells can vary the vascular wall tone and lumen cross-section, by cellular shortening and/or elongation[22,23]. The contractile apparatus

consists of alpha and beta Actin as well as Myosin light chains (MLC) and Myosin heavy chains (MHC), which are netlike distributed throughout the cellular body. Dense bodies within the sarcolemma are used as the anchoring points for (intermediate) actin filaments [Figure 2]. Further intermediary filaments like desmin, vimentin and filamin transduce the generated force of the myosin filaments to the sarcolemma. The contracting of smooth muscle cells can be mediated in several ways, but all seem to work through trimeric G-protein receptors [24].

Like all other muscle cells, the contraction of smooth muscle cells is Ca^{2+} dependent. As soon as the intracellular Ca^{2+} level increases, especially for smooth muscle cells of great lumen vessels, additional Ca^{2+} is released via the IP_3 receptor, which is initiated by the endo-plasmatic reticulum. In its resting phase, the head domain of Myosin is fixed to an actin filament, while the head domain of the heavy myosin chain and light myosin chain is angled 90° . The cross-bridge cycle (CBC) of smooth muscle cells (SMC) is the same as the CBC of straightened muscle cells. However, the initiation is not triggered by Troponin C. Instead, Ca^{2+} ions bind to Calmodulin, resulting in a Ca^{2+} -Calmodulin Complex, which activates the Myosin Light Chain Kinase (MLCK). MLCK phosphorylates the MLC, leading to activation of Myosin ATPase, resulting in cleavage of the myosin head transforming ATP to ADP by releasing a phosphate, triggering the CBC. Due to the biochemical binding in the CBC, the actin-myosin apparatus mechanically moved forward by changing the myosin head angle from 90° to 45° , resulting in smooth muscle contraction.

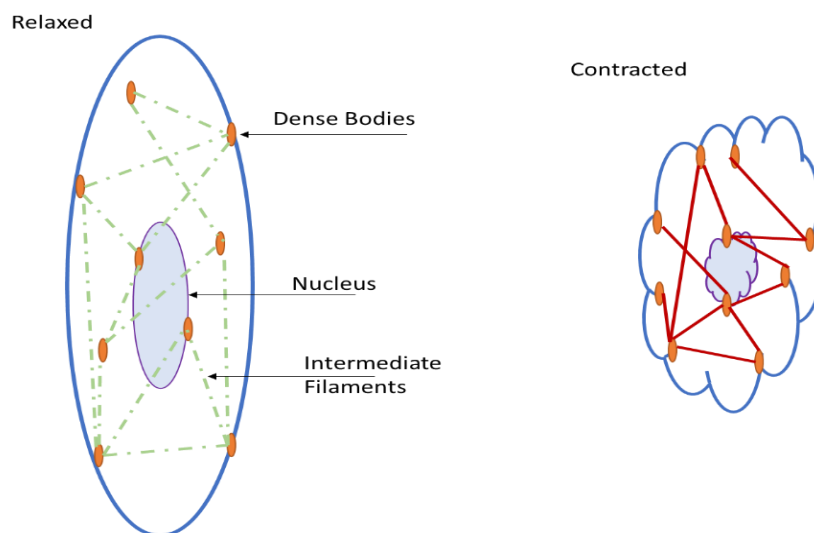


Figure 2 Schematic representation of the net-like distribution of dense bodies and intermediate filaments that cross the sarcoplasm. The contraction of the actin-myosin complex causes the dense bodies and intermediate filaments to shrink, resulting in cellular deformation and shortening[1].

The sensitivity of LCM phosphorylation is increased due to RhoGTP. A parallel signaling-pathway activates the Rho-kinase, which partially inhibits myosin phosphatase, consequently increasing the number of phosphorylated myosin cross bridges and force generation at any given Ca^{2+} concentration[25].

For cellular relaxation, the myosin needs to be removed from the actin, requiring another ATP molecule. The phosphorylation of ATP causes the myosin heads to reach back to the initial resting state. Additionally, intracellular Ca^{2+} needs to be decreased, which is promoted by cyclic Adenosine Monophosphate(cAMP) and cyclic Guanosine Monophosphate (cGMP)[26–28].

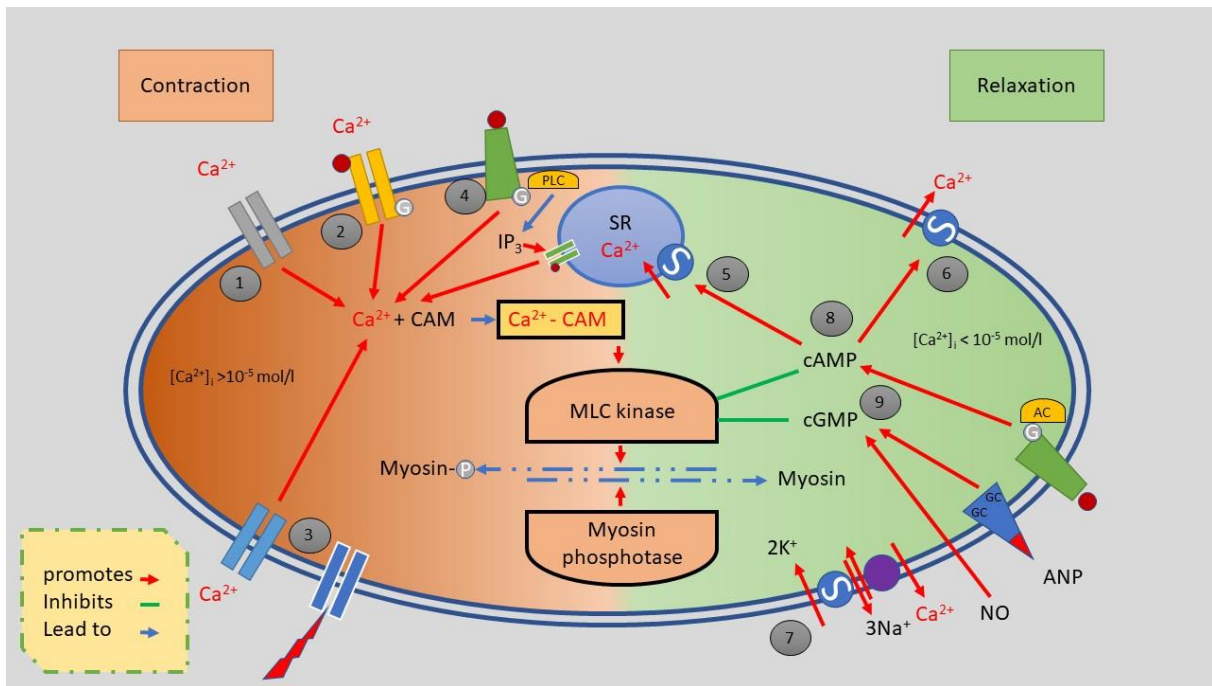


Figure 3 Contraction and relaxation mechanism of a smooth muscle cell as a schematic overview. The left half of the picture describes the contraction by electrical tension (1), receptor (2) and strain (3) dependent Ca^{2+} channels as well as by receptor-controlled (4) release of Ca^{2+} ions from the sarcoplasmic reticulum (SR). Muscle relaxing mechanisms are shown in the right half of the figure. Decrease of the cytosolic Ca^{2+} nucleotide by Ca^{2+} -ATPase(5,6) and $3\text{Na}^+/\text{Ca}^{2+}$ exchange (7) as well as the effect of the cyclic nucleotide cAMP (8) and cGMP (9). Molecular contraction mechanism in the center of the image, CAM calmodulin, PLC phospholipase C, AC adenylyl cyclase, G G protein, IP_3 inositol triphosphate, ANP atriopeptin, GC guanylylcyclase[1] (figure adapted).

The Ca^{2+} exchange is mainly ensured by voltage-dependent Ca^{2+} ion channels, including the L-type and T-type Ca^{2+} channels. Both channels are primarily responsible for the membrane potential of the cell and are activated and opened by depolarization so that Ca^{2+} ions can reach into the cell compartment. The L-Type Ca^{2+} channels describe a group of ion channels with long-lasting activation time and are essential for the contraction of smooth muscles. T type Ca^{2+} channels, on the other hand, have a lower depolarization limit than the L type Ca^{2+} channels and have a shorter activation time. This fast activation behavior enables the cell to react to quick and rhythmically arriving action potentials.

The group of strain-dependent Ca^{2+} ions reacts to mechanical stimuli and allows depolarization and influx of Ca^{2+} by mechanical stretching of the cell membrane[26,29–31].

Another group of Ca^{2+} ion channels is the stored operated channels, which open after the intracellular Ca^{2+} stores of the cell are depleted and to refill the cellular Ca^{2+} storage. The exact physiological function and meaning of these channels are not yet clear at this stage. Furthermore, other ion channels can be summarized, which have a physiological and pathophysiological influence on intracellular Ca^{2+} levels and regulate the myogenic tone. These group of channels include, voltage-controlled K^+ channels, Ca^{2+} -activated K^+ channels with high conductivity, ATP-sensitive K^+ channels, ryanodine receptors, inositol 1,4,5-trisphosphate receptors (IP3Rs), and a multitude of channels of transient receptor[31,32].

4.3. Hypertension

A continuous pathological increase in arterial blood pressure is called arterial hypertension. The subjective perception of increased blood pressure varies from imperceptible to severe impairment. Therefore, hypertension is classified according to various ranges of blood pressure. As soon as the general blood pressure at rest overcomes 140-159mmHg and or systolic 90-99mmHg diastolic blood pressure, a person is diagnosed with hypertension.

Table 1 High Hypertension categorization according to the level of blood pressure [1]

Classification	Systolic mmHg	Diastolic mmHg
Optimum	<120	<80
Normal	120-129	80-84
High-Normal	130-139	85-84
Mild Hypertension (1.)	140-159	90-99
Moderate Hypertension (2.)	160-179	100-109
Severe Hypertension (3.)	>= 180	>= 110
Isolated systolic hypertension	>=140	<90

Hypertension can be divided into two subgroups, primary (or essential) and secondary hypertension, whereas the pathogenesis of primary hypertension cannot be defined in 90-95% of all cases. Secondary hypertension is caused by another primary disease like renal, cardiac and nervous dysfunction, or endocrine imbalance. Both instances can be pathologically subdivided to increase peripheral resistance and increased heart time volume, leading to increased systolic blood pressure, as the diastolic pressure stays normal. Due to the increased load on the peripheral system, structural changes and adaptations of the vascular tissue can occur, which can manifest themselves in the compression of the connective tissue and ECM as well as cellular stiffening. In most cases, hypertension is often a hybrid of described subgroups.

The pathogenesis of primary hypertension is mostly unknown, but various factors were identified, inducing hypertensive pathogenesis.

Genetic deposits could be a decisive factor in the development of hypertension [33]. The most common are polygenic mutations that are responsible for a pathological increase in blood pressure due to malfunctioning of the genomic material, which has been demonstrated in various twin studies. In contrast, Liddle Syndrome is a rare example of monogenetic defects, which mutates the tubulin sodium channel of the distal kidney epithelia, increasing the resorption of water and hypertonic saline[34,35].

Psychosocial factors, in which acute racket and stress might amplify the activation of sympathoadrenal systems, causing increased vascular contraction through neurotransmitters. In addition, excessive sodium intake, obesity and regular alcohol consumption promote pathogenetic development. The coherence of excessive NaCl intake and hypertension was proved by only a partial group of global hypertension patients. It is assumed that the high consumption of NaCl increases cytosolic Na⁺, which deranges the Na⁺/ Ca²⁺ exchange, resulting in an increased intracellular Ca²⁺ level and a steady increased cellular tone[36].

Moreover, a disbalance of the body's natural vasoactive substances like eNO, ET1, AT2[37–39] or imbalanced of the endocrine system affect the blood regulation significantly [Figure 4]. Patients with diagnosed hypertension showing an increased level of catecholamines and norepinephrine in the blood sera, leading to increased vascular tone[40,41]. In the case of pregnancy hypertension, elevated ET1 levels were often found in the blood of affected women.

To understand the multiple pathogenesis and their connections to the genomic level, multidirectional pathways can be described using big data analysis and so-called signature genes can be identified, which may be responsible for the development of hypertension[42–44].

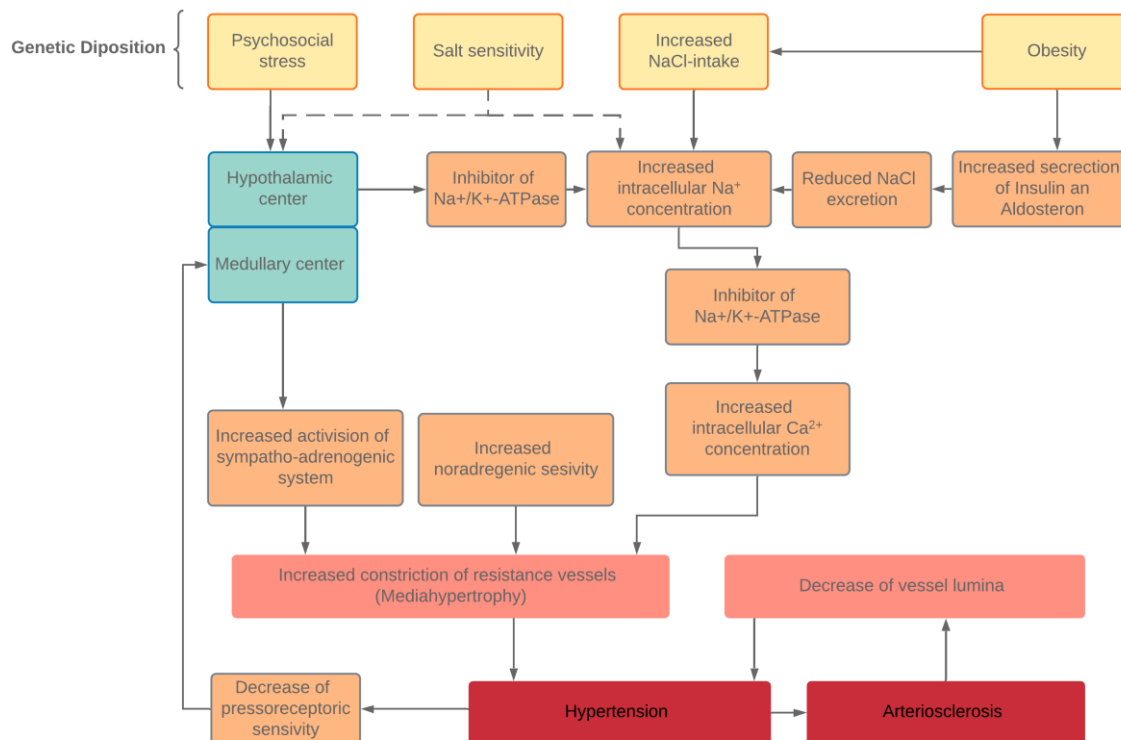


Figure 4 Overview and progress of different causes of high blood pressure[1] (figure adapted)

The development and problems of high blood pressure can also be traced back to changes in the vascular cells. Many of the already mentioned causes lead to uncontrolled cell proliferation or calcification at the macroscopic level, which in turn leads to narrowing of the vascular lumen[45]. As the number of cells increases, the elasticity of the vessel wall is also impaired.

Genetic defects, mechanical overload and increased cell mass, can lead to severe changes in the connective tissue of the vessel wall[12,46]. In particular, the additional production and uncontrolled restructuring of the extracellular matrix can lead to reduced elasticity, strength or defective structures such as fibrosis[47].

Likewise, long-term biochemical and biomechanical changes cause adjustments of the ion channels and receptors located in the cell membrane[48,49]. Such adaptations may shift the resting or activation potential, making the cell more difficult to depolarize, or in the opposite, keep the cell depolarized all the time [50].

Till now, there is no pharmaceutical cure for hypertension. Only a timely adjustment of blood pressure during the pharmacological treatment can be achieved. In severe cases, surgical interventions can diminish hypertension long-dated. There are various drugs to relieve the symptoms of high blood pressure, but due to the multiple sources of hypertension, patients are usually medicated by several compounds at once. The most common anti-hypertensive regulating agents are ACE-inhibitors, AT1-antagonists, Potassium inhibitor, beta-antagonists and thiazides. Aside from their desired effects, the drug administration goes along with side effects, prolonging the pharmaceutical adjustment and additional ailments.

4.4. Mechanical Cellular Stimulation

Mammalian cells need mechanical tension to survive. The mechanical, environmental conditions determine the orientation, growth behavior, force development and essential functions of the cells. Cells in the human body are permanently exposed to mechanical stress caused by movement, digestion, respiration and in the vascular system by the pulsatile ejection of the heart.

Since the mechanical stimulus of the cell plays such a crucial role in tissue development[51] and also in regenerative behavior [52], a wide variety of methods for mechanical cell stimulation have been developed over the last decades[53–55].

Mechanical stimulation at the cellular level can be subdivided according to physiological stimuli so that methodologies can be found in the literature that exposes cells to compression, shear stress and mechanical strain. Besides, the stimulation protocols differ in static and dynamic mechanical load. Static stimuli describe a one-time change in the stress situation to which the cells are exposed. Thus, some studies observe the growth behavior of cells on growth surfaces with varying degrees of solidity. Especially in stem cell research, these protocols gain great attention since the maturation of cardiomyocytes, in particular, is strongly influenced by the growth condition mechanics[56,57].

For the field of vascular research, cyclically dynamic mechanical stimulation methods of shear stresses and strain stresses are of particular interest. Thereby, cells are exposed to different, rhythmic and recurrent stimuli. The rheology of blood vessels has an essential effect on the cellular characteristics of the vascular endothelium. Thus, it has already been possible to show the correlation of mechanical stress and metabolites/messenger secretion[6].

Due to the permanent cyclical blood ejection of the heart, the cells of the vascular system experience mechanical stimulation throughout the organism. To understand the cellular response to this mechanical stimulation and also changes, methods for cellular stretching are of particular interest.

To date, studies have shown that cyclical mechanical stimulation of vascular smooth muscle cells has a fundamental influence on their phenotype[58][59], biomechanics, cell connection, signaling[60][61] and restructuring of both intra- and extra-cellular structures[18,62,63]. All these findings serve for a detailed physiological understanding to better understand pathological developments and regenerative medicine in medical applications as well as biological and biomechanical research[19,64].

4.5. Biomechanics

Biomechanics is an interdisciplinary discipline that applies the laws of mechanics and material sciences to biological organisms, biomaterials and tissue. The resulting data are used in research and medicine to explain mechanobiological phenomena based on experimental and mathematical models.

Over the last decades, mechanical tissue properties have been studied in detail and their fields of application are as diverse as the methods used to determine them[46]. Thus, classical mechanical material parameters serve the necessary physiological characterization and the definition of material requirements for medical and tissue-engineered implants[65,66]. Due to the experimental research work by G.A.Holzapfel mechanical properties of vessels could be measured by dissections and tissue equivalents. This enables to determine both, the tensile strength and the deformation properties of biological material consisting of ECM and cells[67,68].

In extension, pathological or aging-related findings can also be correlated with biomechanical models, which can be reconstructed and improve fundamental understanding and prognosis[69,70].

In classical physiology, biomechanics is mostly applied to the study of movement and tissue consolidation or contraction and relaxation. At the beginning of the last century, the contractile force

of an isolated and perfused heart could be measured using the so-called Langendorff heart, which is still used in physiology today, especially for pharmacological investigations[71].

The measurement of force variations due to muscle shortening can be projected onto all other muscular structures, including vascular structures. Especially this requirement is still used today in so-called aortic rings, whose cross-sectional deformation provides detailed information about mechanobiological processes[72–75]

4.5.1. Cellular Force Measurement

In addition to the macroscopic level, the biomechanical laws can also be applied to the microscopic and subcellular levels. Taking biophysical laws into account, complex and dynamic mechanical properties of individual cells and cell organelles can be measured[76–78].

The state of the art currently offers various methods to measure force changes of monolayers and single cells, both directly and indirectly. Due to different hypotheses of force distribution and stress development of the cells[79,80], diverse force measurement methods are considered, which can measure uniaxial, monoaxial or bi-axial stresses[81–83]. The high sensitivity of the methods is essential to resolve cellular forces in the pN- μ N range.

One of the most common methods for indirect force or stress measurement is atomic force microscopy and traction force microscopy[84–86]. Both techniques allow deformations of the growth substrate to be measured by induced cell forces. In addition, the atomic force microscopy method allows us to assess the strength of single cells. Due to material stiffness analysis, it is possible to infer cell contraction or relaxation indirectly[87].

Probably the most common method for measuring cell forces is tensile testing of cell cultures on defined growth substrates. Usually, biocompatible polymers or matrices in rectangular shape are prepared from which the induced forces of the cells are determined by means of using load cells. However, the geometry and fixation of these preparations usually generate different stress fields on the carrier material by the cells. Thus, in most cases, only an averaged and summed force generation of the cells can be shown. In order to counteract this problem, the group around Kit Parker has developed a procedure that enables the contraction of the cells through the deformation of eyelash structures. By deforming the "lash", a mechanical model can be used to determine the force of shrinking from the eyelash bending radius[88]. Micro-structuring of the carrier material across methods can help to direct the generated strength to a particular preferred direction, which makes the evaluation more precise and sensitive[89].

The bi-axial stress measurement neglects the directional stress distribution, as the stress distribution is the same in all directions in biaxial systems. For bi-axial stress measurement, methods that also serve for mechanical cell stimulation are usually used. Deviations of the parameters for precise adjustment of the strain can thus be indirectly inferred from changes in cell tension[60,90]. The best known and most widely used method for bi-axial stimulation is the FlexCell system, which transfers the principle of the simple tensile test in a round geometry[91,92].

The choice of methodology is therefore extremely versatile and can be made with the scientific question. While most *in-vitro* cell force methods currently serve for basic research and laboratory development, clinical approaches continue to pursue the use of tensile tests and deformation analyses of real tissues *in-vitro*.

4.6. *In-vitro* Model

Developments in cell culture technology and tissue engineering make it gradually easier to produce tissue equivalents from cell cultures. Besides the less ethically questionable handling towards living tissue, isolated cells benefit the reduction of mechanically influencing factors. So that mechanical cell force alterations can be characterized more precisely without the passive contractive influence connective tissue.

Cell culture technics and tissue engineering enables the cultivation of living tissue or tissue equivalents under *in-vitro* condition. Such models are idealized cellular systems for biological analyses. Due to the substantial simplification of a living organism, these models enable to multitudinous aspect elimination compared to *in-vivo* samples.

From an ethical point of view, such *in-vitro* models are much more favorable than animal testing or experiments with living tissue dissections, as the specimen material can be cultured under laboratory conditions and reproduced to a certain extent. According to the 3Rs principle, the development of *in vitro* models makes it possible to reduce and replace animal experiments and to make the experimental set-ups more reproducible and ethically acceptable[93]. Nevertheless, for functional testing, animal testing is still an important matter as the functional testing of pharmaceuticals to complete organisms cannot be simulated entirely[94].

Current studies show that there is an urgent need for disease models and functional physiological assays to support and improve medical findings and diagnostics in order to understand sophisticated mechano-biological phenomena of physiology, pathophysiology and aging *in-vitro*[95,96].

The scientific application and implementation of arterial *in-vitro* models are versatile and depend on the scientific problem and the phenomena to be observed, ranging from single-cell models and monolayers to three-dimensional tissue-equivalent or organoids. The knowledge gained from these models is used to analyze functional physiological processes concerning biochemical, electrophysiological and biomechanical phenomena. Beyond that, they are also used to answer more complex questions that arise at the molecular level or in regenerative medicine, in which processes such as angiogenesis or wound healing are central[56,97,98].

A great variety of model designs depend on the scientific question and observing phenomena and ranging from single-cell model and monolayer to three-dimensional tissue-equivalent or organoids.

The most fundamental way to set up a cell culture model is the cultivation of a single monolayer of one cell type. Due to the isolation of cells, it is easy to characterize and interpret single-cell physiology and experimental findings. In terms of studying rheological effects within the vasculature, flow chambers and organ on a chip approaches became quite famous in recent years[99–103].

Especially while studying vascular walls, the cross-communication between smooth muscle cells and endothelial cells is a highly interesting topic, with high medical impact. To get inside to this topic, it requires a co-cultivation of both cell types, allowing intercellular signaling. According to literature, there are three main subgroups of co-cultures: Conditioned co-culture, direct co-culture and three-dimensional co-culture.

A conditioned co-culture offers no direct contact between the cells. Both cell types are physically separated from each other. Such systems can be realized by so-called inlet membranes, which separates two different culture compartments, but allows cell signaling and molecule transfusion throughout the separation layer. Another approach to achieve a conditioned cell-culture is to exchange or mix the media of two distinct cell cultures. Hence, the effect of metabolites and signaling molecules can be evaluated by employing a mono-culture[104,105].

In contrast to conditioned co-cultures, direct co-cultures describes the cultivation of two different cell types in the same cell culture compartment. Respecting cellular communications, such systems are closer to physiological conditions, but also exacerbate the interpretation and analysis of differentiated results[106]. Concerning the physiology and experimental setup, it is possible to arrange the cell in a physiological pattern by gel structures or decellularized tissue[107–109]. Such a setup benefits the functionality of an *in-vitro* model as the arrangement of cells can be simulated equally to an in-vivo system[110].

Working with vascular three-dimensional cell models requires a well-defined matrix equivalent. In most cases, three-dimensional structures are generated by gel-like structures made of collages, matrices or similar[111–113]. The use of such systems usually has a relatively compact and stable structure due to the matrix components and is, therefore, mostly applied in biochemical and molecular biological research.

A recent trend that is closely related to stem cell research is the application of organoids, which commonly suitable for the study at hollow organs. Organoids are spherically modeled organs made of primary or stem cells[56], promising to have great physiological properties and having similar in-vivo arrangement.

4.6.1. CellDrum Technology

The CellDrum technology was firstly described by Jürgen Tzerwiki, Institute for Bioengineering FH Aachen, in 2001 [114–116]. The CellDrum was developed to estimate the biomechanical properties of standardized cellular monolayer and 3D tissue equivalents[117]. The CellDrum is methodologically an important technology that, in contrast to known indirect electrophysiological methods, quantifies direct lateral bi-axial generated cellular forces in micronewton (μN). Previous studies have shown that the CellDrum is a useful tool to elucidate the mechano-pharmacological characterization of human-induced pluripotent cardiomyocytes[118,119]. This has been shown in the experimental work by M.Goßmann, which has also demonstrated that a three-dimensional arrangement of different types of cells is possible[120]. Besides the possibility to biomechanically analyze cells, the softness of the membranes results in a unique growth surface, which provides mechanically seen an almost physiological growth environment.

Over the past decades, the CellDrum went through various optimizations and changes, leading to the current state of the art, which will be presented in this work. Especially the description of standard operating protocols and automatization are described in detail in a recent publication by R.Bayer[121,122].

The recent developments of the CellDrum technology showed the versatile application of the standard CellDrum. In addition to mechanobiological characterization, the system can be used to expose the cell to mechanical stress. Combining both techniques could be an excellent foundation for biophysical and biomechanical basic research[122,123].

5. Material & Methods

Table 2 Chemicals

Material	Producer	Vendor	Cat.No.
Cell culture			
M200	Gibco	ThermoFisher	M200500
M231	Gibco	ThermoFisher	M231500
DMEM-GlutaMAX	Gibco	ThermoFisher	31966021
DMEM + F12	Gibco	ThermoFisher	11330057
M199	Gibco	ThermoFisher	12340030
DPBS	Gibco	ThermoFisher	14190250
Trypsin/EDTA (0,05%)	Gibco	ThermoFisher	25300054
FBS	Gibco	ThermoFisher	16140071
SMGS	Gibco	ThermoFisher	S00725
SMDS	Gibco	ThermoFisher	S0085
LSGS-Kit	Gibco	ThermoFisher	S003K
Collagen Type I	Merck	Merck	9007-34-5
Human Collagen Type IV	Merck	Merck	CC076
PureCol EZCollagen Type I	Cellsystem	Cellsystem	5074-35ml
Fibronectin Bovine Plasma	Merck	Merck	F1141-2MG
DMSO	Roth	Roth	0728.1
Trypan Blue Solution 0,4%	Gibco	ThermoFisher	15250061
LIVE/DEAD® Viability/Cytotoxicity Kit	Invitrogen	ThermoFisher	L3224
LDH-KIT	Invitrogen	ThermoFisher	-
ET1-ELISA Kit	Invitrogen	ThermoFisher	EIAET1
Staining			
Alexa Fluor® 488 – Phalloidin	Invitrogen	ThermoFisher	A12379
CellTracker™ Deep Red	Invitrogen	ThermoFisher	C34565
CellTracker™ Green CMFDA	Invitrogen	ThermoFisher	C7025
Anti-Actin, α -Smooth Muscle - Cy3™ antibody	Sigma-Aldrich	Merck	C6198-100UL
Antibody CD31	Abcam	Abcam	Ab28364
Gen Analysis			
SYBR Green	Sigma Aldrich	Merck	163795-75-3
RNeasy Mini Kit	Qiagen	Qiagen	74106
QIAshredder	Qiagen	Qiagen	79656
miRNA Kit	Qiagen	Qiagen	217604
QuantiNova Reverse Transcription Kit	Qiagen	Qiagen	205411
SsoAdvanced Universal SYBR Green Supermix	BioRad	BioRad	1000076382
Ultra Pure Water PCR grade	Invitrogen	ThermoFisher	AM9935
ROTIPURAN® Ultra	Carl-Roth	Carl-Roth	HN68.3
RNAseZAP	Sigma	Sigma	R2020-250ML

CellDrum			
Sylgard 184	Dow Corning	VWR	SAFA761036-5EA
Trimethoxy[2-(7-oxabicyclo[4.1.0]hept-3-yl)ethyl]silane	Sigma	Sigma	413321-25ML
MES Buffer	Carl-Roth	Carl-Roth	4256.4
Acetic Acid	Sigma	Sigma	64-19-7
Perdrogen	Sigma	Sigma	-
Muriatic Acid 37%	Carl-Roth	Carl-Roth	4625.2
Gypsum			
2-Propanol	Carl-Roth	Carl-Roth	AE73.2

Test Substances			
Nifedipine	Sigma	Sigma	N7634-1G
BayK 8644	Sigma	Sigma	B112-5MG
Verapamil	Sigma	Sigma	V-002-1ML
Potassium Chloride	Carl-Roth	Carl-Roth	6781.1
Diazoxid	Sigma	Sigma	D9035-250MG
CGRP	Cayman Chemicals	Cayman Chemicals	24405
Glibenclamide	Sigma	Sigma	G0639-5G
Spermine NO-complex	Sigma	Sigma	S150-25MG
DEA/NONOate	Cayman Chemicals	Cayman Chemicals	82100
Norepinephrine	Sigma	Sigma	A7257-500MG
Angiotensin II	Sigma	Sigma	A9525-1MG
Acetylcholine Chloride	Sigma	Sigma	PHR1546-500MG
Endothelin I	Sigma	Sigma	E7764-.1MG
Caffein	Sigma	Sigma	C0750-100G
Cytochalasin D	Sigma	Sigma	C2618-200UL
Sildenafil	Sigma	Sigma	S-010-1ML
L-Citrulline/L-Arginine	GEN	Amazon	X00140JWWS1

Table 3 Systems & Devices

Device	Company
Automated CellCounter TC 20	BioRad
Biophotometer	Eppendorf
Photospectrometer V-560	JASCO
Multi-plate Reader 680	Biorad
BioZero 8000	Keyence
iCycler	BioRad
Axiovert 200	Zeiss

5.1. Technology Overview

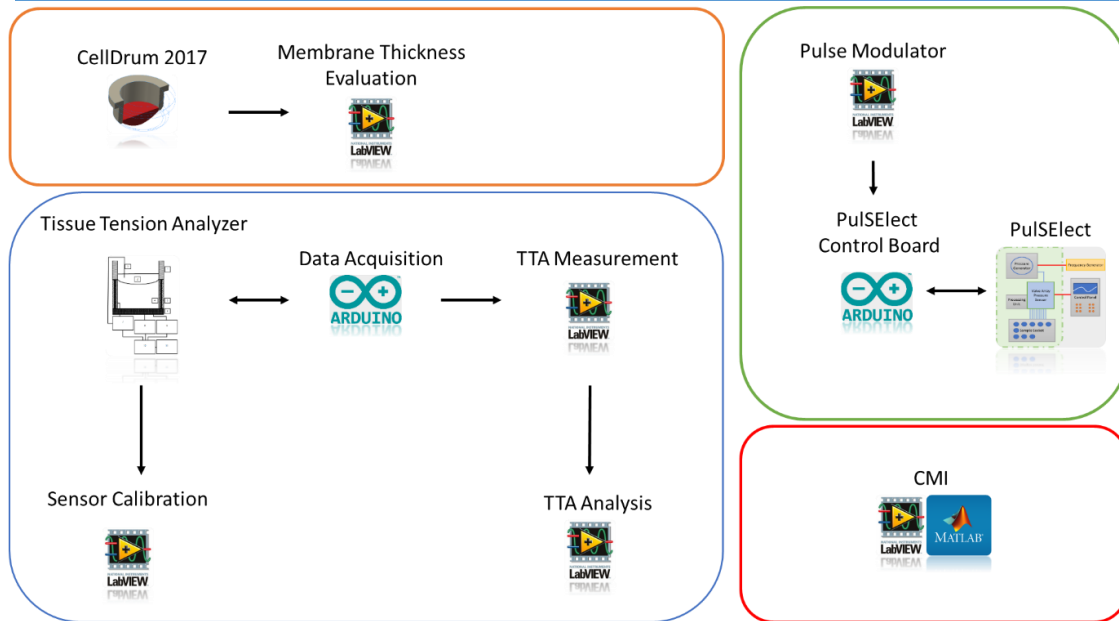


Figure 5 Overview of all systems and programs developed for this work. Orange Box: Adaptation of CellDrum and measurement methods for quality management. Blue Box: Measuring system for the biomechanical analysis of the CellDrums and software for data acquisition, evaluation and sensor calibration. Green Box: Technical development for mechanical stimulation of CellDrum samples. Red Box: Software for the quantification of cytoskeletal distribution.

5.2. CellDrum

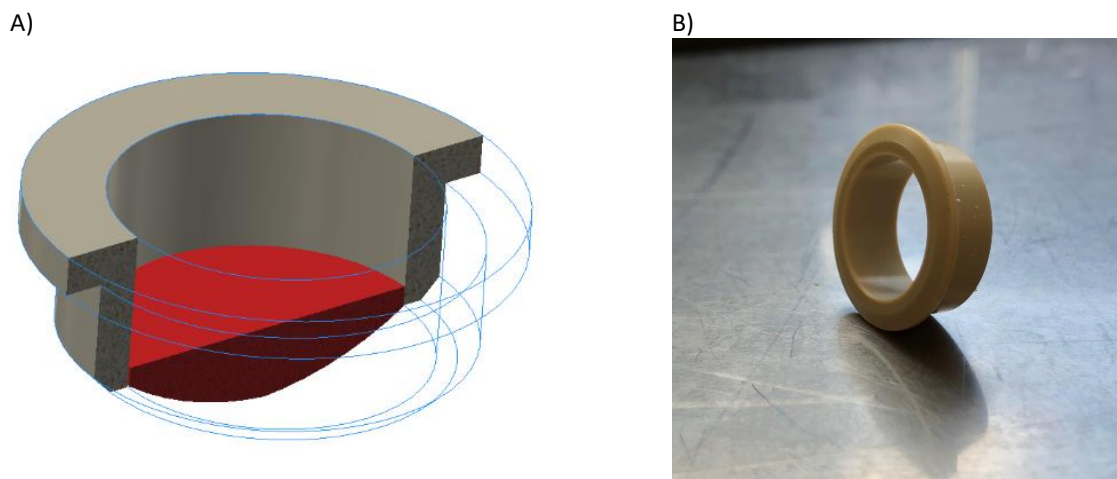


Figure 6 A) Sliced computer-aided design scheme of a CellDrum with membrane and cell culture media. The CellDrum offers a 2cm² cultivation area, consisting of an ultra-flexible polydimethylsiloxane (PDMS) membrane. Due to surface functionalization, cells can attach to the membrane [124] **B)** Photo of CellDrum 2017.

The CellDrum is a round-shaped cell culture well with a highly flexible 2cm² cultivation area made of a 4µm thin polydimethylsiloxane (PDMS) membrane, which was developed to estimate biomechanical properties of standardized cellular monolayer and 3D tissue equivalents[116,117,124].

Especially for this thesis, the “CellDrum 2017” was developed, which has idealized dimensions and tolerances[Figure 6]. Additionally, the new version of the CellDrum does not require a sealing ring for storing anymore. The material is changed from Polymethylmethacrylate (PMMA) to

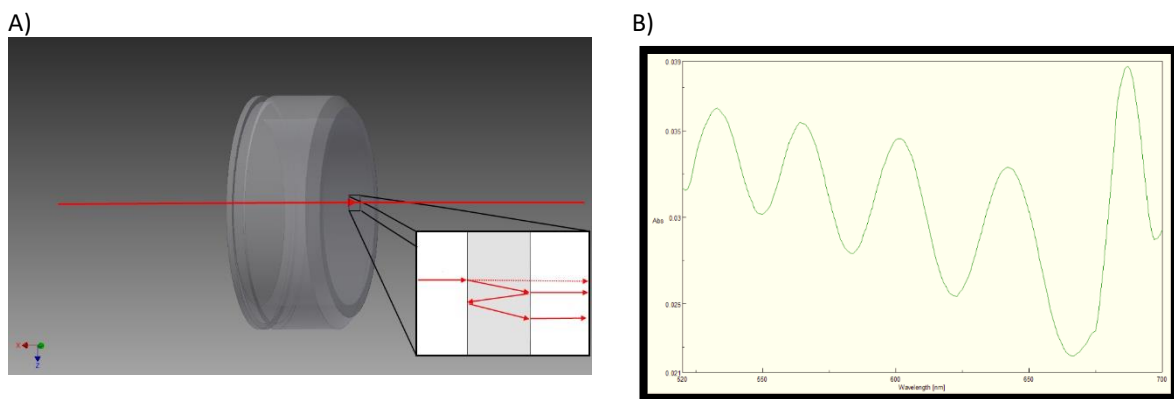
Polyetheretherketone (PEEK), which makes it much more stable for chemical and thermal stress, but is still biological compatible.

All biomechanical experiments were carried out in self-made CellDrums with highly specified membrane properties. The manufacturing protocol has already been described in the dissertation of Dr. M. Goßmann[125]. Only membrane thickness and strength were adjusted to the requirements of this study.

5.2.1. Membrane Characterization

For standardized CellDrum membrane quality, the membrane thickness and initial tension were analyzed before each experiment.

The thickness was measured photometrically and is a crucial parameter for the sample quality, as the thickness is required for the stress calculation[Figure 7]. The working principle is precisely described in the doctoral thesis of M.Gossmann[125]. Afterward, the method was established and automatized by J.Klinkhammer[126].



C)

$$d = \frac{\lambda_1 * \lambda_{21}}{2n * (\lambda_1 - \lambda_2)}$$

Figure 7 A) Illustration of the measuring principle for photometric layer thickness measurement. VIS light penetrates the CellDrum membrane and generates an interference pattern, which indicates the layer thickness by the refractive index, internal reflection and material parameters. **B)** Recorded interference pattern[126] **C)** Formula for determining the coating thickness using the wavelength interference.

Pressure-deflection curves determined the initial membrane stress properties using the Tissue Tension Analyzer(TTA). This method is described in more detail later. For this study only CellDrums with an initial membrane tension without cells and functionalization around 100kPa were used.

5.2.2. Membrane Functionalization

PDMS is a medical-grade polymer with a silicon backbone structure. Due to its inert biological properties, adherent mammalian cells will not adhere to the surface sufficiently. To enable cellular adhesion, the membranes were treated wet-chemically. Surface functionalization is carried out by oxidation and silanization steps, which is detailed described in the work of M.Gossmann[125] and well characterized in the bachelor thesis of R.Bayer[127]. In addition to this, the surfaces are coated with a 1% fibronectin solution to improve cell adhesion.

5.3. Tissue Tension Analyzer

The biomechanical analysis is carried out by a so-called TTA[120]. A TTA is mainly composed of a pressure sensor, deflection sensor and a syringe precision pump[Figure 8A] to analyze biomechanical properties by recording pressure deflection curves.

For the measurement, the CellDrum is airtightly placed into the measurement socket[Figure 8B]. Afterward, the membrane is inflated with a precisely defined volume and flowrate of air by a precision pump. The TTA records the membrane deflection in dependency on the generated pressure progression, resulting in a pressure-deflection-curve. The slope of the pressure deflection curves is used to calculate the internal stress of the cell monolayer and the PDMS membrane[Figure 14].

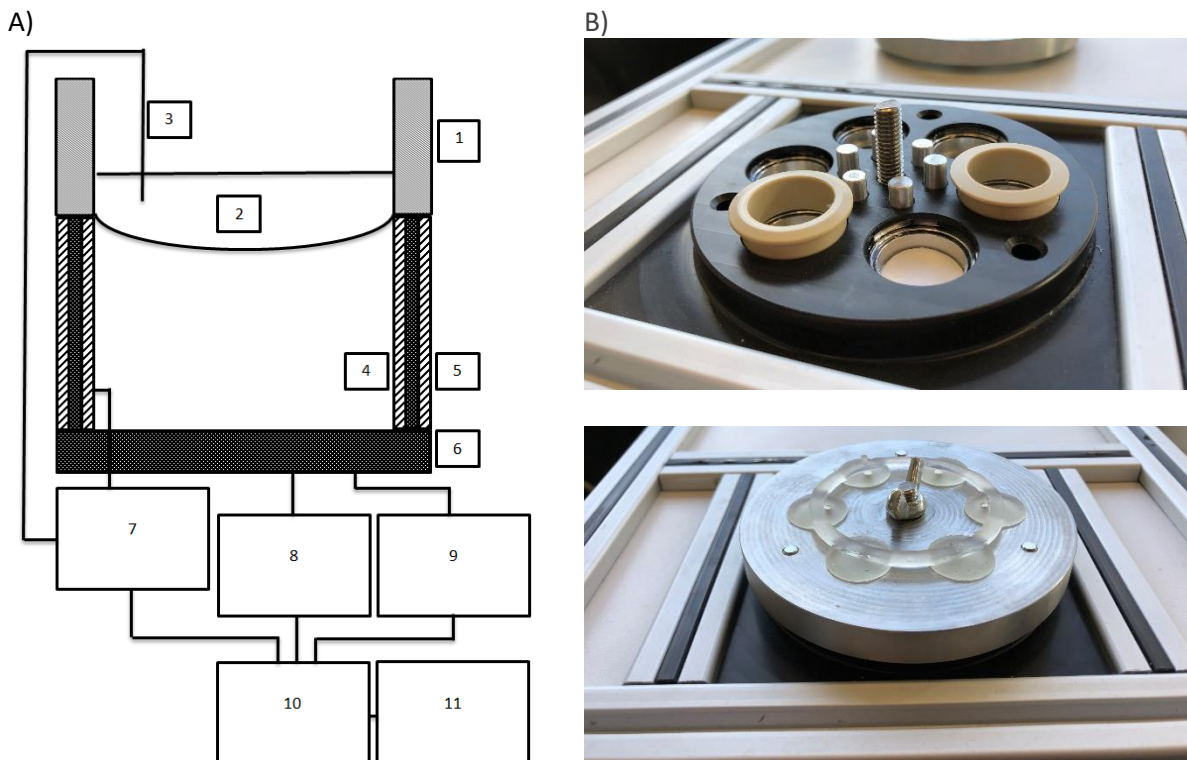


Figure 8 A) Picture of the Tissue Tension Analyzer with a detailed schematic arrangement of the measurement socket - 1) CellDrum; 2) Cells attached to the CellDrum membrane with cell culture media (500 μ l) on top; 3) GND electrode; 4) Counter electrode; 5) Electrical shielding; 6) Measurement socket; 7) Deflection sensor; 8) Pressure sensor; 9) Syringe pump; 10) Processing unit; 11) Peripheral computer and data storage[121,124]. **B)** Photographs of the TTA test base; above: Cover open with two CellDrums and view of the cylinder electrodes; bottom: Closed with cover and protective cap.

5.3.1. Development

For this thesis, a fully re-engineered TTA was developed, designed and improved to exact needs by Robin Bayer[Figure 8 B,C]. The central innovation of this device is the used proximity sensors. For the deflection measurement, a patented capacitive sensor principle is used, which is described in detail in the FH Aachen patent "CellDrum Electrode arrangement for measuring mechanical stress"[128,129].

The latest iteration is capable of holding six samples at once. The measurement time has been shortened from 30 s to only 12 s per measurement, to decrease the cellular damage by overextension. Pauses of 30 s between the single measurement cycles have been established to stabilize the signal. Further, the device was fully automated, allowing measurement rows over extended time frames.

The entire engineering process required designs in the fields of mechanics, electronics and computer technology, the individual segments of which are described in more detail in the following chapters.

5.3.1.1. Mechanical Construction

The mechanical components were designed with Inventor AutoCAD and later on manufactured by the mechanical workshop of the FH Aachen or printed with a Formlabs II Printer.

The sample sockets at the top side are designed to the dimensions of the CellDrum 2017 model, connecting the specimen to the proximity and pressure sensors.

To increase the sensitivity and to minimize the distance between the proximity sensor and CellDrum, the proximity sensing unit is designed as a cylindrical surface for the CellDrum. The proximity sensing units consist of two, and one side closed, high-quality steel cylinders which are separated by a spacer made of polyoxymethylene (POM). The inner component is used as a counter electrode, whereas the outer cylinder is used as shielding to prevent the measurements from interfering with each other. The measurement principle is explained in chapter 0.

The electrical circuit responsible for the displacement measurement is situated directly to sensor cylinders to improve the signal-noise ratio. Therefore, two jack plugs (0,9mm) are designed underneath the sensor heads, which allow cableless connection to the analog-digital converter.

For shielding and improved specimen fixation, a metal cap was designed, which holds a simple electrical board to connect the cell medium via a gold electrode to the inside of the system.

5.3.1.2. Electronic Components

The electronic components of this device were designed with Eagle software and printed to printed circuit boards by the company PCB Pool. All boards and electrical components were designed with surface mounted device components to improve the size and diminish electronic interferences.

The motherboard is the central board, which connects all single components and is designed as a mounting device for the Arduino Due, so failure-prone cable connections are reduced. Its main function is to enable a conversation between the single components and the microcontroller. Plus, the motherboard supplies all necessary components with appropriate voltages ranging from 3,3V-12V[*Figure 9*].

All signals are collected on this board, directed and managed to their final destination. The control of the valve system is realized by transistors circuits, which allow them to select the corresponding pneumatic channel and open the whole system to atmospheric pressure. The pressure data are measured by a customized HCLa pressure sensor (FirstSensor) in the range of $\pm 100\text{Pa}$.

Incoming data from the TTA and further periphery are collected and processed by the Arduino DUE. The Arduino DUE was found to be appropriate as it allows the measurement of high frequencies due to its high clock frequency (84MHz). Additionally, it has preinstalled serial connections that allowed secure bidirectional data transfer via USB to a computer.

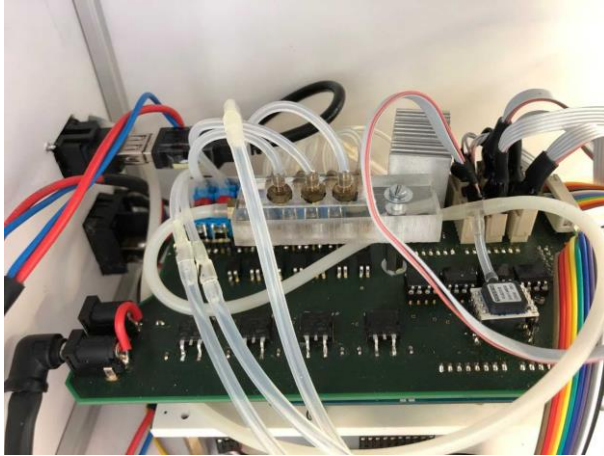


Figure 9 TTA motherboard for data acquisition and control of the system via computer. On the top left, in light blue, you can see the microvalves, which are pneumatically connected to the PMMA pressure distributor in the center. The pressure in the closed system is measured by an SMD pressure sensor on the bottom right. Power supply and voltage regulators can be seen on the bottom left. The slots of the individual measuring chambers can be seen at the top right. Directly below the motherboard is the microcontroller to establish communication with the computer. Underneath it is a mechanical relay that ensures the complete decoupling of the individual sensors.

The electronic circuits for the displacement sensors are designed to single boards that are separated from each other and situated directly to the sensor sockets. These boards contain a self-exciting LC oscillation circuit with a resonance frequency of around 14MHz. For appropriate handling of such high frequencies, the signal is converted directly to the digital TTL level. To prevent electrical coupling, isolators for the signals and voltage supply are implemented. The signals analog to digital conversion are directly done within these circuits as well[Figure 10].

A)



B)

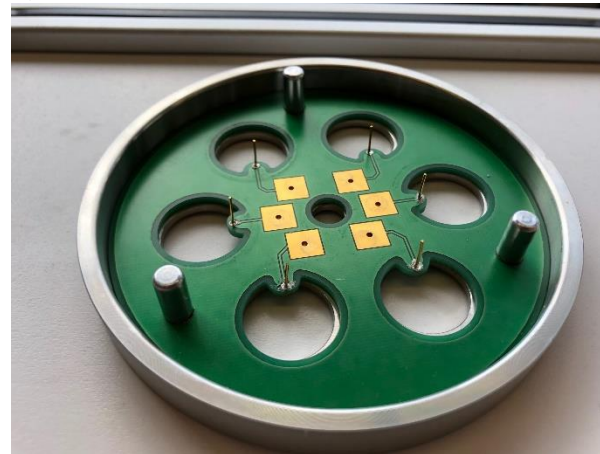


Figure 10 A) Bottom view of the measurement socket. Proximity sensors connected to the base, 0V electrode and pressure connection. **B)** TTA sealing cap bottom view with 0V gold electrodes for contacting the cell culture medium with LC-resonant circuit.

5.3.1.3. Proximity Measuring

The measurement is based on an LC oscillating circuit, in which the dimension of the capacitor or inductivity results in a changing resonance frequency.

In this case, the inductance is constant, while the CellDrum and the sample socket form a dynamic capacitance whose dimension depends on the area and the distance between the electrodes.

A capacitance generally consists of two electrodes, which are separated by a dielectric material. To turn the CellDrum into a moving electrode, the culture medium is connected via a gold wire to the ground (GND) of the electric circuit. The counter electrode is situated directly under the CellDrum and is designed as the bottom plate of the sample socket. In between the dielectric materials are the CellDrum PDMS membrane and air [Figure 11]. This combination results in a capacitance composition of spherical and cylindric electrodes, in which the cellular biomechanics dynamically determines proximity and area of both capacitor electrodes.

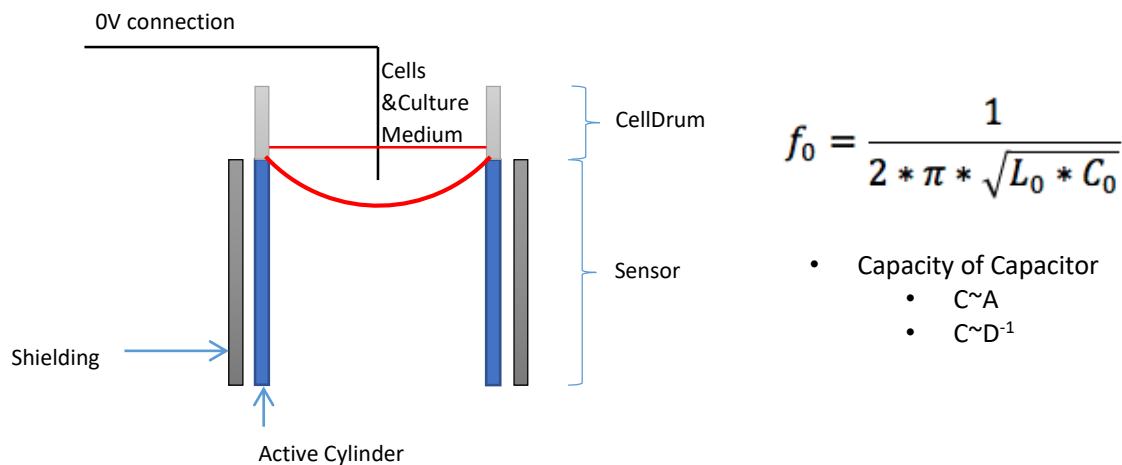


Figure 11 Schematic diagram of the measuring electrode arrangement. All components are connected to one of the separated oscillating circuits. The capacitance change of the system takes place between the red CellDrum membrane and the blue active cylinder surface [129].

Formula 1 Physical law of the resonant frequency of an LC oscillating circuit and the associated capacitance dependence of electrode distance and area.

5.3.1.4. Calibration

Due to the complex geometry of the capacitor arrangement, the proximity sensors require calibration with later on linear fitting. An additional experimental setup was designed, in which pressure deflection curves were measured by the capacitive sensors and an industry standardized triangulation LASER sensor in parallel. Both deflection datasets were correlated over the measured pressure progression.

A LabVIEW based calibration software merged both deflection profiles and plotted them to a combined graph. The resulting plot function was used for sensor linearization. As each sensor has unique characteristics, this calibration was carried out for each sensor head. The linearization function was implemented into the analysis software.

5.3.1.5. Programming

For the biomechanical evaluation, three software programs were required: Controlling, Data collection and data analysis.

The controlling software is uploaded to the Arduinos as so-called sketches. Sketches are program codes in a C++ like programming language, which can be coded, compiled and uploaded using Arduino IDE. The installed sketch of the microcontroller(μC) can detect high-frequency signals via external clock input, which is coming from the displacement sensors. The pressure data are read via 12bit analog input.

Controlling of the valves and relays is realized by case-structures, which can be triggered by incoming commands send from the graphical user interfaces (GUI). For serial data transfer, all outgoing data are put into a Byte array of high and low bytes and later on encoded by the data collection software. Due to the optimized data conversation, data can be recorded with a sample rate $>1\text{kHz}$ of each sensor type.

The data collecting software is written in LabVIEW and is mainly designed for the application in the lab [Figure 12]. The GUI allows real-time visualization of the current measurement and allows to enter all necessary data to the measured specimen. Due to the implemented automation, the operator only needs to choose the sample number. Afterward, the appropriate signals are sent to the μC automatically. Every measurement is saved automatically and is written in a customized data format (.rb), which contains all necessary data for the data analyzation and customized user information.

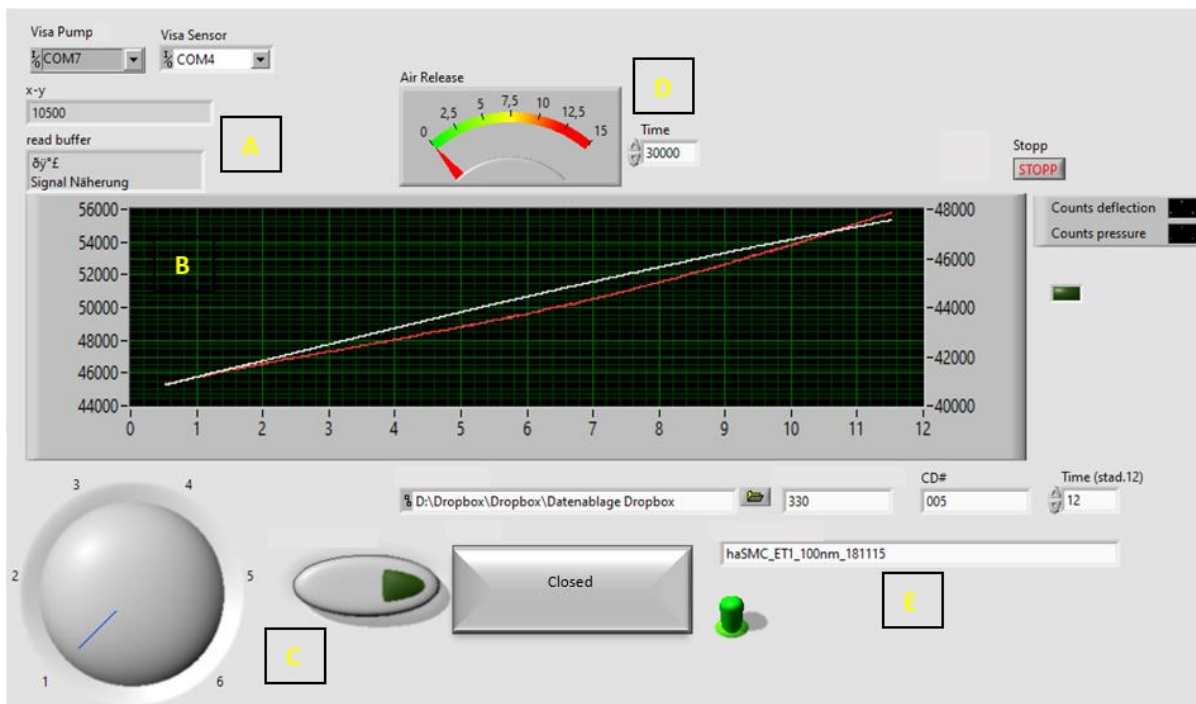


Figure 12 Interface of the measurement software. (A) Configuration of serial communication between TTA and computer. (B) Real-time monitoring of data acquisition. (C) Controlpanel to select sample chamber and control valves. (D) Timeout control and indicator enables automated pressure equilibration between the measurements. (E) Datafile configuration and save options.

The data analyzation software requires high computational performance[Figure 13]. Therefore, the software was written as a standalone program. The operator needs to choose the folder of desired

measurements and software proceeds the analyzation automatically. All comprehensive steps are visualized to enable a follow up of the data processing.

To calculate the mechanical tension, pressure and deflection data are merged. The Levenberg–Marquardt algorithm is used for the curve fitting. The inflection point of the fitted plot is used to apply and calculate in the mathematical model for stress evaluation. All data are collected and saved into an array that can be exported.

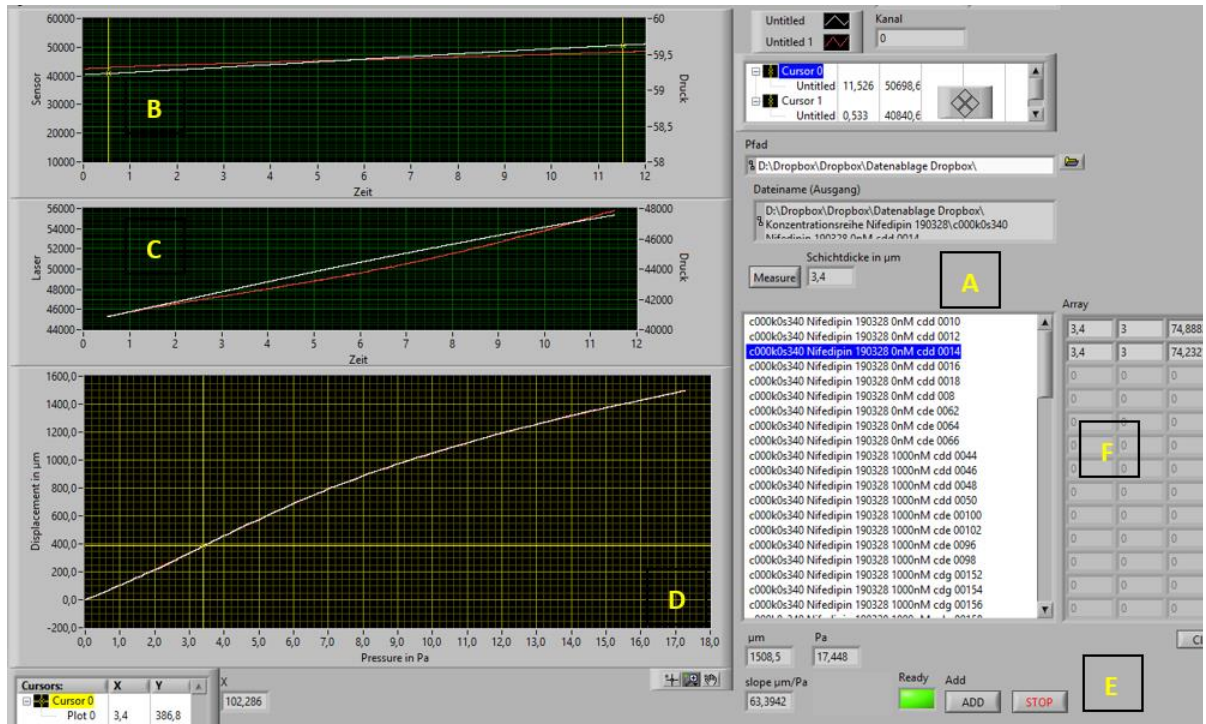


Figure 13 Interface of the analysis software. In (A) all data of the selected file path are listed. The file selected in (A) is opened in (B) where the data can be trimmed. The default settings for the analysis range is the time interval 0.5s-11.5s. The data is cut out and displayed in (C). Both data series are merged and the deflection over the pressure course is displayed in white. (D) also represents the best non-linear adaptation in red. The resulting data is presented in (E) and can be buffered in (F) using ADD.

5.4. Physical Model

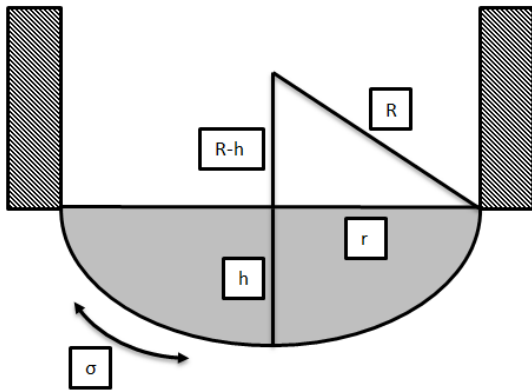


Figure 14 Key figure for the CellDrum physical model with CellDrum fitted Barlow's formula to derive the cellular tension from recorded pressure deflection curves. *r*) Radius of the CellDrum (16mm). *h*) Indicates the deflection of the CellDrum membrane to the baseline (in μm). *R*) Radius of the theoretical hemisphere. The formula is used to derive the tension from the recorded pressure deflection curves. σ) Calculated axial stress (N/m^2). *p*) measured pressure (in Pa). *s*) CellDrum membrane thickness (in μm).[124]

The calculation of the mechanical stress the CellDrum membrane and is based on the Barlow formula [Figure 15]. In the particular case assumed here, the silicone membrane is deflected by the medium to an idealized spherical cartilage. Thus it is possible to calculate the tangential stress of the membrane by using the Barlow formula from the ratio of the spherical cap radius of the pressure difference and the layer thickness.

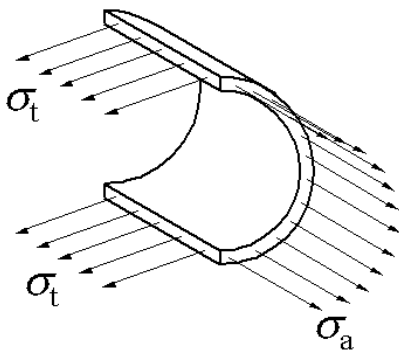


Figure 15 The starting point of the mathematical model is the Barlow formula, which allows calculating the stress distribution in thin-walled boilers. For the calculation of the mechanical stress within the CellDrum membrane the calculation of the tangential stress σ_T is necessary. The formula for calculating a hemisphere is shown below the drawing

$$\sigma_T = \frac{p * R}{2 * s}$$

Considering the special case that the membrane behaves similar to a spherical carotte, the radius of the spherical carotte can be described with the theorem of Pythagoras.

Formula 2 Adaptation to the correlation of pressure and deflection using the Pythagoras Theorem.

$$R^2 = (R - h)^2 * r^2$$

$$R^2 = R^2 - 2Rh + h^2 + r^2$$

$$2Rh = h^2 + r^2$$

$$R = \frac{1}{2h} * (h^2 + r^2)$$

$$R = \frac{r^2}{2h} * \left(1 + \frac{h^2}{r^2}\right)$$

By combining the formula 2 and formula 1, the tangential stress of a ball cartilage is obtained as a function of pressure and deflection.

Formula 3

$$\sigma_{TP} = \frac{p}{h} * \frac{r^2}{4s} * \left(1 + \frac{h^2}{r^2}\right)$$

The ration $\frac{\Delta p}{\Delta h}$ corresponds to the reciprocal value of the pressure-deflection curves inflection point-slope.

Formula 4 Adapted Barlow formula to the geometry of the CellDrum, which is used to evaluate the mechanical stress change due to tangentially induced cell forces.

$$\sigma_{TP} = \frac{\Delta p}{\Delta h} * \frac{r^2}{4s} * \left(1 + \frac{h^2}{r^2}\right) = kPa$$

Formula 5 Conversion of the measured mechanical stress into force (N), with an calculative example of 5% tension deviation.

$$F = \sigma_{TP} * d * S$$

$$F = \Delta\sigma_{5\%} * 16mm * 4\mu m = 160\mu N$$

5.5. General Biomechanics

In terms of protocol standardization as well as proof of concept, the very first measurement correlated the number of seeded cells to the resulting biomechanical stress. Therefore, CellDrums were prepared as usual and measured after fibronectin coating. Afterward, the CellDrums were cultured with different cell densities. haSMC with 2.5×10^4 , 5×10^4 , 1×10^5 , 1.5×10^5 and 2×10^5 cells per CellDrum. As haECs are smaller in size, a higher amount of cells were seeded, 5×10^4 , 1×10^5 , 2×10^5 and 3×10^5 . The specimens were acclimated and incubated for seven days under cell culture conditions. On day eight, the specimens were measured again and the results before and after cell seeding were compared. The difference and optical appearance were key results to define the developed vascular mode.

Also, the dependency between temperature and stress alteration was determined. Therefore, the cultivation media was entirely replaced by previously chilled media (4°C). Temperature and biomechanics were measured every 45 seconds and compared. This experiment was meant to examine the temperature sensitivity and impact on the cells.

5.6. Cell Culture

5.6.1. Human Aortic Smooth Muscle Cells

Primary haSMCs (ThermoFisher) were used and cultured in growth media [Figure 16 A]. For cell proliferation, the haSMCs were cultured in T75 flasks until they reached a confluence level of ~80-85%. Afterward, growth factors and supplements are changed to induce cellular differentiation. From this point on, the cells are kept in a cell culture flask for another eight days to establish a complete cellular differentiation. As the cells reached their final differentiation stage, the proliferation is stopped and the maximum capacity of contractility is developed. Due to quiescent, it is ensured that the biomechanical measurements are not affected by either proliferation or cell migration. Subsequently, the cells were passaged to the CellDrums. For maintaining the Cells within the T-flasks and CellDrums, the medium was changed every second day and was kept at a temperature of 37°C and 5% CO₂ atmosphere.

For passaging, the cells were washed with magnesium and calcium-free phosphate-buffered solution (PBS) once. The addition of 0,05% Trypsin detached the cells. To inhibit the trypsin, media with a high content (10%) of Fetal Bovine Serum (FBS) was added. To remove the trypsin from the cell suspension, the sample was centrifuged with 280g for four minutes. After centrifugation, a cell pellet has formed and the supernatant needs to be removed by the suction pump. Subsequently, the cells were resuspended in 1ml of cultivation media. The cells were counted and checked for their viability with trypan blue staining by an automated cell counter (TC 20 -Biorad).

For plating the cell to another flask, the cell suspension was filled up with an appropriate amount of media to split the cell suspension even to the number of culture flasks (min. 2500cell/cm²).

To passage the cells to CellDrums, differentiated haSMC's were seeded in a density of 75.000 cells/cm² to the previous surface-functionalized CellDrum membranes. Twenty-four hours after seeding the cells were resupplied by fresh media containing 1% fibronectin to enhance mechanical durability for external mechanical stimulation.

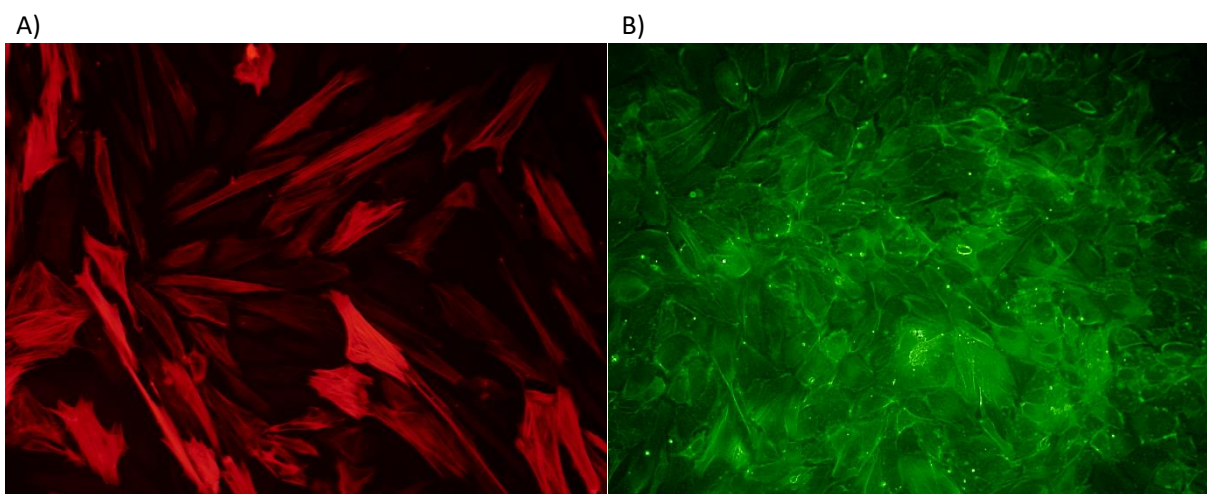


Figure 16 A) haSMC in cultivated on slides. Fixed and stained smooth muscle cell-alpha-actin. B) haEC grown on slides. Fixed and CD31 antibody stained.

5.6.2. Human Aortic Endothelial Cells

Primary haECs (Thermofisher) were cultured in basal media with low serum growth supplements [Figure 16 B]. The cultivation of these cells required an additional collagen type I coating of the T-Flasks. To maintain the cells, they were kept at the same incubator conditions as the haSMCs and media was changed every second day as well. As the cells are reaching a confluence level of 100%, cell proliferation is inhibited. The passaging procedure is executed as described by the haSMCs. Seeding haECs to the CellDrums requires 200.000cells/cm² to achieve an entire cell monolayer.

5.6.3. Co-Cultures

Co-Cultures describe cell cultures consisting of more than one type of cell. The co-culture of cells allow to the evaluation of cellular communications and the analysis of cell coupled phenomena. Various approaches are used for the mutual cultivation of different cell types, depending on the scientific question and systematic setup[105,130].

5.6.3.1. Conditioned Co-Culture

For conditioned co-culturing, the cells are physically separated from each other and do not have direct access to each other [Figure 17 a]. This kind of co-culture was supposed to give information if the media taken from endothelial cells contains vasoactive substances, which either lead to a contraction or relaxation of haSMCs. The conditioned medium was collected from CellDrums seeded with endothelial cells. As a control, fresh medium was used to see if the components of the media might lead to biomechanical deviations.

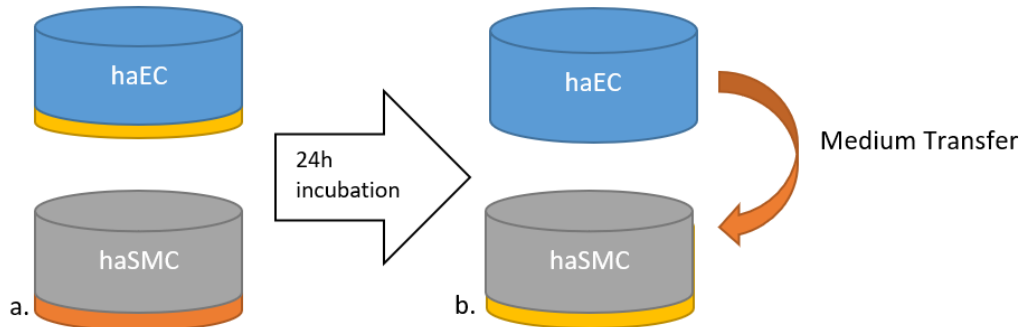


Figure 17 Drawing of the conditioned co-culture. Conditioning was carried out inside the CellDrums with 150.000 haSMCs and 200.000 haECs a.) Cells were cultivated in separate cell culture vessels with the cytospecific media. b) After 24h the medium of the haSMCs is removed and then replaced by the medium of the haEC.

For evaluation, haSMCs were cultured on CellDrums, as written in the SOP (Standard Operation Procedure). The conditioned medium was analyzed as like as the pharmacological substances, except 500µl of the medium was changed [Figure 17 b]. Afterward, a series of measurements were carried out over a time progression of ~30min.

5.6.3.2. Direct Co-Culture

In contrast to indirect, the direct co-cultivation of cells enables direct cell contact and bi-directional exchange of cell signals and secreted cell metabolites.

Media composition plays a crucial role in the co-cultivation of different cells. Each media contains specific ingredients to provide certain cellular characteristics. While the endothelial cells are maintained in a low serum basal medium, the haSMC cultivation requires a proliferative and differentiation media. EC proliferation is contact inhibited, which means that the proliferation is stopped as soon as the cells reach 100% confluency. In contrast, haSMC proliferation is stopped as they reach their contractile phenotype. These quiescent proliferation states benefit the measurement conditions for the biomechanical evaluation.

In search of an appropriate medium blend that provides high viability while maintaining cell-specific characteristics and quiescent proliferation behavior, various media compositions were tested. Commonly used basal medium was combined with essential supplements listed in Table 4. Viability parameters via proliferation curves and trypan blue viability tests were generated to evaluate the blended medium effects.

Additionally, the cells were observed via phase-contrast microscopy over 14 days of culture in different media. Afterward, the cells were stained by cell-specific antibodies, alpha Actin (haSMCs) and CD31 (haEC) to prove that the cells did not dedifferentiate.

After a series of trials, the cells were cultured in M199 basal media with 1% FBS, 30µg/ml Heparin and 10ng/ml hEGF most successfully.

Table 4 Overview of media additives and growth factors

haEC Supplements	haSMC proliferation supplements	haSMC differentiation supplements
<ul style="list-style-type: none"> - 2% FBS - 1µg/ml hydrocortisone - 10 ng/ml human epidermal growth factor(hEGF) - 3ng/ml basic fibroblast growth factor (bFGF) - 10µg/ml Heparin 	<ul style="list-style-type: none"> - 5% FBS - 0,5ng/ml hEGF - 2ng/ml bFGF - 2µg/ml Insulin 	<ul style="list-style-type: none"> - 1% FBS - 30µg/ml Heparin

Table 5 Overview of media additives and growth factors effects on haSMCs and haECs respectively

Component	EC	SMC
FBS	<ul style="list-style-type: none"> - Amplify cell growth - Contains growth and adhesion factors 	<ul style="list-style-type: none"> - Amplify cell growth - Contains growth and adhesion factors
Heparin	<ul style="list-style-type: none"> - ECs degrade high-molecular-weight heparin fragments into low-molecular-weight fragments - ECs produce heparan sulfate[131] - Inhibits FGF dependent proliferation 	<ul style="list-style-type: none"> - Antiproliferative effect of low weight Heparin - Inhibits thymidine and uridine uptake - Blocks SMC in the G0/G1 state[132]
bFGF	<ul style="list-style-type: none"> - Mitogen → support cell growth - Induces cell division in vitro, Angiogenesis in vivo[133] - FGF localized in the ECM bound to heparin-like glycosaminoglycans 	<ul style="list-style-type: none"> - Binds to specific receptors on the surface of SMCs - Leads to Initiation of DNA synthesis - Mitogen[131] - bFGF can be displaced from extracellular matrix binding sites by heparin[134]
EGF	<ul style="list-style-type: none"> - Promote endothelial cell growth, migration and survival[135] - Mitogen 	<ul style="list-style-type: none"> - Associated with changes in cation movements like calcium - Stimulates proliferation of these cells in vitro - Mitogen[136]

5.6.3.3. 3D Co-Culture

The three-dimensional co-culture can as well be described as a direct co-culture but with a specific cell arrangement. The overall aim of the study is to establish a vascular wall like cell culture model. Therefore, the cells should be arranged like in vivo system. The setup of this model intends to have a base layer of haSMC with haEC on top[Figure 18]. As the arrangement is build up in a sandwich arrangement, an appropriate number of cells can be used.

150.000 haSMCs were seeded to previously functionalized CellDrums. After 24 hours, SMCs were covered with a 1% fibronectin media solution. On day seven, cultivation media was supplemented by 1% Collagen Type IV. The next day, 200.000 haECs were seeded on top of the haSMC monolayer.

For an even cell distribution, the media volume was raised from 300µl to 500µl over two days. After another five days, the samples were ready for analysis and testing. Additionally, staining with different CellTrackers was carried out.

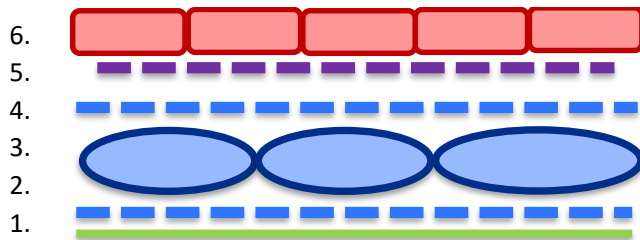


Figure 18 Graphic illustration of the planned three-dimensional co-culture model consisting of smooth muscle cells and endothelial cells. 1) CellDrum membrane 2) Fibronectin coating 3) haSMC monolayer 4) Fibronectin coating 5th) collagen type IV coating 6) haEC monolayer

5.6.4. Vitality Test

Cell viability and amount were observed with various methods.

Microscopic observation allows quick and subjective viability control. Especially for the fast control of CellDrum models, to ensure no monolayer rupture and cell detachment in large areas.

For general cell cultivation and passaging, cell amount and viability was checked by trypan blue staining and an automated cell counter by BioRad (TC20™ Biorad). This procedure was always carried out for experimental preparation and CellDrum plating.

Additionally, the cells were stained by a LIVE/DEAD assay (Thermofisher) [Figure 19]. The kit bases on two components staining with calcein AM and ethidium homodimer-1, allowing distinguishing optically between viable and damaged cells. This method was mainly used to create the SOP of mechanical stimulation. It allowed fast and precise evaluation of the viability of cells and also visualized cells that have taken damage but were still attached to the membrane.

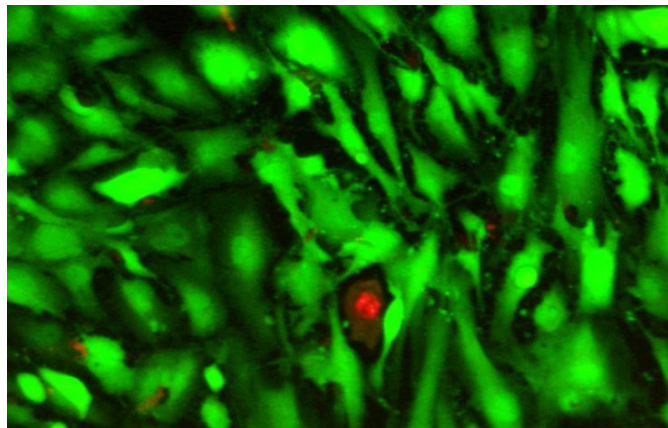


Figure 19 Representative live/dead staining of haSMC monolayer on CellDrum. For functional testing, cell lesions were induced by excessive mechanical stress. Intact cells are displayed in green and damaged cells in red fluorescence[124].

Long-time observation, especially during mechanical stimulation, an L-lactatdehydrogenase (LDH) screening, was used to record a time profile of the LDH secretion within the media. LDH is leaked by dead and damaged cells. The amount of LDH can be followed by removing 50µl of media, which can later be on photometrically screened.

5.6.5. Microscopic Analysis

For cell culture purposes, a phase-contrast microscope was used to monitor cellular viability, attachment, confluency and especially for haSMC state of differentiation. Due to the high transparency of the PDMS CellDrum membrane, it was even possible to check the cell models for ruptures and homogeneity.

For fluorescent imaging, a BZ-8100 by Keyence was used. It was used in the experimental setups, which are described in chapters 5.11 and 5.6.4.

For visualization of haSMCs and haECs in monocultures, Phalloidin 488 and DAPI were used. Phalloidin 488 is specifically binding on f-Actin structures. Aside from the display, this dye was also used for the CMI evaluation 5.11. DAPI exclusively binds to the cell nucleus. Staining with Phalloidin 488 / DAPI was carried out as follows:

Remove medium and washout for three times with PBS. For fixation, 4% Formaldehyde diluted in deionized water was added. Incubate for 5 min at room temperature. Afterward, two washing steps with PBS. Membrane permeabilization was made possible by a 0,1% Triton X solution, which was incubated for 5 min at room temperature. Subsequently, two washing steps were followed. Phalloidin 488 stock solution was dissolved in 1,5ml, 100% methanol and stored at -20°C. Phalloidin 488 1:40 and DAPI 1:100 working solution was prepared with PBS. The working solution was added to the cells and incubated for 35 min, protected from light at room temperature. After the incubation time, the sample was rinsed for at least three times with PBS to remove residual dye particles. The specimen was ready to be observed.

For distinguishing different cell types in co-culture, an antibody linked fluorescent dyes were used. Anti-Actin, α -Smooth Muscle - Cy3™ antibody, Mouse monoclonal antibodies bind to contractile actin structures, which are exclusively present in the haSMCs. To indicate haECs cells mouse monoclonal[JC/70A] to CD31 (Alexa Fluor® 488) was used. These antibodies bind only to membrane structures of the endothelial cells.

Staining with α -Smooth Muscle - Cy3™ antibody and Mouse monoclonal[JC/70A] to CD31 were carried out as followed:

Antibody staining requires the same fixation as a permeabilization procedure as described before. After permeabilization and washing steps, 3% BSA was added and incubated for 1h at room temperature. Afterward, the antibodies are diluted 1:200 with PBS and added to the samples. Incubation has been carried out overnight at 4°C. The sample was washed at least three times with PBS. The samples are ready for use or for optional double staining.

5.7. Pharmacological Testing

The evaluation of pharmacological agents is the essential measurement of this thesis. These measurements were carried out as proof of concept, to ensure the functionality of the system and also to establish the physiological *in-vitro* cell model.

For the biomechanical investigation, six CellDrums per test group were prepared and an additional number of six CellDrums were used for each control group. During the measurements, the CellDrums were kept in the Tissue Tension Analyzer socket, which prevents undesired shaking or temperature drop. The test substances were applied through a hole of the apparatus cap from above. Before the measurements, six successive measurements were carried out, purposing the normalization of each CellDrum and to describe the initial tension of the cells.

The TTA system allows various measurement protocols. To determine the most suitable one, we have tested three different analysis modes: the "particular time mode" (PTM), the "long term mode" (LTM) and the "real-time mode" (RTM)[124].

The LTM describes the recording of a serial measurement, which is observed on the biomechanical effect of a sample for at least 25 minutes. This mode was used and established for testing new

substances in order to test the vasoactive effect of the test substances and to resolve it in time roughly. This mode was used for single test substances as well as for substance combinations.

The PTM compares the biomechanical tension between five measurements per sample before and after substance application. The incubation time between the two measuring points can be adapted to the respective test substance. In most cases, an incubation time of five minutes was chosen, except for norepinephrine measurements (1 min), during which the sample was left alone. This mode has been used to record dose-response curves and to detect load variations by mechanical stimulation [124].

The RTM focused exclusively on the precise observation of membrane deflection without monitoring the generated pressure deviation. This mode is only suitable for concentric muscle contraction so that isometric contraction remains undetected. In this mode, the membrane deflection is monitored at a sampling rate of 1 kHz to make the membrane movement visible in the nanometer range. This measurement was only used in this study as proof of principle.

In accordance with the scientific problem and task definition, we have referred exclusively to the two analysis modes in this work: PTM and LTM

All substances were kept as a stock solution of 10mM at -80°C. Immediately before the measurements, the stock solutions were diluted to the final concentrations and acclimated to 37°C in the water bath. For the addition of substances, 50µl of media was removed and replaced by the agent, so the media reached the final concentrations.

All control groups were only exposed to the corresponding solvent of the agent DMSO or ultrapure water.

The contraction of muscle cells depends on the presence of Ca²⁺ ions. For that reason, the first measurements focused on L-type Ca²⁺ channel modulators, regulating the ion influx of Ca²⁺. In this thesis, we evaluated Bay K8644 as a Ca²⁺ channel agonist and Verapamil and Nifedipine as Ca²⁺ channel antagonists.

Table 6 L-Type Ca²⁺-channel modulators

Agent	Concentration in nM	Results	Literature
BayK 8644	1; 10; 50; 100; 1000	6.2.1; 6.2.6; 6.3	[137–139]
Verapamil	1; 10; 50; 100; 1000	6.2.1; 6.2.6; 6.3	[140–142]
Nifedipine	1; 10; 50; 100; 1000	6.2.1; 6.2.6; 6.3	[138,143]

K⁺ dependent vasoactivity was tested with a KCl, Diazoxid, Calcitonin Gene related peptide (CGRP) and Glibenclamide. According to the literature, CGRP and Glibenclamide are competing agents, which bind to the same ATP dependent K⁺ channel. Especially for these two agents, an experiment with blended agents was carried out, to show that the presence of Glibenclamide does affect the addition of CGRP

Table 7 K⁺ channel modulators

Agent	Concentration in µM	Results	Literature
KCl	50.000 / 50mM	6.2.2	[144–146]
Diazoxide	1	6.2.2	[147],[148]
Glibenclamide	5	6.2.2; 6.2.6	[146]
CGRP	5,2	6.2.2; 6.2.6	[146,148,149]

The release of nitric oxide is one crucial vasodilation mechanism in the in-vivo system, most commonly derived from the intima endothelial cells (eNOs). To simulate the presence of endothelial cells and the natural release of NO, two NO donators were analyzed. NO groups are attached to molecular

complexes, which are released over time. Here we used Spermine-NO-Complex and Diethylammonium NONOate.

Table 8 Nitric oxide donators

Agent	Concentration in nM	Results	Literature
Spermine-NO-complex	0,1; 1; 10; 100; 1000; 5000	6.2.3; 6.2.6	[150]
DEA NONOate	1000	6.2.3	[150,151]

In-vivo, the body's vasoactive substances are permanently secreted to maintain homeostasis of blood pressure. The secretion of these messenger substances varies according to physical requirements or situations. We have placed particular emphasis on the two most potent vasoactive messengers, ET1 and AT2. In addition, we investigated the effect of NE and acetylcholine, which are mediated by the autonomic nervous system.

Table 9 Biological vasoconstrictors and catecholamines

Agent	Concentration in nM	Results	Literature
Norepinephrine	0,1; 1; 10; 100; 1000;	6.2.4;6.2.7;6.3	[152]
Angiotensin II	0,1	6.2.4	[26,73,153]
Endothelin I	0,1	6.2.4; 6.2.7;6.3;6.4	[26]
Acetylcholine	1	6.2.4	[152,154]

In a last series of experiments, we tested known examples with vasoactive effect. Among these were the impact of caffeine and sildenafil, which is known for its potency-enhancing effect. Furthermore, cytochalasin-D was applied to investigate the complete deactivation of the myosin actin complex and experimentally, the spider venom GsMTx4 affecting stretch-activated Ca²⁺ channels.

Table 10 PDE5 inhibitor

Agent	Concentration in μM	Results	Literature
Sildenafil	1	6.2.6	[155]

Table 11 List of stimulants and toxins

Agent	Concentration in μM	Results	Literature
Caffeine	1	6.2.6	[156]
Cytochalasin D	0,1	6.2.6	[157]
GsMTx4	0,25	6.2.6	[158,159]

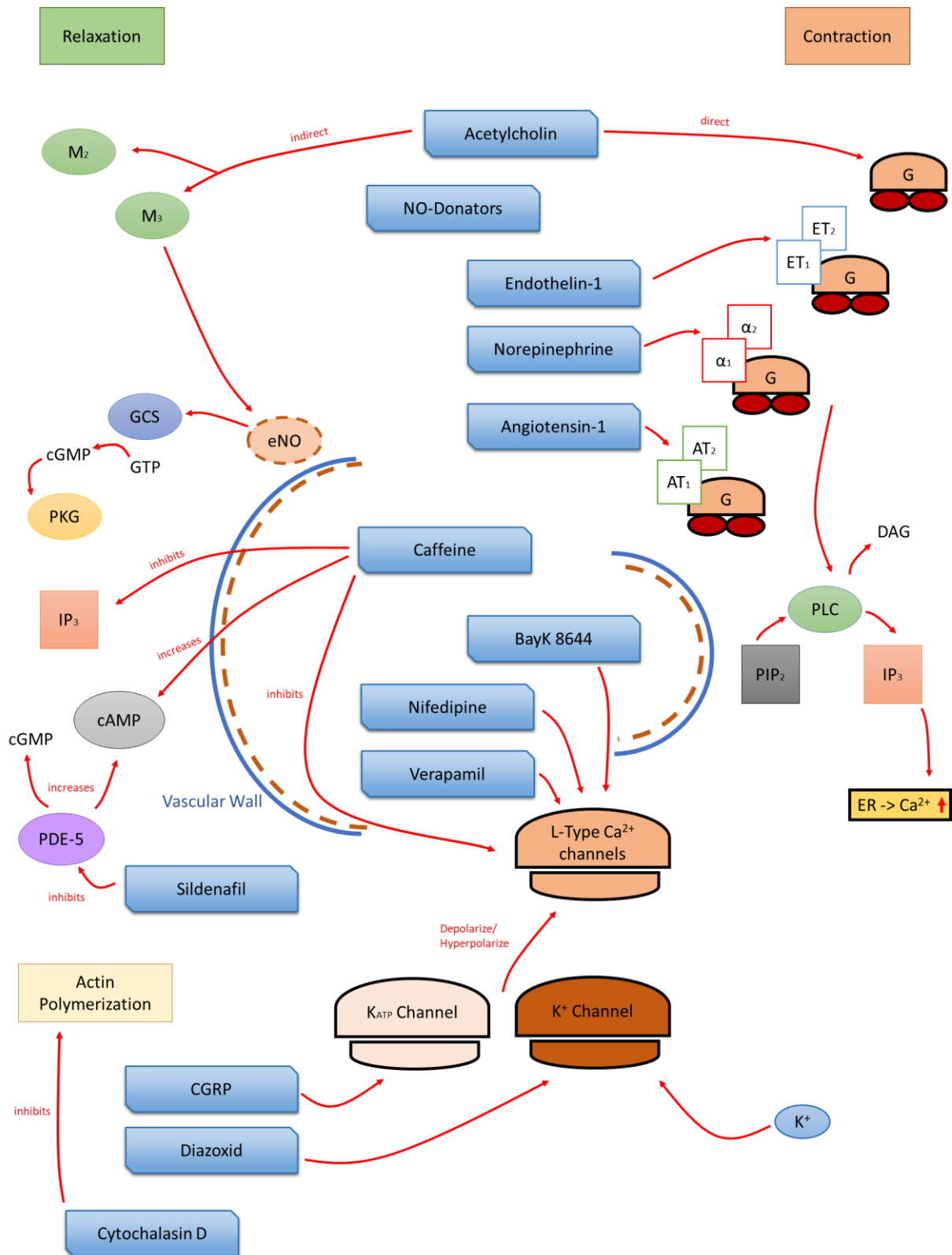


Figure 20 Overview of the vasoactive mechanisms of action of all substances used in this study. cAMP(cyclic adenosine monophosphate); cGMP (cyclic guanosine monophosphat); DAG (1,2-Diaglycerol); ER (endoplasmatic reticulum); GC-S (Guanincyclase-S); G-Protein; GTP (guanintriphosphate); IP3 (Inositol-1,4,5-triphosphate); M2,M3 (Muscarinreceptor 2,3); PDE-5 (phosphodiesterase type 5); PIP2 (phosphate idyilonositol-4,5-biphosphate); PKG (Proteinkinase G); PLC (Phospholipase C).

5.8. Blood Sera Screening

5.8.1. Blood Collection and Sera Extraction

The investigations of the biomechanical effect of blood sera were carried out in a self-experiment. The blood sera required for the analysis were taken and prepared by Mr. Robin Bayer under medical supervision.

Blood sera were taken from male 30 years old healthy donor. The subject carried out two exercise ECG tests. Fresh blood was taken from the donor as control right before the first exercise ECG test. The ECG test was carried out until the subject was wholly exhausted. Afterward, another 15 ml of fresh blood was donated.

After a break of 20 minutes, the ECG stress test was repeated. Fifteen minutes before the second ECG test, a mixture of arginine (3,3g) and citrulline(3,3g) was administrated to the proband. Citrulline and arginine are amino acids used in supplementation food to increase physique energy levels. Both substances increase the overall blood flow by vasodilation. Afterward, the second exercise ECG was started, with subsequent blood donation (15ml). This experiment was repeated on three consecutive days.

For transport, the sera were kept at a temperature of $\sim 4^{\circ}\text{C}$ in special blood sera tubes. To separate the sera from the full blood sample, the tubes were centrifuged with 1000g for 10 minutes.

5.8.2. Blood Sera Analysis

The blood sera were handled as the pharmacological substances in chapter 5.7. The sera were warmed up to 37° in a water bath just before the measurement starts. Subsequently, 500 μl of sera was applied to the CellDrums. Afterward, a time progression curve of 20 minutes was recorded (LTM).

For the evaluation, four groups of each three CellDrums have been prepared: Control (media only), serum control (before exercise), stimulated serum (after exercise) and supplemented serum (after exercise and nutritional supplementation).

5.9. PulSElect

The PulSElect system was developed to stimulate CellDrum models with customized pressure pulses mechanically[122,123]. Deformations of the CellDrum membrane by pulsatile pressure waves cause cellular stretching and compression of the cells attached to the membranes[Figure 21]. The system is composed of a pressure generator, a control unit and a sample socket.

The pressure generator is build up by an eight-inch speaker, which is driven by an Arduino self-engineered frequency generator, offering a defined wave signal and frequency. The pulse wave shape can be programmed via a LabVIEW software, enabling to customize the pulse waves to any desired wave shape.

For exclusively cellular elongation, a negative Gaussian bell-shaped pressure curve was created. Also, resting phases between the stimulation phases have been implemented, in which the cells expire no additional stress. The sample socket allows to stimulate twelve CellDrum at once and can be situated entirely in an incubator. Via a valve array, the mechanical stimulation can be turned on or off. A remote control was designed, allowing access to the valves from outside of the incubator. Even more, a display allows supplying the operator with necessary information and data plots. The detailed engineering and characterization of the PulSElect system are documented in the master thesis of Till Creutz[123].

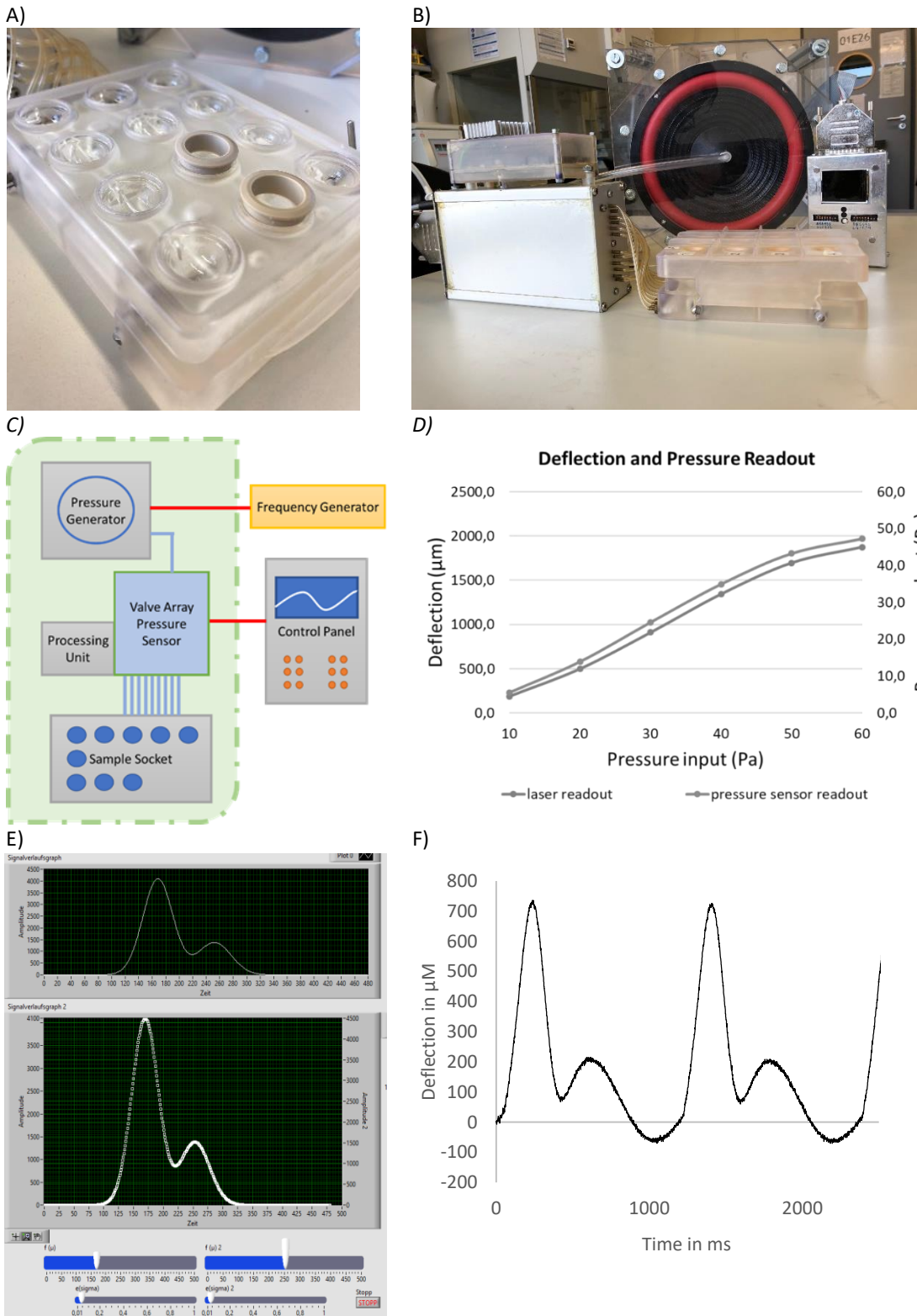


Figure 21 A) PulSElect sample sockets for the mechanical stimulation of twelve CellDrums. A printed component made of clear resin with a FormLabs 2 3D printer B) Compilation of all components of the PulSElect system C) Sketch of the individual components of the PulSElect system and arrangement in operation. The green box indicates the incubator, including all parts which can be placed in the incubator during mechanical stimulation D) Calibration of the PulSElect system. The deflection is plotted against the increasing pressure applied to the system. The pressure is measured directly below the CellDrums, which is displayed in the second Y-axis[123]E) Software for creating user-defined pressure waves. The waveform can be generated from two Gaussian functions using the controllers. The data is then transposed into the appropriate data format to be compiled on the microcontroller. F) Real-time recording of the waveform created in Figure 21 E. The measurement was recorded using laser-assisted TTA at a sample rate of 1kHz[122].

5.10. Stimulation Protocol

The stimulation protocol describes the cell cultivation and mechanical stimulation routine for all experiments in which we exposed cells to mechanical stress.

Differentiated haSMC cells were seeded to functionalized CellDrums, which is described in more detail in chapter 5.6.1.

To define an appropriate dose and interval duration of mechanical stress, a series of experiments has been done. The main criteria were to prevent cellular detachment and to induce a measurable cellular response. The cellular viability was followed by an LDH assay and microscopic observation, as described in chapter 5.6.4. To determine a cellular response to the applied mechanical stress, the change of cytoskeletal structure arrangement by the cell morphology index (CMI) described in chapter 5.11 was observed.

For all experiments related to mechanical stimulation, a negative Gaussian-shaped pulse wave has been generated with a frequency of 2Hz. By choosing negatively directed pressure waves, we were dealing with cellular stretching exclusively. Furthermore, the cellular stimulation does have a few milliseconds of the resting phase, in which the cells are in their initial state. The stimulation rate refers to a heartbeat rate of 120 bpm [Figure 232].

Due to the calibration of the system, we are aware of the cellular stretch according to the applied pressure. The SOP was carried out with -40Pa, which equals a deflection of around 1,3mm and 1,5-1,6% strain.

A crucial stimulation parameter is the applied stress duration. The longer the mechanical stress duration, the higher the risk of monolayer ruptures. From our experimental results, we decided to stimulate the cells two times per day for 30 min each with at least 4 hours resting phase. With this stimulation characteristics, it was possible to measure intact cells over a period of five days. Proofing the specimen viability, the CellDrums were checked for cellular ruptures microscopically after each training. In between the stimulation periods, the cells were kept in the incubator under cell culture conditions. The cell medium was changed after every mechanical stimulation routine.

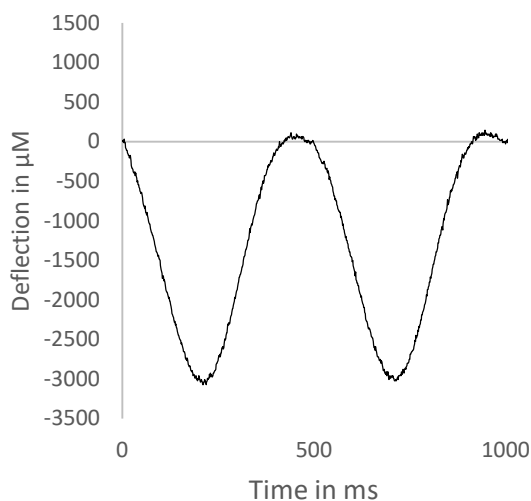


Figure 22 Real-time recording of the mechn stimulation SOP signal. The measurements were recorded by laser-assisted TTA with a sampling rate of 1kHz.

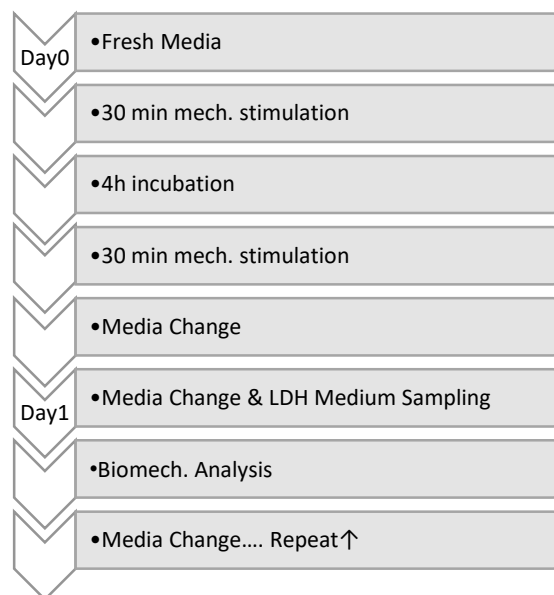


Figure 23 Flowchart of the stimulation SOP represented on a daily cycle.

5.11. Cell Morphology Index (CMI)

The Cell Morphology Index (CMI) [Figure 24]. was developed to quantify the morphological changes of cytoskeletal structures within the cells objectively[160][161]

The software was developed via LabVIEW [Linder, Goßmann & Bayer]and later on translated to Matlab by Mascha Schmitt[162].

Due to cytoskeletal fluorescence staining, the internal structures of the cell can be evaluated by angle-dependent frequency analysis. The application of the CMI was used mainly to determine the SOP for the mechanical stimulation but also to understand the biomechanical stiffening of the cell by cytoskeletal rearrangement.

To determine the CMI, 30 pictures of single cells from a single CellDrum have been taken and analyzed by the software. Each sample consisted of a sample and a control group, each consisting of three CellDrum. For data analysis, the data were pooled and evaluated.

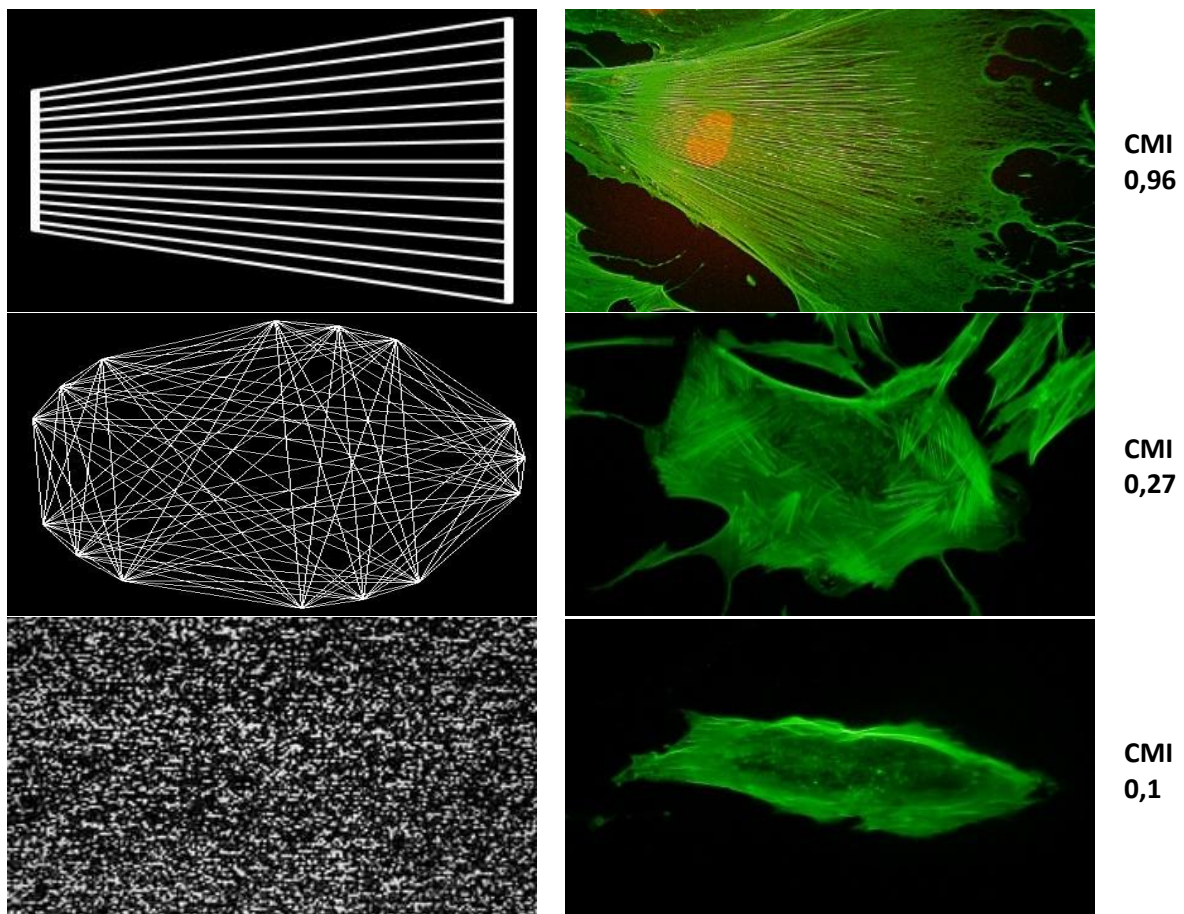


Figure 24 Explanation of the CMI analysis. Comparison of example models (left), similar cell examples (middle) and the resulting CMI value. Linear ordered structures result in a higher CMI value, whereas chaotic structures result in a CMI value close to zero.

5.12. Gene Analysis

Gene analysis describes techniques to quantify potential cellular regulatory mechanisms on the transcriptomic level. Due to this work, the collected data should support the validity of the biomechanical measurements and enlighten the reasons for measured mechanical changes.

5.12.1. Microarray Analysis

Microarray analysis is a method for the complete analysis of the transcriptional level of the cell. The study was performed by the Gene Expression Affymetrix Facility of the Center for Molecular Medicine Cologne (CMMC).

For the analysis, the complete RNA of the cell was obtained using the miRNA kit of Qiagen. The isolation was performed according to the manufacturer's instructions. The technical requirement for successful transcriptome analysis was 2µg/20µl total RNA necessary with A260/A280 ratio >1.8 and A260/A230 >2.0. The quantity and purity of RNA were determined by photometric analysis first and later on checked again by the CMMC Affymetrix core facility via nanodrop technology. Transportation was done on dry ice around -80°C.

The samples were analyzed by Clariom™ S Assays and an Affymetrix System. The focus on this part of the study was to elucidate the cellular stress management and support the collected data from mechanical stimulation within the CellDrum system. The purpose of the whole transcriptome analysis was to determine the impact of mechanical stimulation on the full transcriptomic level.

The specimen was cultured on CellDrums and mechanically stimulated according to the SOP 5.6.1 & 5.10. Three groups each six CellDrums were prepared. Six CellDrums as control and each six CellDrum for three and five days of stimulation. All specimens of each group were pooled and analyzed.

5.12.1.1. Microarray Analysis Evaluation

Data evaluation was carried out by TAC 4.0, a freeware software for the analysis of Affymetrix generated data. The data were evaluated by cluster and heatmap analysis to show general differences in mechanobiological relevant expression profiles. Special attention was paid to the genes and similar genes that had already been evaluated by qPCR. For further interpretation, the web-based g.profiler was used to show molecular pathways of specific regulation profiles.

5.12.2. Quantitative PCR

qPCR allows quantification of the gene expression levels, respectively, to a previously determined housekeeping gene. Due to this method, it is possible to determine the quantitative gene expression of target genes. For this gene expression analysis, we primarily focused on genes, which are directly related to structural changes, mechanosensitive and genes that are affecting the cellular contraction of smooth muscle cells.

The specimen proceeded like described in 5.10. The same stress profile and the number of samples were analyzed.

Description	Gene	Primer	
Glycerinaldehyd-3-phosphate-Dehydrogenase	GAPDH	Forward Primer	GGAGCGAGATCCCTCCAAAAT
		Backward Primer	GGCTGTTGTCATACTTCTCATGG

Table 12 Housekeeping Gene

Description	Gene	Primer	
beta Actin	ACTB	Forward Primer	GTCTGCCTTGGTAGTGGATAATG
		Backward Primer	TCGAGGACGCCCTATCATGG
Tropomodulin 4	TMOD4	Forward Primer	CCCAAATCCCACAAACATTGAGG
		Backward Primer	ACAGCTCACTTAGCATGGGTATT
Filamin A	FLNA	Forward Primer	CTTATCGCGCTGTTGGAGGT
		Backward Primer	GCCACCGACACGTTCTCAA
Smoothelin	SMTN	Forward Primer	CCCTGGCATCCAAGCGTTT
		Backward Primer	CTCCACATCGTTCATGGACTC
Transgelin	TAGLN	Forward Primer	AGTGCAGTCCAAAATCGAGAAG
		Backward Primer	CTTGCTCAGAATCACGCCAT

Table 13 Genes which are associated with changes in the cytoskeleton.

Description	Gene	Primer	
CD49a	ITGA1	Forward Primer	GCTCCTCACTGTTGTTCTACG
		Backward Primer	CGGGCCGCTGAAAGTCATT
P38	MAPK14	Forward Primer	TCAGTCCATCATTATGCGAAA
		Backward Primer	AACGTCCAACAGACCAATCAC
MMP2	MMP2	Forward Primer	CGACCACAGCCAACACTACGAT
		Backward Primer	GTCAGGAGAGGCCCATAGA
MMP9	MMP9	Forward Primer	TGTACCGCTATGGTTACTCTCG
		Backward Primer	GGCAGGGACAGTTGCTTCT
JNK 1	MAPK8	Forward Primer	GGGTATGCCCAAGAGGACAGA
		Backward Primer	GTGTTGGAAAAGTGCCTGG
P4H α 1	P4HA1	Forward Primer	AGTACAGCGACAAAAGATCCAG
		Backward Primer	CTCCAACACTCACTCCACTCAGTA
P21	CDKN1A	Forward Primer	ACATCGCCAAGGAAAAACGC
		Backward Primer	GTCTGTTTCGGTACTGTCATCC

Table 14 List of mechanosensitive genes that contribute to biomechanical adaptation and cellular signal transduction

Description	Gene	Primer	
Desmin	DES	Forward Primer	GAGACCATCGCGGCTAAGAAC
		Backward Primer	GTGTAGGACTGGATCTGGTGT
Tropomyosin	TPM1	Forward Primer	GCCGACGTAGCTTCTCTGAAC
		Backward Primer	TTTGGGCTCGACTCTCAATGA
MYH11	MYH11	Forward Primer	CGCCAAGAGACTCGTCTGG
		Backward Primer	TCTTTCCCAACCGTGACCTTC
Calponin	CNN1	Forward Primer	CTGTCAGCCGAGGTTAAGAAC
		Backward Primer	GAGGCCGTCCATGAAGTTGTT
Calmodulin	CALM1	Forward Primer	TTGACTTCCCCGAATTTTTGACT
		Backward Primer	GGAATGCCTCACGGATTTCTT
α -smooth muscle actin	ACTA2	Forward Primer	AAAAGACAGCTACGTGGGTGA
		Backward Primer	GCCATGTTCTATCGGGTACTTC

Table 15 Selection of genes that are directly related to the contractile force of the cell via the contractile mechanism

In a second series, we focused on the gene expression of haSMC receptors and various ion channels, which are associated with the cellular tone, to elucidate potential increased reactivity of contraction and dilatation depending on ion channel and receptor transcription. Therefore, three groups of each twelve CellDrums have been prepared. Again, one control group and two stimulation groups. Six CellDrums were used for RNA isolation and six were used for pharmacological testing. To measure a variation in biomechanical response, we applied Bay K8644, verapamil, nifedipine and norepinephrine.

For comparable results, the cells were measured before and after drug application. As the measurements were carried out entirely after mechanical stimulation, the biomechanical changes according to the stimulation protocol are normalized.

Description	Gene	Primer	
L Type Ca ²⁺ Channel	CACNA1C	Forward Primer	GAAGCGGCAGCAATATGGGA
		Backward Primer	TTGGTGGCGTTGGAATCATCT
T Type Ca ²⁺ Channel	CACNA1G	Forward Primer	TGTCTCCGCACGGTCTGTAA
		Backward Primer	AAGCCGGTTCCAAGTGTCTC
K ⁺ ATP Channel	KCNJ1	Forward Primer	GGTCGCTTCGTCAAGAAAGAC
		Backward Primer	CACGCATGTGGTGAACAGG
Transient Receptor Potential Canonical1	TRPC1	Forward Primer	AGGATAGCCTCCGGCATTCC
		Backward Primer	TTCCACCTCCACAAGACTTAGT
IP ₃ Receptor	ITPR1	Forward Primer	GCGGAGGGATCGACAAATGG
		Backward Primer	TGGGACATAGCTTAAAGAGGCCA
Alpha-1 Adrenergic Receptor	ADRA1A	Forward Primer	CGCTACCCAACCATCGTCAC
		Backward Primer	GAACAGGGGTCCAATGGATATG
Alpha-2 Adrenergic Receptor	ADRA2A	Forward Primer	TCGTCATCATCGCCGTGTTC
		Backward Primer	AAGCCTTGCCGAAGTACCAG
Beta-2 Adrenergic Receptor	ADRB2	Forward Primer	TTGCTGGCACCCAATAGAAGC
		Backward Primer	CAGACGCTCGAACTTGGCA

Table 16 Selection of different genes that are related to the expression of receptors and ion channels responsible for cell contraction.

Gene analysis via qPCR requires to isolate and convert the specimen genomic material to cDNA. Hence, there are two necessary steps in advance to prepare an qPCR.

5.12.2.1. RNA Isolation

The RNA isolation is carried out by the RNeasy mini kit by Qiagen. This kit uses one column to isolate RNA from different types of cells.

Working with RNA is a time-critical procedure, which also requires stable low temperatures and clean surroundings. The whole extraction was carried out on crushed ice to keep the temperature as low as possible. To clean the working area from RNase, all tools and surfaces were wiped with RNaseZAP. The used disposables were Ribonucleases free certified and sterile. Besides, the material was stored in separate boxes to keep them away from potential contamination sources.

In order to keep the genomic material as unaffected as possible, the cells were directly lysed on top of the CellDrum membrane without previous trypsinization. To ensure ideal lysis, the samples were homogenized in QIshredder tubes and centrifuged for at least 3min with 8000g. Afterward, the protocol was followed as described in the kit manual.

5.12.2.2. Reverse Transcription

Subsequent isolation, the single-stranded RNA was transcribed to a double-stranded cDNA for stabilization and further procedure. For this step, the QuantiNova reverse transcription kit was used. The protocol was followed without any changes to the kit manual.

After successful transcription, the amount and purity of the yield cDNA were measured by an Eppendorf photometer. Specimen quality was determined by the photometric relation of $260/280 = 2.0 \pm 0,2$ and $260/230 = 2 \pm 0,5$. Samples showing impurities were discarded. The total amount of cDNA

was diluted to 500µg/ml with PCR grade water and evenly distributed to microtubes. Afterward, the samples were stored at -80°C till the qPCR analysis started.

5.12.2.3. qPCR Analysis

For qPCR applications, the SsoAdvanced Universal SYBR Green Supermix and the iCycler™ from Biorad were used. Preparation of the working space was performed like described before. To prevent the samples from warming, the microplate was kept on top of crushed ice. The qPCR agents were mixed to a master mix, which was prepared as followed:

Component	Volume per 20µl Reaction
SsoAdvanced universal SYBR Green supermix (2x)c	10µl
Forward and reverse primers	2µl (each)
Template	2µl

Table 17 Components of SsoAdvanced universal SYBR Green supermix

The following protocol was implemented to the I-Cycler software:

			Amplification			
System	Setting/ Mode	Polymerase Activision and DNA Denaturation	Denaturation at 98°C	Annealing/ Extension + Plate read at 60°C	Cycles	Melt-Curve Analysis
Biorad I-Cycler	Std.	30 sec at 95°C for cDNA	15 sec	10 sec	40	65-95°C increment 5 sec/step

Table 18 Biorad I-Cycler Settings

The qPCR analysis was carried out with four individual specimen batches, consisting of pooled material taken from at least five CellDrums. Additionally, two technical replicates for the qPCR was prepared. The measurement depicts the comparison of mechanically stimulated and non-stimulated cells over different periods. The used training protocol is described in chapter 5.10.

5.12.3. Endothelin-1 ELISA

To evaluate endothelial ET1 secretion due to mechanical stimulation, an ELISA ET1 Kit by Thermofisher was used to screen the media for ET1 concentration.

Two groups of each six CellDrums were prepared as a control group and an experimental group that was exposed to mechanical stress. The mechanical stimulation protocol follows the SOP described in chapter 5.10. A medium volume of 200µl was removed daily after every second stimulation interval. The sample evaluation was carried out by a Model 680 Microplate Reader by Biorad.

The samples have been pooled and technical triplicates were measured. The protocol was carried out according to the kit manual, attached to the Appendix.

6. Results

6.1. Biomechanics – Proof of Principle

The first data sets represent the results of the proof of principle measurements, which are used to verify the functionality of the fundamental procedure.

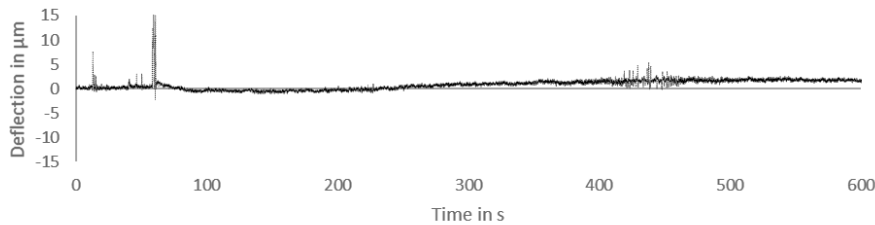


Figure 25 RTM measurement of haSMC cells treated with 100nM Bay K8644 over time. The data points represent the movement of the CellDrum membrane in μm [124]

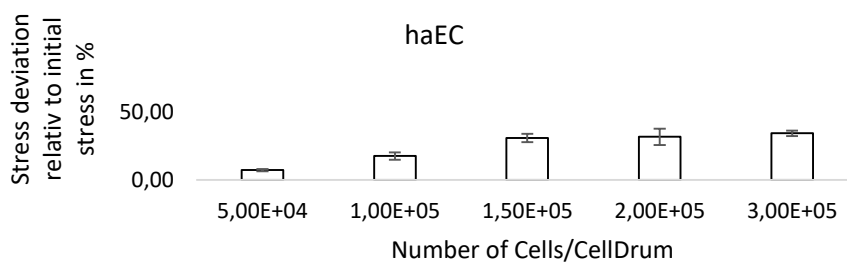
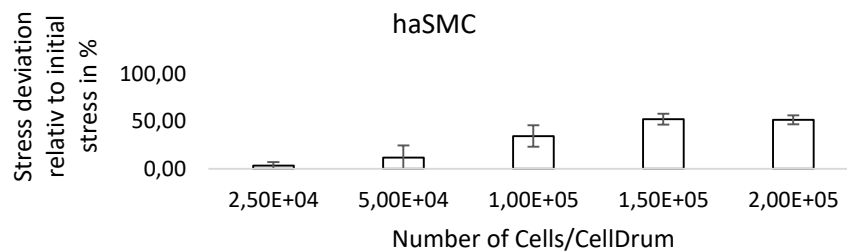


Figure 26 Cell number dependent rise of mechanical tension. Each bar represents the mean value of three individual samples. The error bars show the SEM. All measurements show the change in mechanical stress compared to non-populated CellDrum, both with smooth muscle cells and endothelial cells.

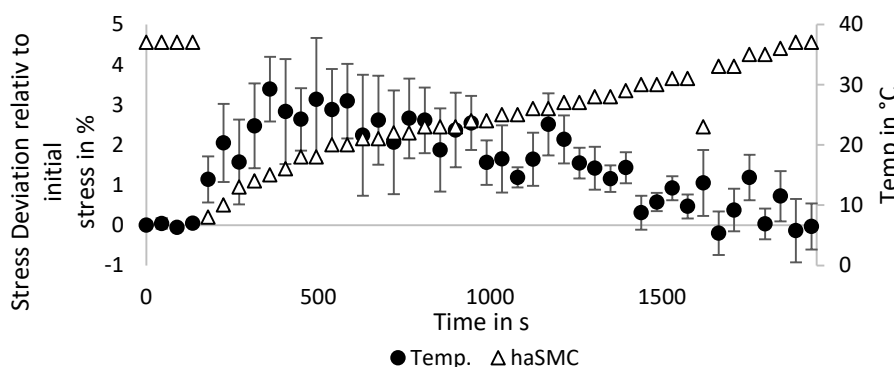


Figure 27 Temperature-dependent cell tonus measurement over time. The points represent the mean value of 6 individually measured CellDrums, each loaded with a previously chilled medium. The error bars represent the SEM.

The dependency between cell number and biomechanical stress is shown in Figure 26. CellDrums were measured with and without cells resulting in stress variation. $1,5 \times 10^5$ cells per CellDrum are required to aim for the most significant stress variation. More than $1,5 \times 10^5$ cells do not increase cellular stress further.

Regarding biomechanical properties, also $1,5 \times 10^5$ haECs are required to result in the highest stress variation. Nevertheless, much more cells could have been cultured on this space. The cellular stress does not vary with more than $1,5 \times 10^5$ cells of both cell types. Comparing both cell types, haSMC generate 20% greater cell stress.

Figure 27 shows the effect of cooling on the mechanical properties of haSMCs. The Graph represents two curves, the temperature progression and the cell stress. After replacing the culture media with previous chilled media, cellular stress increases. Whereas, when the media are reheated to incubator temperatures of 37°C, the stress level of the haSMCs went back to the initial stress level.

6.2. Pharmacology

6.2.1. Ca²⁺ Channel Modulators

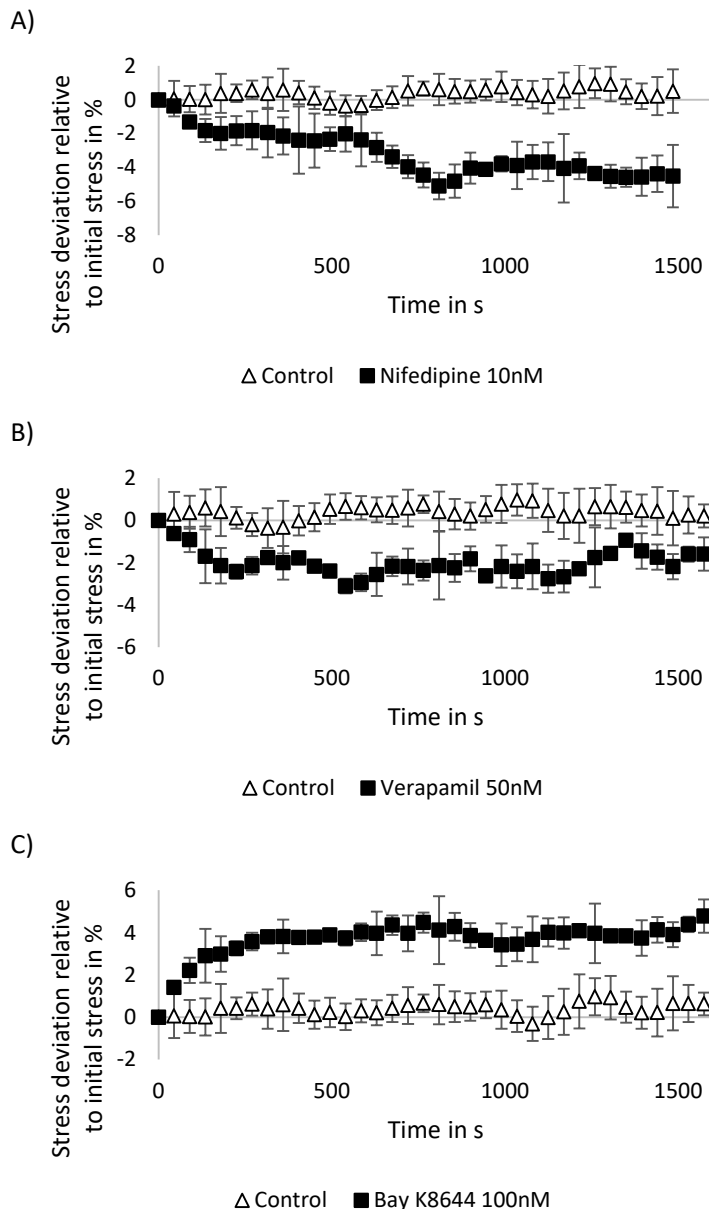


Figure 28 Time courses of L-Type Ca²⁺ channel modulators CellDrum investigation via LTM (N=6 mean ± 1 SEM). The change in the mechanical stress caused by the test substance is expressed as the relative difference of the mechanical stress (%) to the initial value. **A)** Application of 10nM nifedipine **B)** Analysis of the biomechanical effect of 50nM verapamil **C)** Biomechanical effect over time by S-Bayk8644[124]

Due to the L-Type Ca²⁺ channel blockage of verapamil and nifedipine, the cellular stress was decreased. Compared to nifedipine, the effect of Verapamil is lower by about 3%. The result of nifedipine was increased after an incubation time of 600 seconds.

Bay K8466 is a Ca²⁺ agonist, which increases the influx of Ca²⁺ ions, resulting in a cellular contraction. This measurable effect was visible directly after drug application and reached a plateau after 500 seconds.

6.2.2.K⁺ Channel Modulators

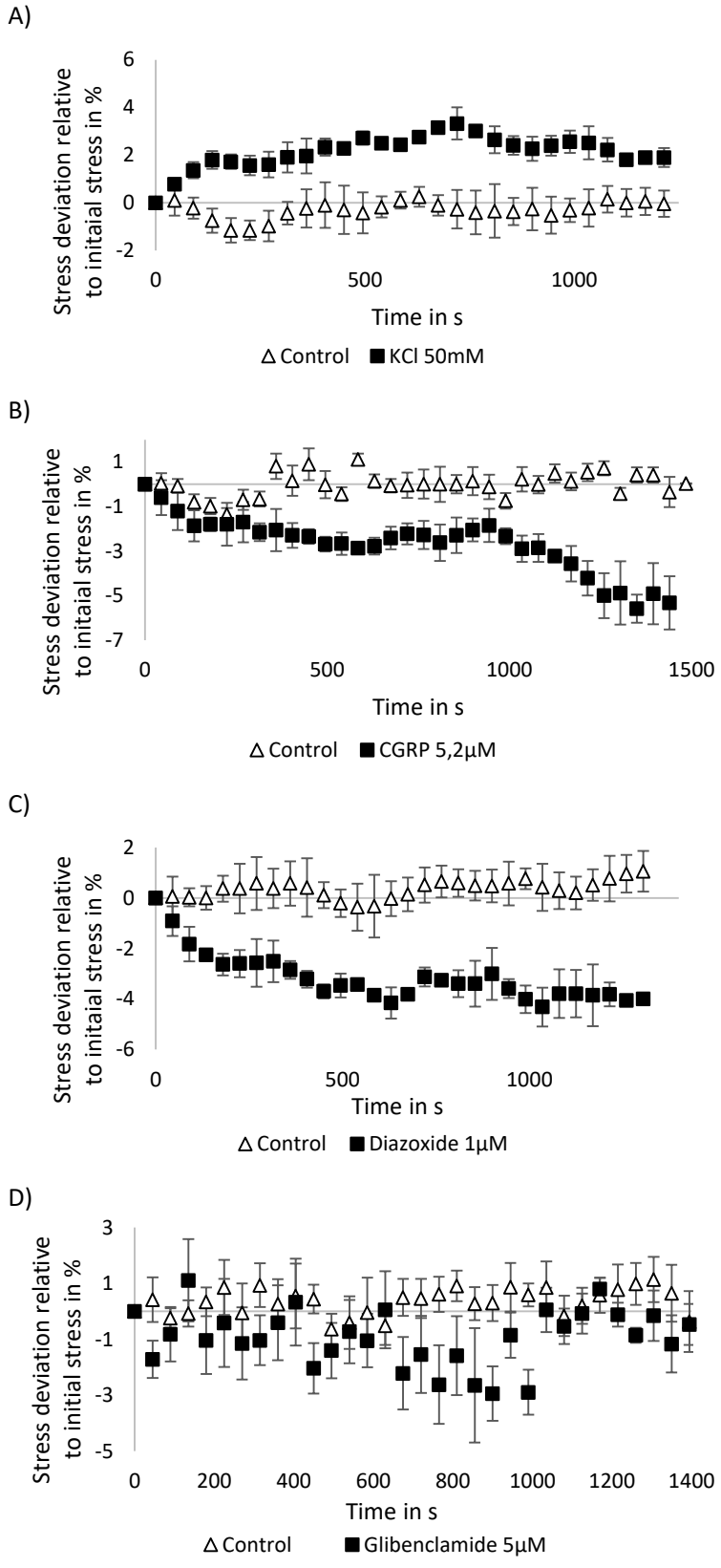


Figure 29 Time courses of substances acting on K⁺ channels, CellDrum investigation via LTM (N=6 mean ± 1 SEM). The change in the mechanical stress caused by the test substance is expressed as the relative difference of the mechanical stress (%) to the initial value. **A)** 50mM KCl **B)** 5,2µM CGRP **C)** 1µM Diazoxide **D)** 5µM Glibenclamide

The application of KCl shows a slow increase in cellular stress compared to the effect of the Ca²⁺ channel modulators. Diazoxide and CGRP were acting on ATP sensitive potassium channels, which were blocked by the substances. By blocking the potassium channels, the intracellular Ca²⁺ content decreases, which leads to a relaxation of the cell.

CGRP was tested in two different concentrations, showing a dose-dependent difference. In both cases, the effect increases after 1200 seconds and reaches a plateau.

Glibenclamide did not show an apparent biomechanical effect. In contrast to the control group, there was a slight deviation between 600 to 1000 seconds, plus an overall increased standard deviation. This suggests a vasoactive effect, which, however, cannot be described as a significant change in cellular tone.

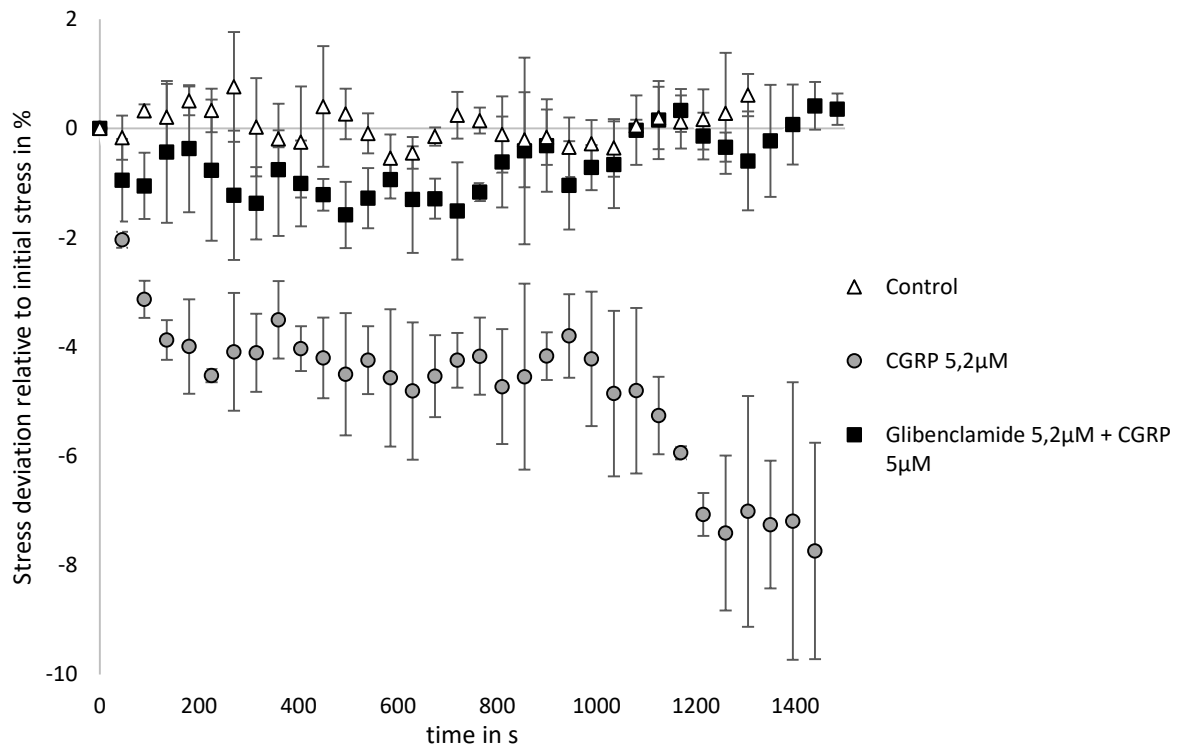
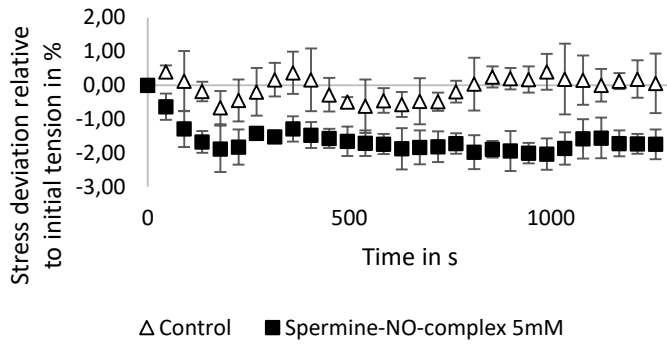


Figure 30 Analysis of the single and combined biomechanical effect of CGRP and glibenclamide on haSMC over time. CellDrum investigation via LTM ($N=6$ mean \pm 1 SEM). The change in the mechanical stress caused by the test substance is expressed as the relative difference of the mechanical stress (%) to the initial value. All substances were measured on separate CellDrum samples. The sample of the measurement series glibenclamide+CGRP was first pretreated with glibenclamide for 30 minutes. The measurement was started when the CGRP was added to illustrate the competitive substance effect.

Figure 30 shows the experimental data, in which the cells were exposed to Glibenclamide and CGRP. The samples were pretreated with a concentration of 5µM glibenclamide. Afterward, GCRP was added. The addition of CGRP did not show any remarkable tension deviation as compared to the effect of only CGRP.

6.2.3.NO

A)



B)

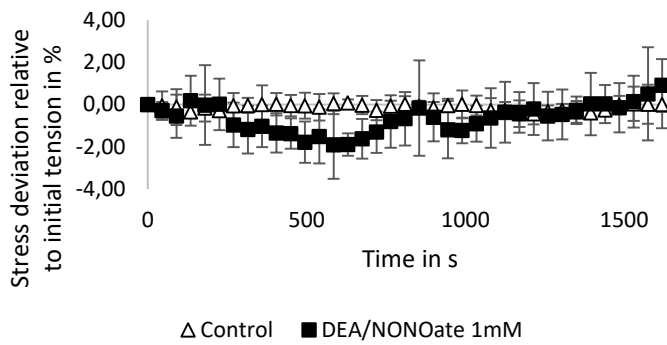


Figure 31 Time courses of NO-Donators. CellDrum investigation via LTM (N=6 mean \pm 1 SEM). The change in the mechanical stress caused by the test substance is expressed as the relative difference of the mechanical stress (%) to the initial value. **A)** 5mM Spermine NO-complex KCl **B)** 1mM DEA/NO

Spermine-NO-complex and DEA/NONOate are nitric oxide-releasing substances. The cell dilation is measurable around 1-2% relative to initial stress and stood stable over the whole measurement. While the effect of spermine-NO-complex continues over the entire measurement period, the effect of DEA/NONOate disappears after 1200s and the cellular tension returned to their original stress level.

6.2.4. Vasoactive Mediators

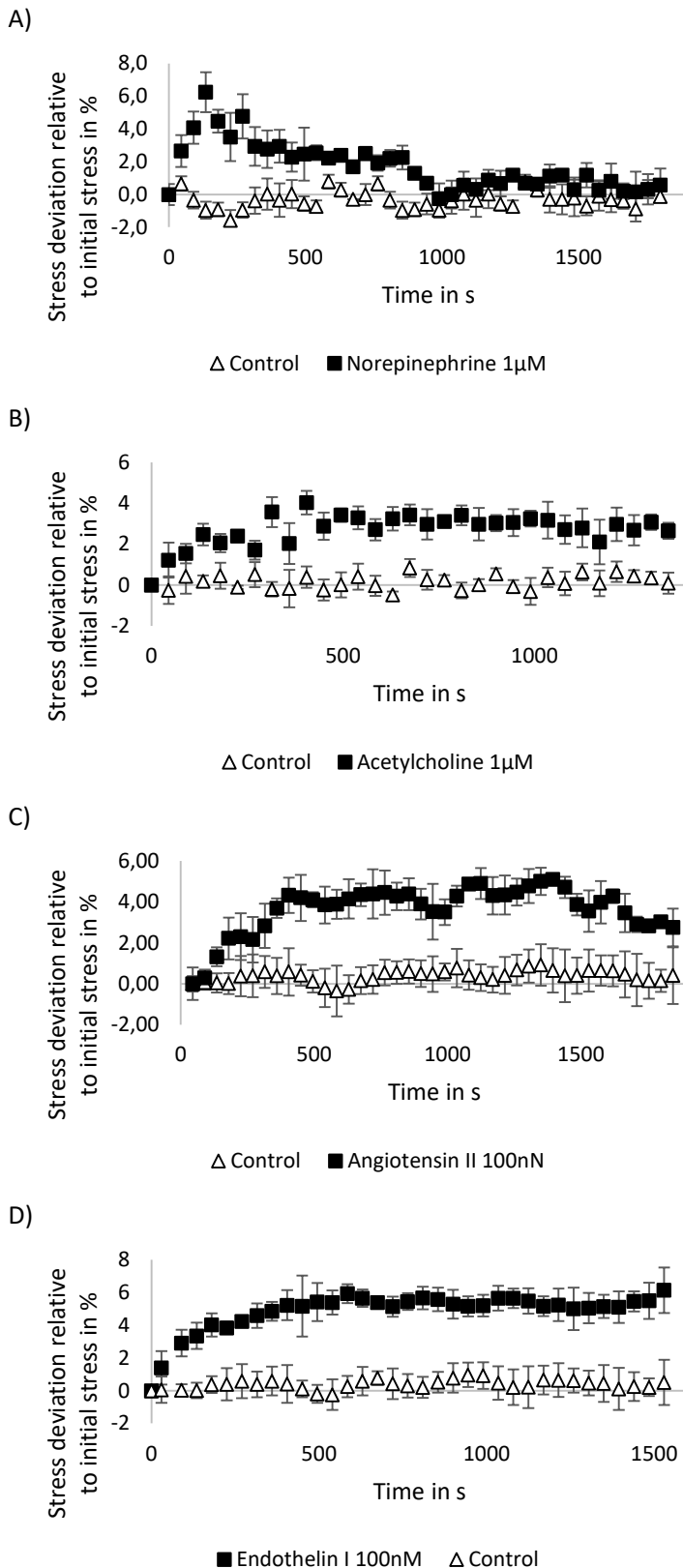


Figure 32 Time courses of measurement of various hormonal vasoactive agents. CellDrum investigation via LTM (N=6 mean \pm 1 SEM). The change in the mechanical stress caused by the test substance is expressed as the relative difference of the mechanical stress (%) to the initial value. **A)** 1 μ M Norepinephrine **B)** 1 μ M Acetylcholine **C)** 100 nM Angiotensin II **D)** 100nM Endothelin I

All tested substances lead to cellular contraction. The direct application of NE to smooth muscle cells leads to a fast and vigorous contraction, which affects lasted only around 1000s. Afterward, the cellular stress went back to the initial stress level. Acetylcholine used on a monoculture of haSMC lead to a cellular contraction. The measured effect persists over the entire time observed. AT2 and ET1 are natural vasoactive substances to increase the vascular cell tone. Compared to AT2, the effect of ET1

was more intense and lasted over the whole measurement period, whereas the cellular contraction by AT2 was decreasing in the end.

6.2.5. PDE5 Inhibitor

A)

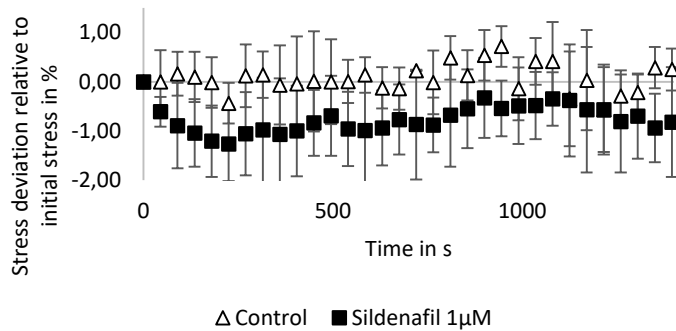


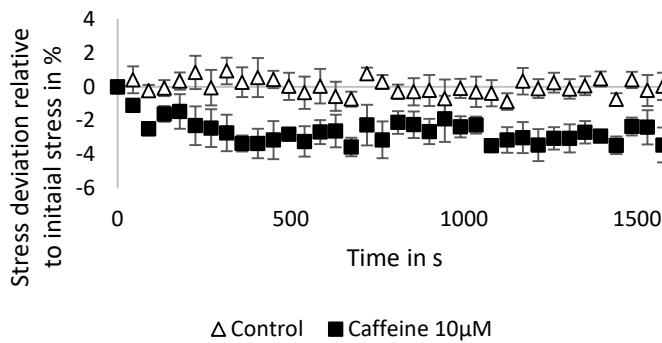
Figure 33 Time courses of vasoactive agents with various mechanisms of effect. CellDrum investigation via LTM (N=6 mean \pm 1 SEM). The change in the mechanical stress caused by the test substance is expressed as the relative difference of the mechanical stress (%) to the initial value. **A)** 1µM Sildenafil

The addition of 1µM Sildenafil reduces the cell tonus slightly and varies between 1-2% mechanical tension relative to the initial value. The measured data show a negative trend, but with a comparably high standard deviation.

6.2.6. Stimulants & Toxins

Figure 34 shows the effect of 10 μ M caffeine. The relaxation started immediately after the application and went over to a plateau phase after 400s. The spider toxin GsMTx-4 caused an apparent relaxation of the cells at the beginning of the measurement, which is reproducible with repeated measures. This heavy relaxation ended after a few measurement cycles and ends in a slight decrease in the cell tone, which varies between 0-2% relaxation. Cytochalasin-D caused a fast and intense relaxation of the cell, with a minimum standard deviation between the individual samples.

A)



B)

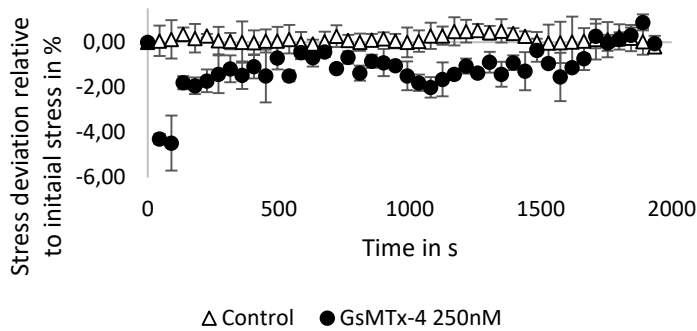
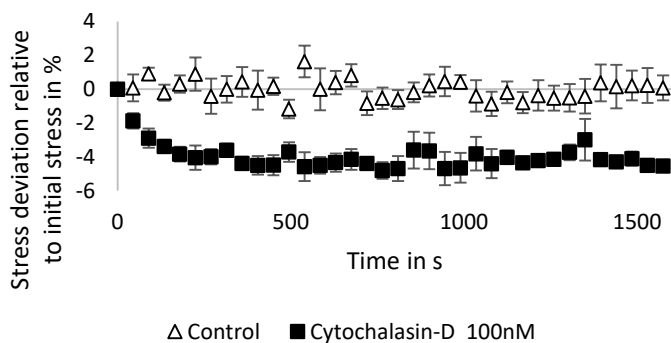


Figure 34 Time courses of vasoactive agents with various mechanisms of effect. CellDrum investigation via LTM (N=6 mean \pm 1 SEM). The change in the mechanical stress caused by the test substance is expressed as the relative difference of the mechanical stress (%) to the initial value. A) 10 μ M Caffeine B) 250nM GsMTx-4 Spider Venom C) 100 nM Cytochalasin D

C)



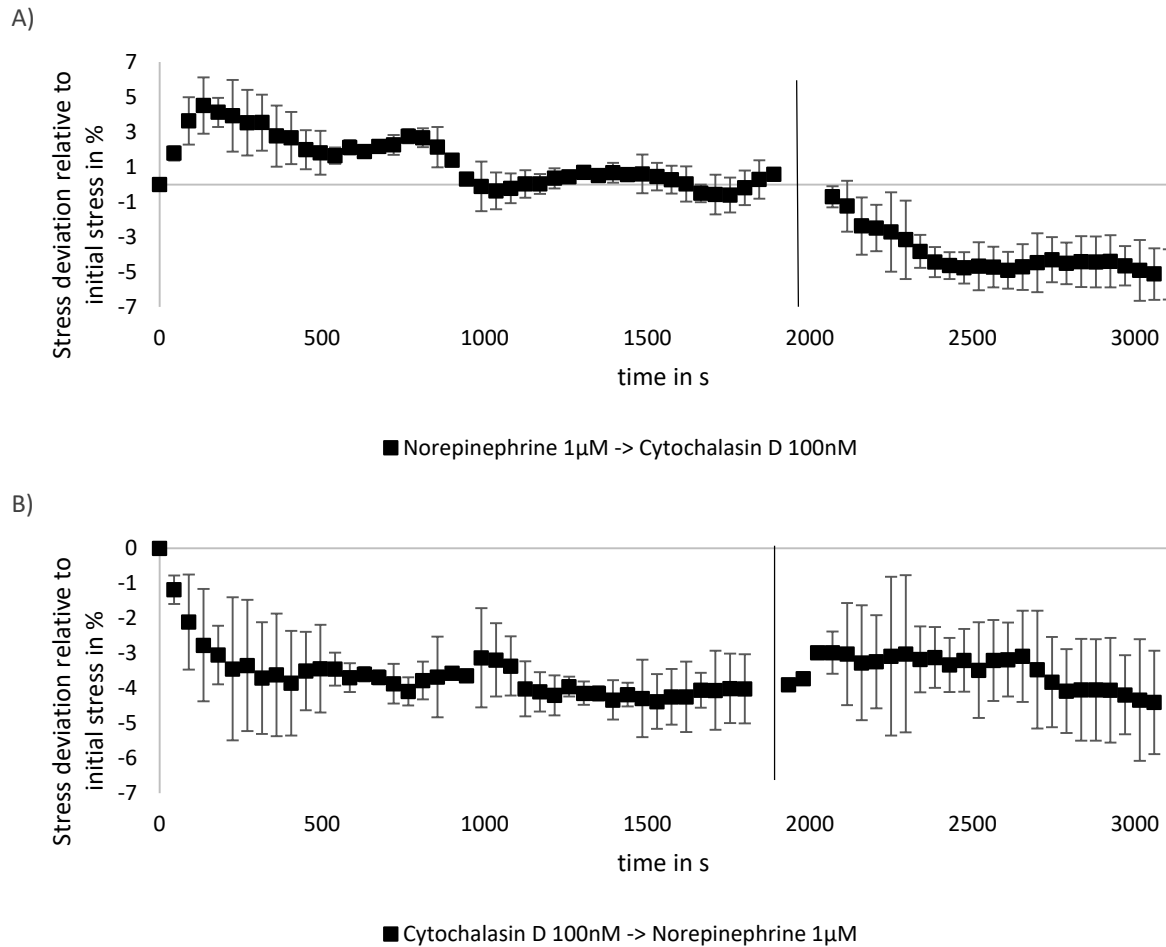


Figure 35 Analysis of the biomechanical effect of serial application of cytochalasin D and norepinephrine over time. CellDrum investigation via LTM (N=6 mean \pm 1 SEM). The change in the mechanical stress caused by the test substance expressed as the relative difference of the mechanical stress (%) to the initial value. Both substances were added in series to the same sample to show the effect of the substance mixture. **A)** Addition of 1µM norepinephrine followed by 100nM cytochalasin D. **B)** Stimulation of 100nM cytochalasin D followed by 1µM norepinephrine

Results of *Figure 35* show an attempt of a measurement series, in which cytochalasin-D was applied first and NE after 2000 seconds. The effect of cytochalasin-D was comparable to the single substance measurement, showing a fast and intense decrease in cellular tension. The followed application of NE increases cellular stress by 1% only. Both drugs show the same time responses in the single drug tests, whereas the effect of norepinephrine was comparably low.

The same setup was repeated in the reverse chronology. Here NE was applied first and cytochalasin-D after 2000 s. The time course shows correlating results to the measured data from the single drug experiments, regarding time progression and effect.

6.2.7. Dose-Response Model

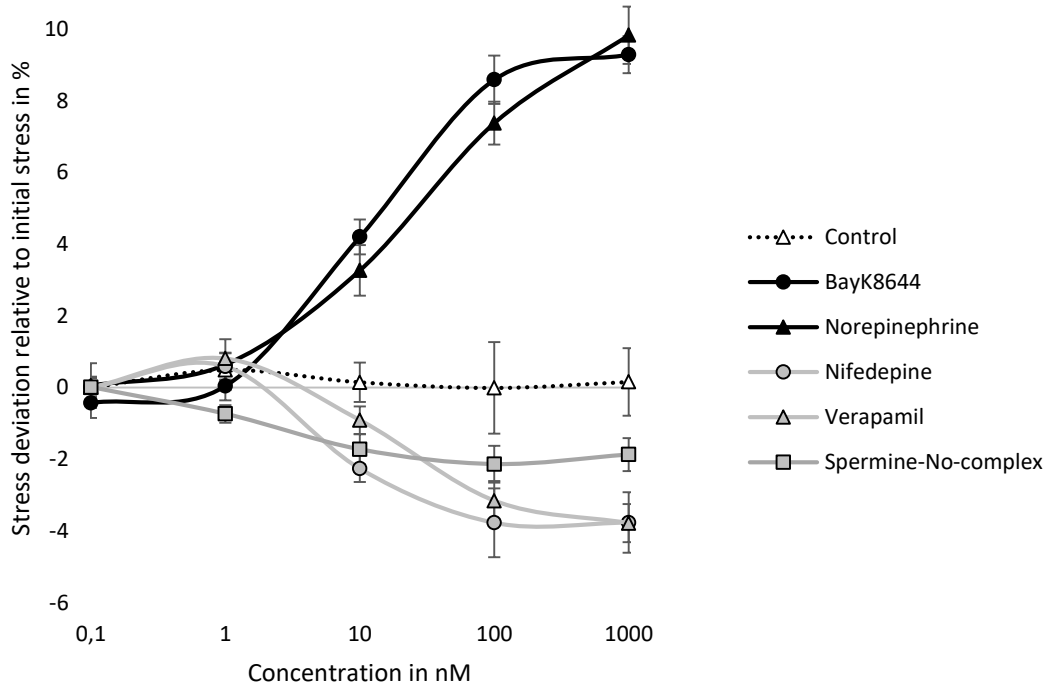


Figure 36 Dose-response model of all tested agents in the concentrations of 0.1nM, 1nM, 10nM, 100nM and 1µM. Y-Axis indicates the deviation in mechanical stress relative to control in % to the initial stress. The X-Axis represents the substance concentration on a log scale. Every data point represents five (n=5) measurements taken from three individual samples(N=6). The error bars indicate the SEM [124](figure adapted)

Figure 36 shows the dose-dependent biomechanical change of haSMC on the addition of Bay K8644, NE, nifedepine, verapamil and spermine-NO-complex, measured by PTM. The application of verapamil and nifedepine decreases the tension around 4% with comparable high standard deviation. In contrast, the use of Bay K8644 and norepinephrine increased mechanical stress around 10,6%, representing the greatest vasoconstriction during this study. The concentration dependency of the spermine-NO-complexes was also tested, which showed its most potent effect already at a concentration of 10nM.

6.3. Mechanical Stimulation

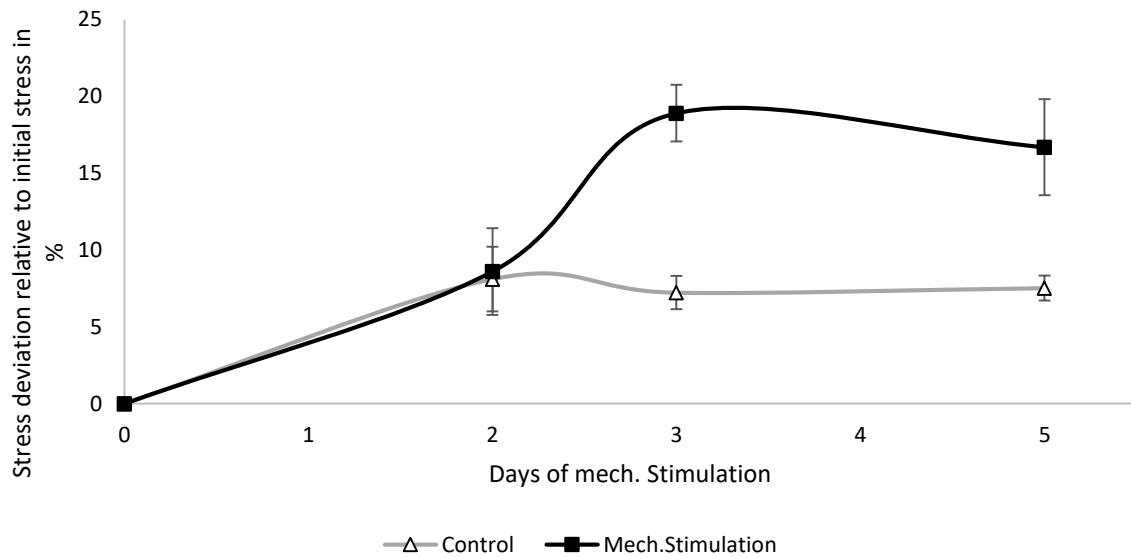
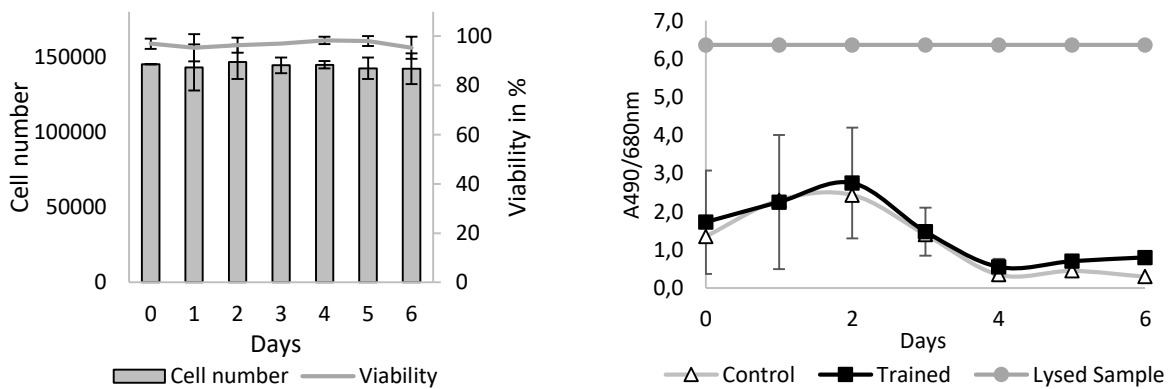


Figure 37 Showing the biomechanical changes of haSMC induced by mechanical stimulation over five days. CellDrum investigation via PTM. Every data point represents the mean value of five independent measured specimens and the error bars represent the SEM ($N=6$ mean $n=5 \pm 1$ SEM). The time course data represent the stimulated specimen compared to the unstimulated specimen.

Nevertheless, the mechanical stress of the cells increased, whether the cells were stimulated or remain in steady-state. After day three, the tension of the stimulated cells increases, whereas the control went over in a plateau phase. After five days, the cellular tension was around the values measured on the third day. The stress of the stimulated cells decreased minimally as the standard deviation increased.



A

Figure 38 Monitoring of cell vitality and cell count of haSMC throughout mechanical stimulation according to SOP for six days. **A)** Quantification of cell count and viability by automatic cell counter and trypan blue staining ($N=6$; $n=2 \pm SEM$) **B)** Viability test by LDH assay and photometric analysis Comparison of stimulated and unstimulated samples ($N=6$; $n=2 \pm SEM$).

Figure 38 shows the results of the viability test, which was carried out analogous to the mechanical seat simulation. While the LDH assay initially indicates an increase in the LDH value secreted into the medium, cell count and viability of the haSMC remained stable over the stimulation period of six days with cell viability of greater than or equal to 90% on the CellDrums.

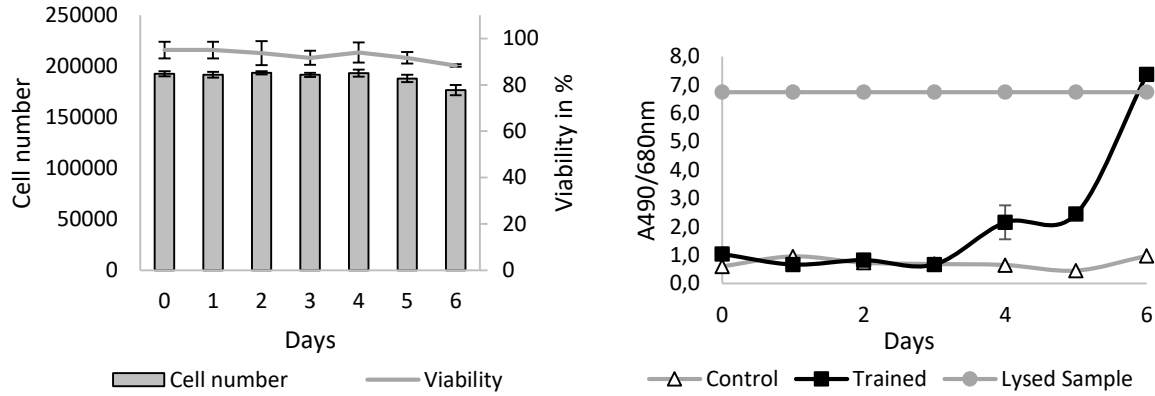


Figure 39 Monitoring of cell vitality and cell count of haEC throughout mechanical stimulation according to SOP for six days. A) Quantification of cell count and viability by automatic cell counter and trypan blue staining ($N=6$; $n=2 \pm SEM$) B) Viability test by LDH assay and photometric analysis Comparison of stimulated and unstimulated samples ($N=6$; $n=2 \pm SEM$).

Figure 39 represents the results of the same experiment described above but performed with haEC. At the beginning of the experiment, cell count, vitality and LDH secretions indicate a remarkably intact sample. From day four on, a slight increase in LDH value is visible, whereas a minimal reduction of the cell number is perceptible with minimally decreasing cell viability. On day six, the maximum LDH value of the samples was measured, which indicates that the samples were severely damaged. Among other things, the SOP of the mechanical stimulation was aligned with this.

In addition to the LDH assays, cell live and dead stainings were prepared to visually control the quality and functionality of the cell monolayer[Figure 40]

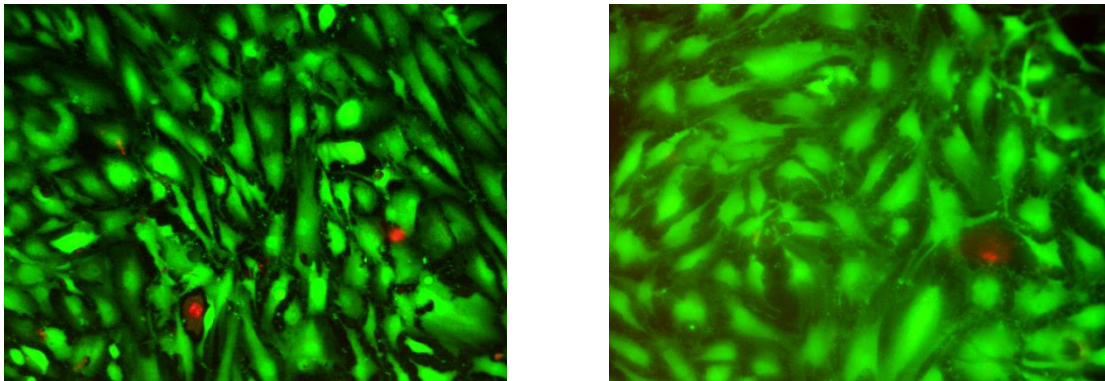


Figure 40 Representative images of live/dead stainings, showing dead cells that have not detached from the CellDrum membrane. The parameters of the training were adjusted so that no more damaged cells could be detected.

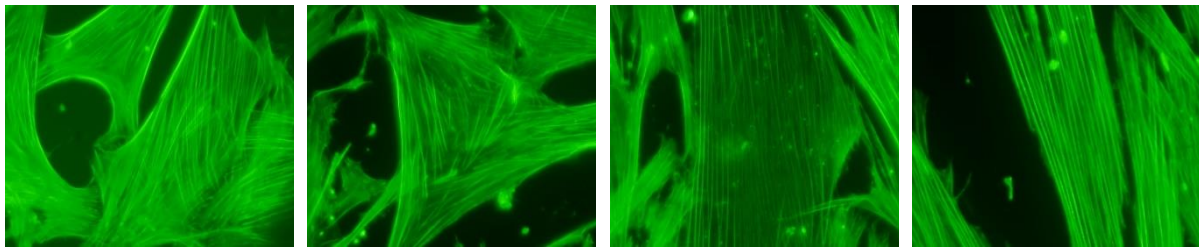
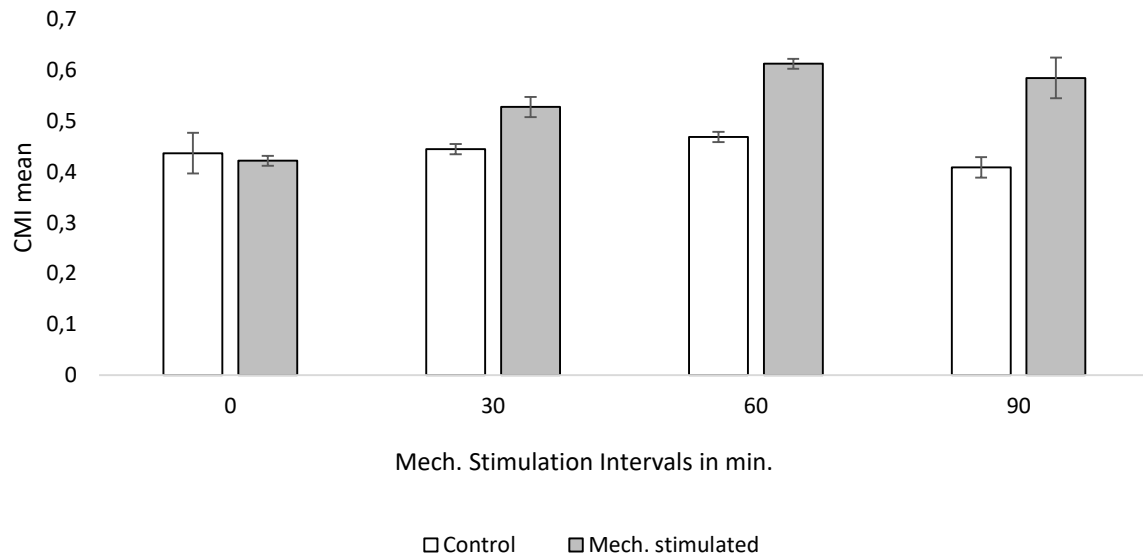


Figure 41 CMI evaluation for the quantification of cytoskeletal f-actin alignment by mechanical stimulation on CellDrums. Each data set was stimulated and unstimulated with three individual CellDrums for the stimulation intervals 0min, 30min, 60min, 90min ($N=3$; $n=30 \pm SEM$). The intensity parameters correspond to the parameters of the SOP ($f=2\text{Hz}$, $P=-40\text{Pa}$). Below representative images of the corresponding stimulation protocols of haSMC, fixed and stained with Alexaflour Phalloidin 488.

The results of the CMI evaluation [Figure 41] show that the cytoskeletal alignment correlates with the stimulation duration. The longer the cells were mechanically stressed per day, the more aligned the cytoskeletal structures are. Despite biaxial stretching, the fibers seem to align in a particular direction. Due to the individuality of the samples, the data are always presented in groups of stimulated versus control. So the effect triggered by the mechanical stimulation becomes clear.

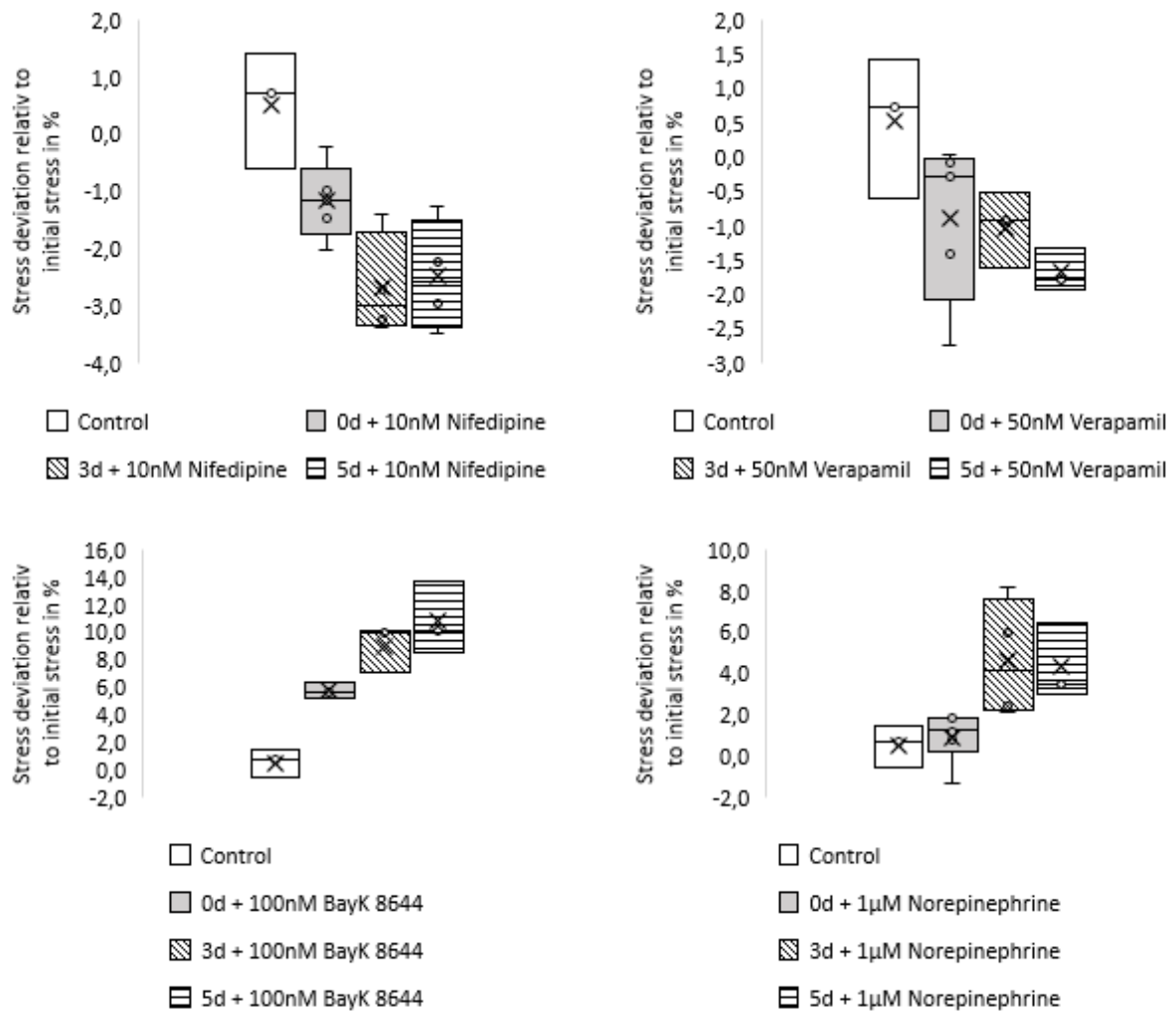


Figure 42 Showing how mechanical stimulation affects the biomechanical response of haSMC to vasoactive agents. Every substance was tested by six individual CellDrums, which were measured after mechanical stimulation after 0 days, three days and five days via PTM and the error bars represent the SEM ($N=6$ mean $n=5 \pm 1$ SEM)[163](figure adapted).

The datasets above visualize the variation in response to vasoactive substances after mechanical stimulation. The stimulated cells were exposed to mechanical stimulation over five days and vasoactive agents were added after three and five days of stimulation. Each group consists of a set of six CellDrums. The data show the change in cell tone in direct comparison to the initial measurement, which was made shortly before the test substance application so that the overall increased cell tone did not affect the result shown.

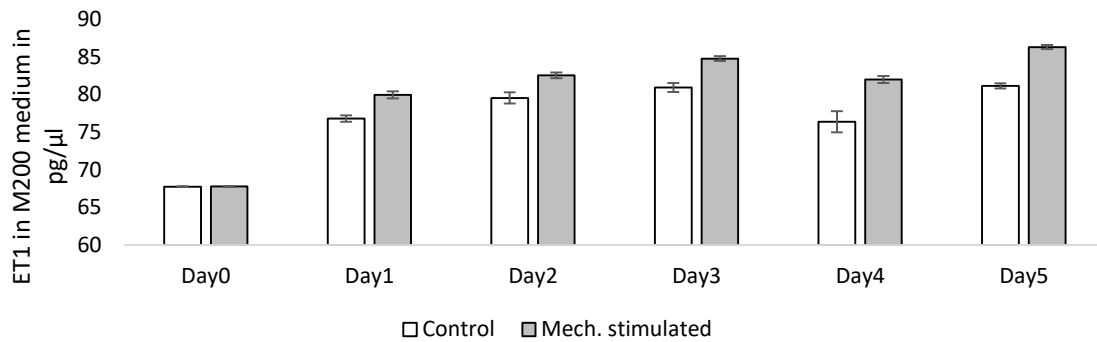


Figure 43 Endothelin secretion measured via ET1 ELISA Kit over the time of 5 days. Every dataset represents the pooled values of three individual samples with two technical replicates of stimulated and unstimulated Cells(N=3 mean $n=2 \pm 1$ SEM). The used CellDrum model consisted of each 200.000 haEC monolayer.

Figure 43 shows the ET1 content determined by ELISA kit in the cell culture medium of haEC mechanically stimulated cells over time. Already on day 0, before the cells were exposed to mechanical stimulation, ET1 concentration of approx. 67pg/μl was measurable. In the course of time, a significant increase in the ET1 level was noticeable. When comparing the stimulated and unstimulated sample, the mechanical stress seemed to have only a slightly more substantial effect on the ET1 secretion, as the ET1 concentration of the control increases at a similar rate over time. Already after three days, an ET1 concentration maximum was measured, which does not significantly differ from the measurement after five days of mechanical stimulation.

6.3.1. Microarray Analysis

The data collected by the Affimatrix system was analyzed by TAC 4.0 from the company applied biosystem. Figure 44 summarizes the results of up- and down-regulated genes from transcriptome analysis. The two stimulation durations were compared and each stimulation duration was compared with the unstimulated control.

Quantity distribution clearly shows that more genes are addressed by more extended or more frequent mechanical stimulation. Thus, after three days, a change of 118 genes can be measured, while after five days, 1208 genes have already have been regulated.

Furthermore, by comparing the two training cycles, it can also be shown that the expression profiles of the genes with the length of the stimulation sharply differ from each other. These deviations were later also made clear in the investigation of individual genes, that the genes addressed vary at different points in time

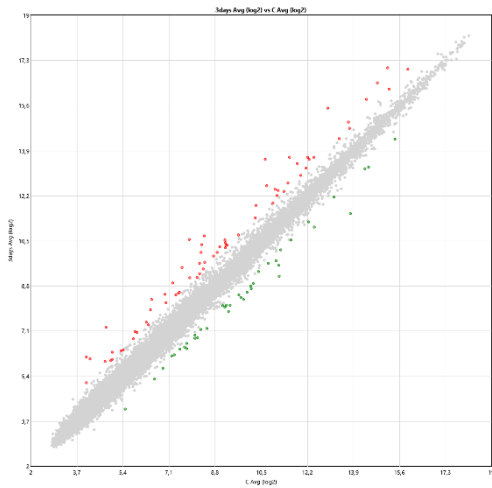
Figure 45 shows the transcriptome comparison of not mechanical stimulated cells to the cells, which were stimulated for three days and five days, according to the SOP described in 5.10.

Significantly down-regulated genes with a foldchange greater equal two are depicted in green color. Red dots indicate upregulated genes for the same conditions.

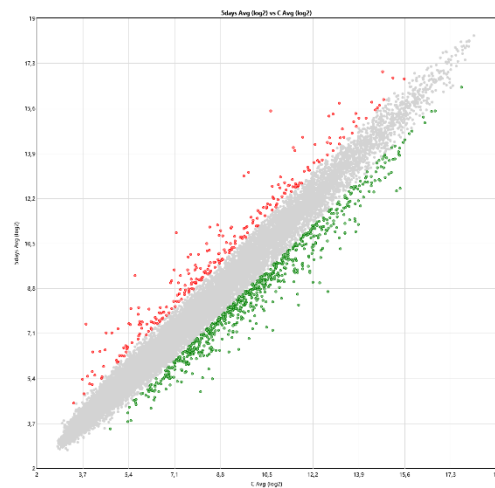
The analysis of the transcription level showed that the response goes along with mechanical stimulation. Hence, the more stimuli, the higher the effect of the transcription level.

For a more detailed examination of the data sets, genes that could be directly related to the development of hypertension were examined. Genes from different epidemiological studies were combined and projected onto the data collected in this study. The change in the expression profile is shown in Figure 45 C, based on a heat map.

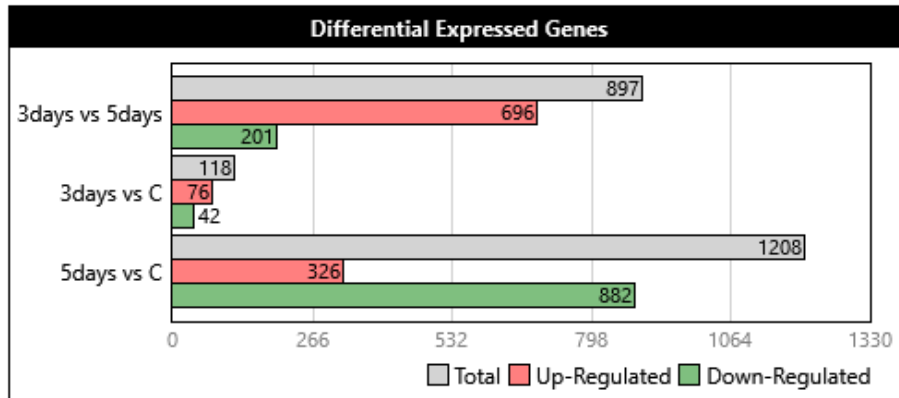
A)



B)



C)



D)

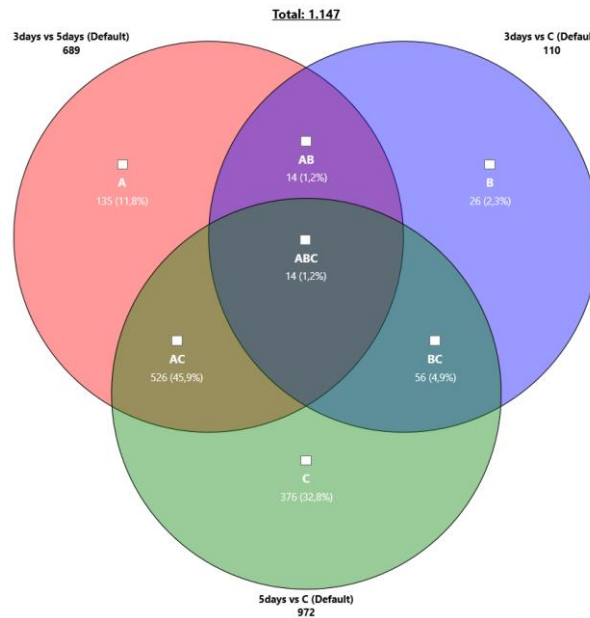


Figure 44 A+B) Comparison of gene expression profile due to mechanical stimulation according to stimulation SOP after three and five days. Genes have been highlighted at a significant change in expression level ($p < 0.05$; foldchanges > 2 ; < -2). C+D) Comparison of gene expression profile due to mechanical stimulation according to stimulation SOP after three and five days. Venn diagram to visualize the diversity of regulated genes. Data were evaluated by microarray analysis (Affymetrix) and TAC4.0 Software

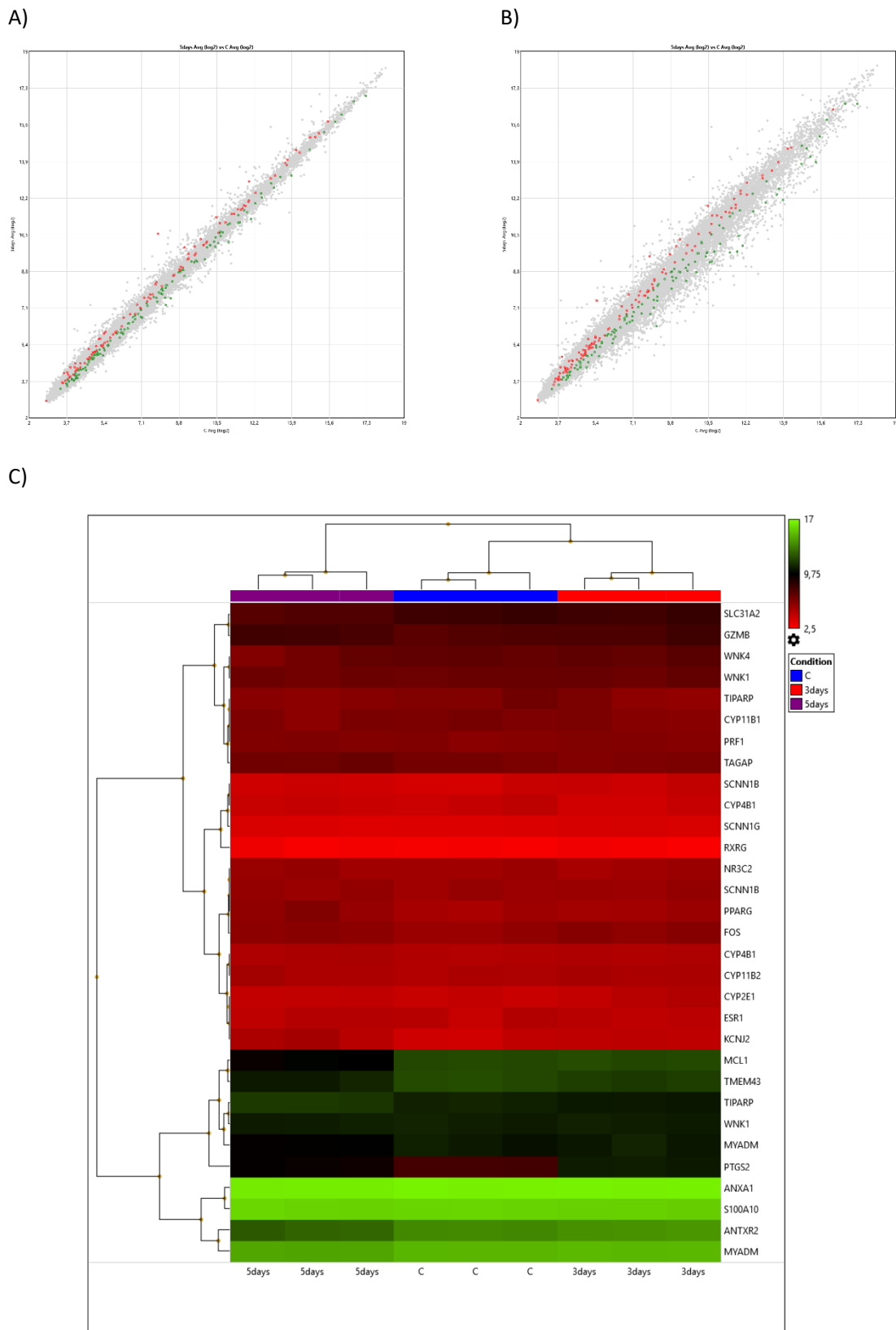


Figure 45 A+B) Comparison of gene expression of pooled genes from different epidemiological studies, which could be related as signature genes for the pathogenesis of hypertension, after three and five days of mechanical stimulation[43,164–167]. Genes have been highlighted without consideration of significant fold change ($Fold >0$; $p > 0$). The arrangement of the data points suggests that the majority of signature genes were not significantly affected by mechanical manipulation. C) Heatmap of pooled signature genes. Data were evaluated by microarray analysis (Affymetrix) and TAC4.0 Software.

6.3.2.qPCR

The qPCR results were split into subgroups for better evaluation. First data show the gene expression level of cytoskeletal related genes in a comparison of different mechanical stimulation protocols. A high deviation was detected for Filamin A after three days of stimulation. Compared to this, β -actin and tropomodulin 4 were highly expressed after five days of mechanical stimulation.

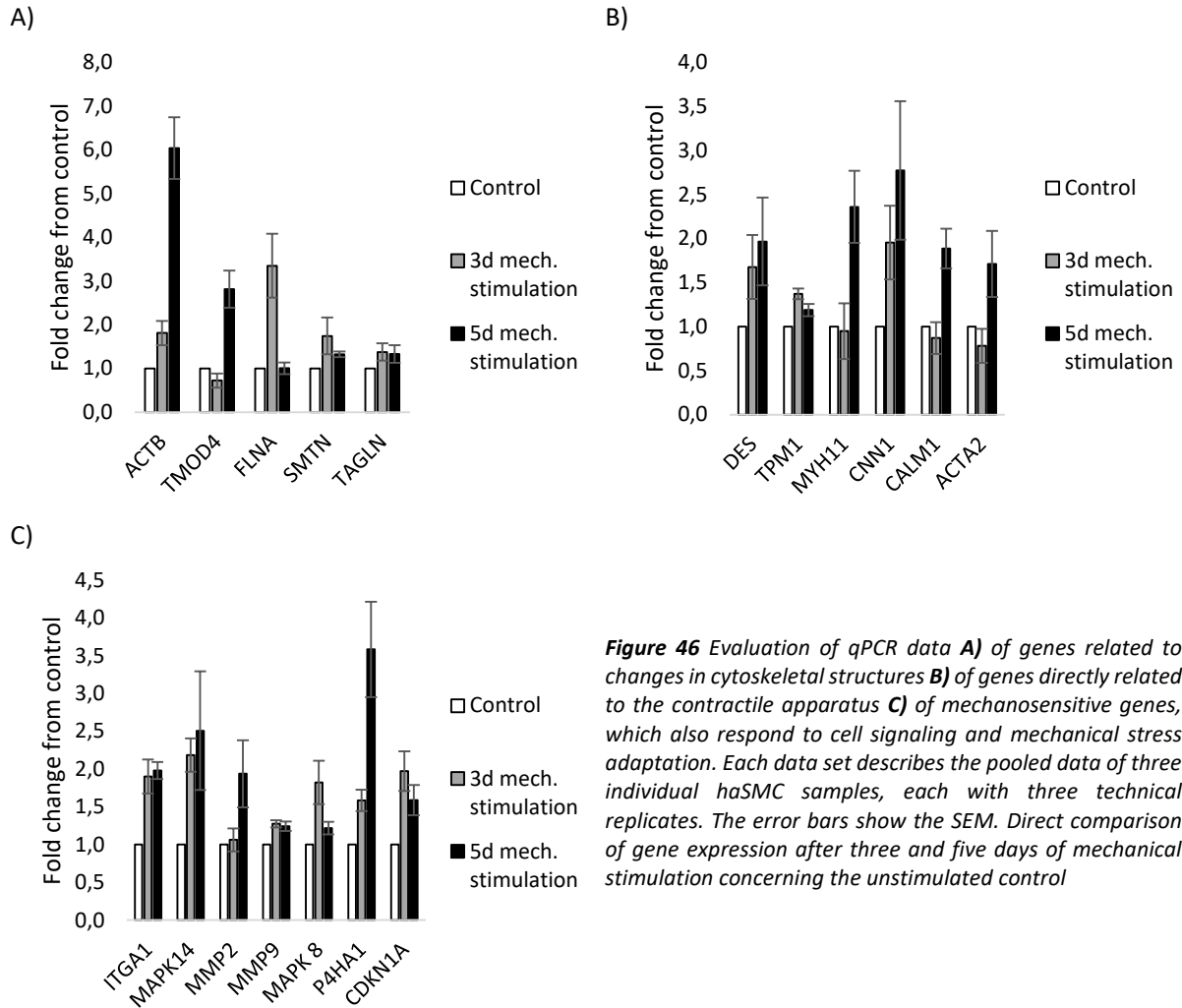


Figure 46 Evaluation of qPCR data **A)** of genes related to changes in cytoskeletal structures **B)** of genes directly related to the contractile apparatus **C)** of mechanosensitive genes, which also respond to cell signaling and mechanical stress adaptation. Each data set describes the pooled data of three individual haSMC samples, each with three technical replicates. The error bars show the SEM. Direct comparison of gene expression after three and five days of mechanical stimulation concerning the unstimulated control

Figure 46 B shows the expression level of genes that are directly related to the contractility of the cells. All genes except tropomyosin, experience increased gene upregulation at least after five days of mechanical stimulation. At last, the gene expression of genes that are sensitive to mechanical stimulation and also related to hypertension pathogenesis.

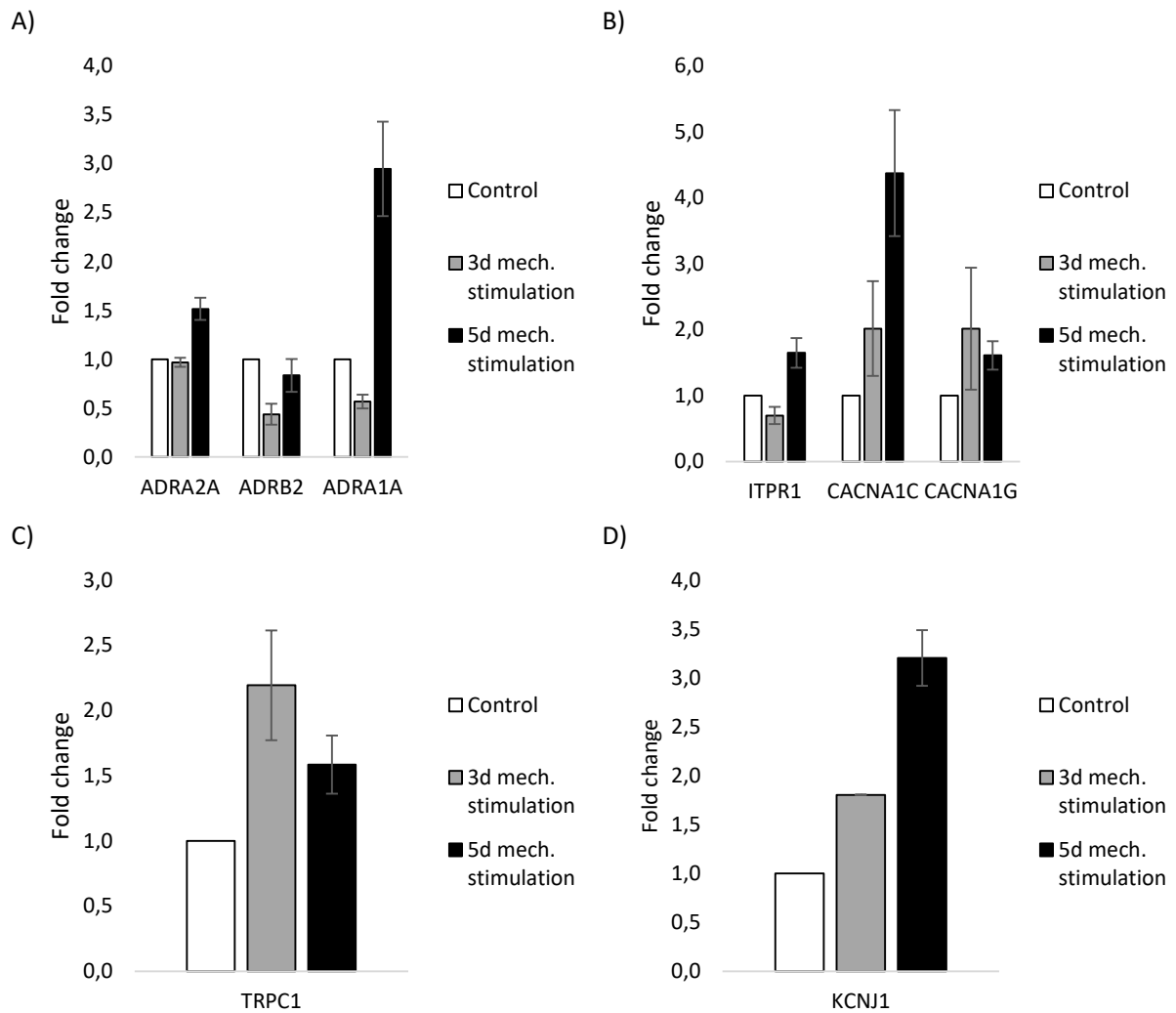


Figure 47 Evaluation of the qPCR data **A)** androgenic receptors **B)** of different calcium channels **C)** of strain-dependent calcium channels **D)** of potassium channels in a direct comparison of gene expression after three and five days of mechanical stimulation with the unstimulated control. Each data set describes the pooled data of three individual samples with three technical replicates each. The error bars show the SEM.

Focussing on gene expression levels related to ion channels and receptors which are responsible for cellular contraction is shown in *Figure 47*.

Three days of SOP stimulation protocol induced a slight variation on gene expression. Exclusively, *TRCP1* was significantly increased after three days. According to the qPCR analysis, five days of stimulation lead to significant upregulation of *ADRA1A*, *CACNA1C* and *KCNJ1*.

6.4. Co-Culture

The most promising media blend was composed of basal media M199 with 2% FBS, 30 μ l/ml heparin, 0,5ng/ml hEGF and 1% penicillin-streptomycin. The presented results were carried out with the final medium blend. Cell proliferation behavior and viability over time are represented in *Figure 48 A/B*. The number and viability of haSMC stood consistent over the whole period of observation. The cell count on days five and seven shows a high standard deviation. This was caused by cellular detachment from particular wells. We estimate this as an outlier, which was not representative.

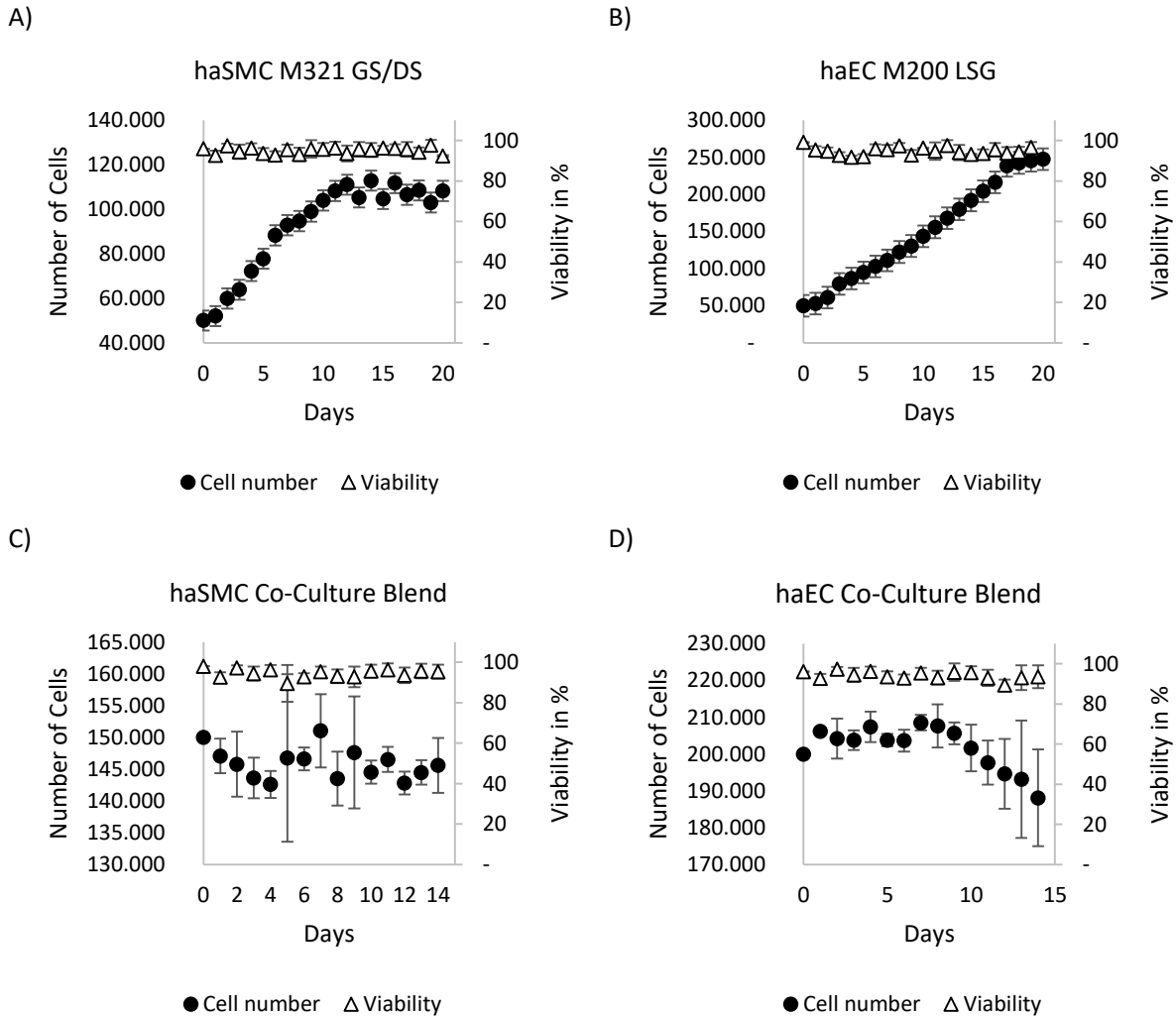


Figure 48 Reviews the cell number and cell viability due to exposure to standard media and co-culture media. The X-axis represents the time course in days, Y-axis 1 represents the total cell number and Y-axis 2 represents the cell viability in percentage. The displayed data show the mean values from three individual biological samples and two technical replicates, and the error bars show the standard deviation. **A)** Proliferation curve of haSMC with initial growth supplement. On day eight, the medium for cell differentiation was added. **B)** Proliferation curve of haEC with M200 medium and low serum growth supplement. **C+D)** Cultivation of haSMC and haEC in final co-culture medium. The initial cell count was adjusted according to the defined cell models.

In contrast, endothelial cell number decreases by day nine, whereas the cellular viability stood consistent >90%. haECs was highly sensitive and had weak adhesion characteristics. Even during cell maintain, the cell always needed collagen-coated surfaces to grow on. The haEC graph (*Figure 48 D*) shows that even with collagen type 1 coated multi-well dishes, the cells started to detach. Since the samples were washed with PBS prior to trypsinization, the number of cells decreased while viability remained the same.

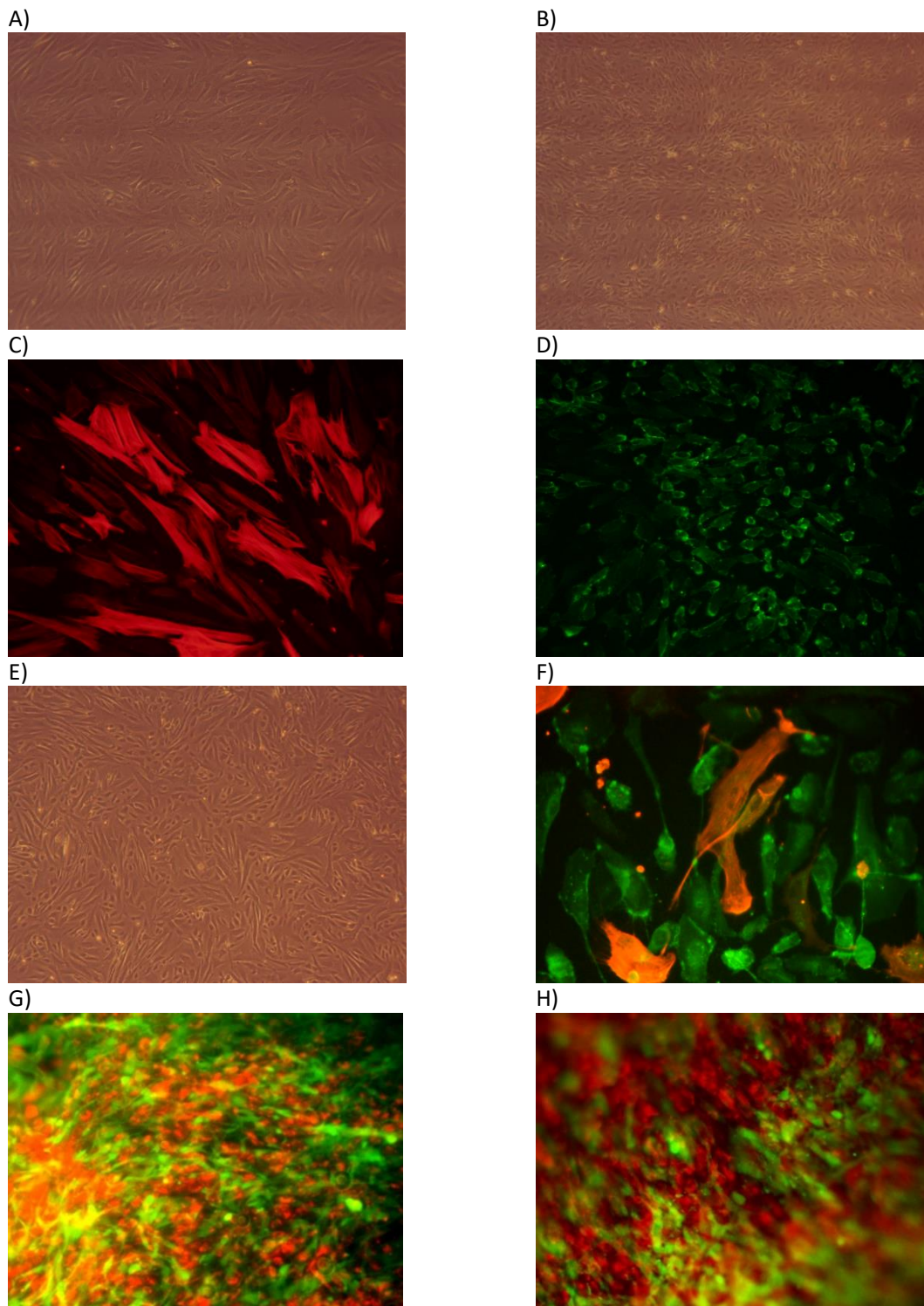


Figure 49 Strategic microscopic investigation of haSMC and haEC single and co-cultures in monolayer and three-dimensional arrangement. **A)** Phase-contrast image of differentiated haSMC on polystyrene slides cultivated with co-culture medium. **B)** Phase-contrast image of haEC grown on polystyrene slides in co-culture medium. **C)** Smooth muscle cell alpha-actin antibody staining of haSMC cultivated in co-culture medium. **D)** CD-31 antibody staining of haEC in co-culture medium. **E)** Phase-contrast image of a direct co-culture of haSMC and haEC in monolayer. Cell ratio 1:1, cultivated on polystyrene slide in co-culture medium. **F)** Co-culture of haSMC and haEC cultivated on polystyrene and stained with antibodies CD31 and smooth muscle cell alpha action. **G+H)** co-culture of two monolayers consisting of haSMC and haEC arranged three-dimensionally on top of each other in CellDrums. They were cultivated in the co-culture medium. Endothelium stained with CellTracker Deep red and smooth muscle cells with CellTracker green.

Microscopic analysis (*Figure 49*) showed that the cells contained cell-specific markers even after long time exposure to the co-culture media blend. Additionally, we were able to show successful co-cultivation via light microscope evaluation and immunocytochemistry staining in a monolayer. Utilizing different Cell Trackers, we tried to display a three-dimensionally arranged co-culture on the CellDrums. It was possible to show both cell types independently of each other and to record them using microscopic Z-stack and full focus recordings.

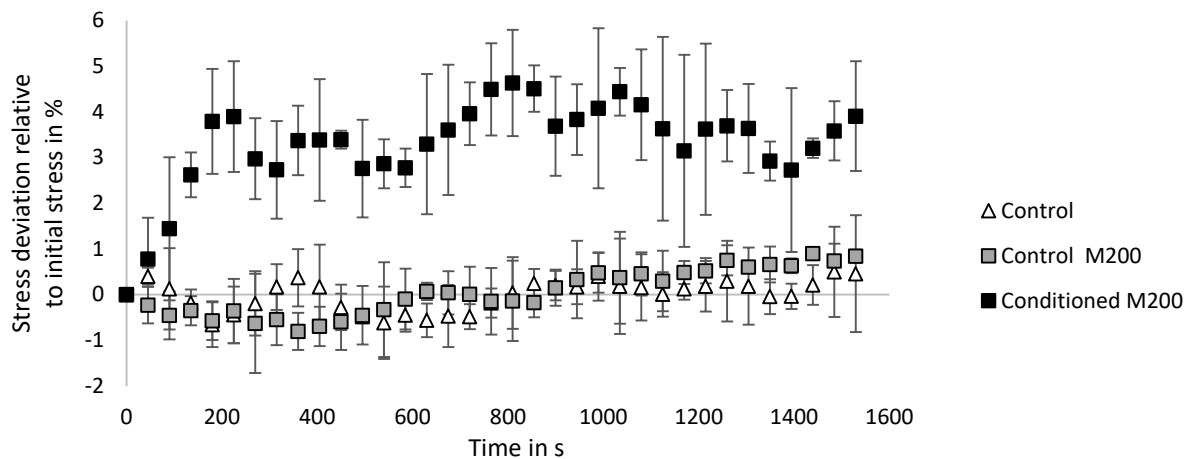


Figure 50 Time courses observation of biomechanical effect induces conditioned medium. CellDrum investigation via LTM ($N=6$ mean ± 1 SEM). The change in the mechanical stress caused by the test Media expressed as the relative difference of the mechanical stress (%) to the initial value. The control measurement was performed using M231 medium. The control measurement M200 was carried out with fresh M200 medium. Conditioned M200 was conditioned for 24h on CellDrums with 200.000haEC before application.

The data in *Figure 50* depicts the biomechanical impact of conditioned culture media. Media from previously mechanical stimulated haECs was removed and added to a CellDrum cultured with haSMC. The control group was supplemented with fresh M200 media and M231. The data revealed that the SMCs started to contract in the presence of ECs conditioned media. The cellular tension increased within the first 400 seconds and stabilized in a plateau phase with relatively high SEM over the whole measurement time.

6.5. Blood Sera

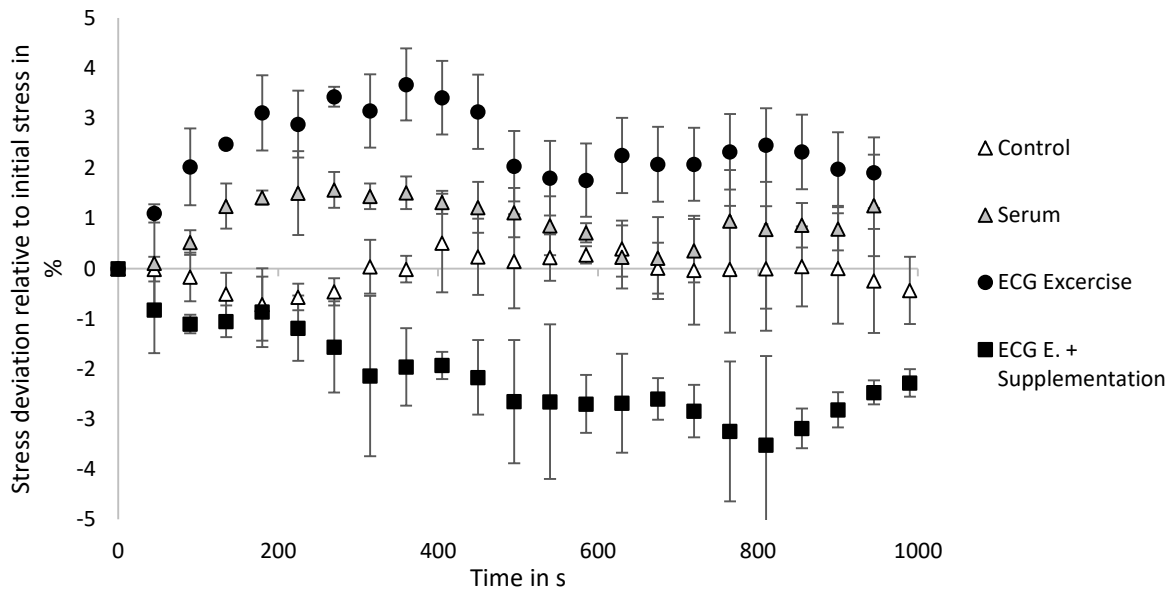


Figure 51 Analysis of the biomechanical effect of blood sera obtained from fresh blood collected from different scenarios over time. CellDrum investigation via LTM (N=6 mean \pm 1 SEM). The change in the mechanical stress caused by the test substance is expressed as the relative difference of the mechanical stress (%) to the initial value.

Figure 51 depicts the data from the exercise ECG test. Application of control sera leads to a slight increased haSMC tone, and the ECG exercise stress amplifies the effect. In contrast, the vascular tone was decreased after administering the arginine and citrulline mixture to the subject. It should be mentioned in particular that the contraction caused by the first two measurements have a maximum, which in both cases fall off again after 400s. On the other hand, the evaluation of the supplemented sera showed a more continuous tonus-lowering effect, but with enlarged variations of standard deviation.

The test person was monitored by a medical specialist during the procedure. Figure 52 shows the monitoring of the subject representatively during the experiment.

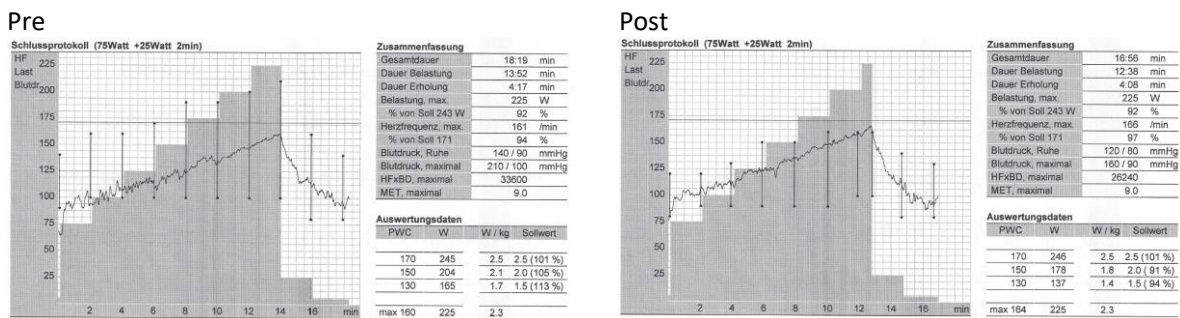


Figure 52 ECG patient monitoring during the two ECG measurements. The curve **Pre** shows the ECG course of the first run without taking the sports supplements, whereas **Post** shows the ECG course after taking the supplements. It can be seen that the heart rate increases in the second run while the blood pressure is lower compared to the first run.

7. Discussion

7.1. Mechanobiological Vascular *in-vitro* Model

To establish the functional vascular CellDrum model, the *in-vitro* models were exposed to different stimuli and agents with known mechanisms of action to compare their biomechanical response with the physiological behavior of vascular cells.

The determination of the temperature depending biomechanics of the cells was initially decisive as to whether the measurement would take place under the clean bench or in the incubator. Due to the cellular cooling with chilled media, a measurable contraction of the haSMC was shown. Especially for temperature $<10^{\circ}\text{C}$ the cellular tension has changed remarkably. After 1500 seconds, a temperature of $\geq 30^{\circ}\text{C}$, the cell tension has normalized. A considerable temperature drop from 37°C to 25°C room temperature is noticeable but not distressing. By these results, we assume that the measurements from the perspective of the biomechanical analysis can be done as well under clean bench conditions. Nevertheless, metabolic and molecular mechanisms could be affected by the temperature drop and the decreased CO_2 saturation as well but were not inspected in this work. The measurements also provided interesting insights into the biomechanical temperature dependence of vascular smooth muscle cells[168].

Pharmacological testing:

The application of calcium channel modulators has been discussed in detail in the publication “Mechano-pharmacological testing of L-type Ca^{2+} channel modulators by a human vascular CellDrum model” which we have published in April 2020. Modulation of Ca^{2+} channels leads to measurable relaxation and contraction of the cells with permanent effects. In addition to the application of Ca^{2+} , we have evaluated different measurement protocols.

All three Ca^{2+} channel modulators are capable of inducing significantly measurable changes in cellular strength. With the application of Bay K8644, the increase in cell tonus indicates an increased Ca^{2+} influx. Bay-K8644 increases the transient Ca^{2+} concentration in the cell from which an increased calcium-induced calcium release from the sarcoplasmic reticulum is assumed, leading to a raised cell[136,137,139]. In contrast, the Ca^{2+} channel antagonists nifedipine and verapamil block the Ca^{2+} inflow, which leads to a reduction of the intracellular Ca^{2+} and, in turn, to a relaxation of the cell[143,169,170]. While verapamil has a specific effect on the L-type Ca^{2+} channel, reference studies suggest a further non-specific effect of various other voltage-dependent Ca^{2+} channels. Besides the lower bioavailability, especially the blockade of various Ca^{2+} channels, could explain the significantly stronger relaxing effect of nifedipine[171,172].

KCl

The stimulation via KCl leads to a depolarization of the smooth muscle cell and opens voltage-dependent Ca^{2+} channels. The resulting influx of extracellular Ca^{2+} activates the Ca^{2+} -dependent contraction mechanism and leads to an increase in cell tone, which can be measured biomechanically[31]. Compared to the measurements of Ca^{2+} channel modulators, the plateau phase was reached later around 600s.

Diazoxide reduces the cell tone endothelium-independently by the presence of low concentrations of KCl. The vasodilatory properties of diazoxide are related to the inhibition of the Ca^{2+} influx, which seems to result from the activation of the ATP-dependent K^+ channels[147,173].

The endocrine factor CGRP has a strong relaxing effect on haSMC, which can be explained by the activation of adenylyl cyclase. In addition, both agents also seem to act on ATP-dependent K^+ channels, which we will be discussed later via substance combination experiments[146].

Glibenclamide also acts on the ATP-dependent K^+ channels and regulates the Ca^{2+} flux by decreasing the influx of K^+ . In theory, it should lead to a relaxation of the smooth muscle cells. However, this effect could not be measured in our experiments. On the basis of the unsteady signal and comparably large SEM deviation, an effect can be suspected, but no significant difference can be determined[149,174].

NO donators:

Spermine-NO-complex and DEA/NONOate are nitric releasing substances used to mimic the eNO release *in-vivo*. Both substances lead to a slight cellular relaxation of the haSMC layer, but not as much as the previously used agents have shown. Unlike the vasoactive substances, the NO donators releasing their NO in doses over a more extended period. In addition, these molecules are quite unstable at room temperature. Hence they decay and lose their potency over time. According to the results, spermine releases NO over the whole measurement span. The limited release and the effect NO induce a cellular relaxation around 2-3%. The dose-response model showed that the cell response correlates to the concentration of the applied substance. Spermine-NO-complex as NO donator was applied in two different doses. Even by increasing the dose by a factor of 100, the relaxation does not increase significantly, which is contrary to the literature data. In previous investigations, stronger relaxation effects were measured, so that it can be assumed that the maximum relaxation potential of NO could not be represented in this test arrangement. By this, we consider that even the lower concentration reached the maximum relaxation, which can be caused by NO, possibly caused by the low NO release of the substance or by its rapid decomposition within the CellDrum setup[175].

Following the literature, DEA/NO does not have a significant relaxational effect on smoothing muscle cells [176]. We were able to measure slight relaxation over the first 800s. Compared to the control group, the addition of DEA caused a more significant SEM deviation. These fluctuations can be indicators of some measurable effects, which might go down within the signal-noise ratio. Nevertheless, the amplitude reaches initial tension after ~900s, which we interpret as that DEA has completely decayed.

Vasoactive Mediators:

ET1 and AT2 have been tested as natural vasoactive substances. Endothelin-1 is known as the most potent natural vasoactive substance to regulate vascular tone. The measurements showed a stable and robust increase in the cellular tone. Compared to this, angiotensin II is described in literature a less potent than ET1. Even though AT2 increased the tension by 5%, the effect decreased after 1400 s.

Additionally, norepinephrine has been tested. Unlike all other tested substances, NE increased the cellular tension within the first 200s to a maximum contraction. Almost instantly, the effect diminishes and the cellular tone went back to initial stress within the early 1000s. This very short phase of concentration can also be traced back to the stability of the substance in solution, so that the active ingredient may no longer be present after 1000s. Studies on the half-life of norepinephrine show that it is dependent on concentration and light exposure[48,177]. NE loses its effect only after a few seconds, whereas comparable *in-vitro* studies show that the measurable contraction of vSMC decreases at a similar rate[145].

According to the literature, acetylcholine application *in-vivo* leads to vasodilatation by triggering the production of eNOs via the endothelial cells. As we are using only haSMC for the pharmacological study, the effect mechanism is acting on the muscarinic IP_3 pathway, which leads to vasoconstriction by intracellular Ca^{2+} release. This has been shown in several publications and is also suspected to be a cause for coronary vessel constriction[178].

Stimulants and Toxins:

Caffeine is one of the most widely used stimulants and is taken in by most people every day through drinks, food and medication. Caffeine belongs to the group of xanthines and affects the vascular system through various direct and indirect mechanisms of action[156]. Indirectly, caffeine affects VSMC via the endothelial cells located in the lumen. Caffeine increases the cytoplasmic Ca^{2+} of the endothelial cells, by forming the calcium-calmodulin complex that activates the nitric oxide synthase enzyme to produce nitric oxide. This diffuses into the VSM and leads to NO-induced vasodilation. In addition, caffeine leads to an increase in cAMP, thereby decreasing the non-contractile intracellular Ca^{2+} and inhibiting MLCK. Caffeine also has a direct inhibitory effect on MLC kinase and actin-myosin interaction, resulting in smooth muscle cell relaxation in both cases. In contrast, caffeine also blocks the adenosine receptors in vascular tissue, which in turn, will lead to vasoconstriction[179,180].

Based on the data in *Figure 34*, we were able to measure a moderate but steady relaxation of haSMC in our experiments by the addition of caffeine. Based on the data, it cannot be ruled out that both mechanisms of action are effective or that the vasodilative effects compensate for the vasoconstrictive ones. Since the experiments were tested exclusively on haSMC, only direct mechanisms of action can be considered.

GsMTx4 is a spider venom peptide that has an inhibitory effect on mechanosensitive cationic channels of cells[181]. Our measurements in *Figure 34* show that after the addition of the substance, an intense relaxation occurs with a fast onset, which could be measured reproducibly with a relatively small SEM. The measurements correlate with data from the literature and can be explained as follows. GsMTx4 is integrated into the cell membrane in a voltage-dependent manner, which distorts the mechanical stress distribution around the corresponding mechanosensitive channels, thus making the transmission of force to the channel less efficient [159]. According to the literature, it can be assumed that GsMTx4 has no direct influence on channel activity and cell contraction[182]. The measured relaxation would therefore be due to the basic tone of the cells, which the cells develop on the soft substrates of the CellDrum. In addition, the signal becomes inconsistent after the initially very intense relaxation and alternates between 0% and 3% relaxation. These fluctuations could possibly be due to the mechanosensitive activation of the cell by the inflation measurement. Electrophysiological studies would enlighten the action of mechanism and the cellular response to the substance.

Sildenafil is a substance that is mostly used as a drug for the treatment of erectile dysfunction. Through specific phosphodiesterase type 5 (PDE5) inhibition, NO-mediated vasodilation is enhanced by inhibition of cyclic guanosine monophosphate degradation of tissues[183]. As with the above-mentioned substances, sildenafil acts both directly and indirectly on the tissue. Studies have shown that sildenafil can promote vSMC relaxation via cGMP, cAMP and K^+ channel-dependent signaling pathways even without a nitrogen-mediated pathway, but this is the far less dominant effect [184]. Since sildenafil can only act via the direct vSMC signaling pathway due to the lack of endothelium in our model, only a marginal and not significant change in cell tension was measured despite the high dosage. As in the other experiments, the measurement was performed without endothelial cells, which means that the NO signaling pathway is entirely negligible.

Cytochalasin D is known to inactivate the contractile apparatus of the cell entirely irreversibly. Aside from the cellular relaxational effect, cytochalasin-D measurements were essential to define maximum relaxation. Due to its irreversible effect, it is not useful for previous sample calibration but can be used to estimate the expected measurement range. Moreover, it may give insight into the residual tension which is build up by the ECM and cytoskeleton[11,185].

Agent combinations:

Serial measurements were used to demonstrate the cooperative and or competitive effects of multiple substances. These kinds of measurements were roughly examined, as the CellDrum technology needs further technical adjustments for a wash in and out experiments. The first experiment was based on a publication of Nelson et al., who showed that CGRP acts via ATP-dependent K^+ channels[146]. CGRP causes intense vSMC relaxation, as shown in *Figure 30*. GCRP, in combination with glibenclamide, does not lead to any biomechanical vSMC response, as glibenclamide blocks the corresponding channel. Nelson et al., proofed that mechanism biomechanically and electrophysiologically. In this thesis, we have reconstructed the experimental setup and were able to prove the results via CellDrum technology. As glibenclamide does not have any measurable biomechanical effect, it was possible to apply glibenclamide in advance and add CGRP just as the measurement has started.

A real wash in measurement, in which two substances have been added during a serial measurement, was carried out with NE and Cyochalasin D. This kind of measurements was only performed with one substance combination, as the pipetting procedure effort maximal precision to prevent a baseline shift of the whole measurement series. For futures analysis, this procedure needs to be automated.

Dose-response model:

The dose-response model proved that the biomechanical substance effects are dose-dependent and can also be resolved like that. From this data, we predict a maximum measurement range from approximately -4% to +10% tension deviation from initial tension, with unstimulated haSMC on CellDrums. Measurement was carried out by the PTM. Solely the effect of norepinephrine was evaluated after three minutes, whereas the other substances were incubated for five minutes according to the SOP. As shown in the single-dose experiments, the effect of NE diminishes over time. The maximum amplitude was no longer detectable for NE after five minutes.

Spermine-NO-complex reaches the maximum effect already at the application of 10nM and, from then on, went into the saturation of relaxation. This supports our hypothesis that the effect of NO on our model is limited to -2% relaxation.

General biomechanics:

Comparing to similar studies that deal with the pharmacological effects of vasoactive substances, the results presented here seem comparably small [*Table 19*]. It should be noted that the samples for the experiments performed were neither chemically nor mechanically pretreated. Thus, the presented results are not scaled based on a pre-stress or maximum contraction but normalized to the initial mechanical tension. The defined mechanical initial stress of the model was set to $50\pm 5\text{kPa}$ so that the calculated percentage deviation can be transformed into kPa in each case and further on in μN as well.

Cell contraction and relaxation could be measured without prior pharmacological or mechanical stimulation, suggesting that the flexible CellDrum membrane and the components of the medium allow the cells to generate and maintain a certain biomechanical tone, which is slightly higher than the membrane tension alone.

Table 19 Comparison of the data acquired by us with comparable studies. Subject species: Rat (R); Human (H); Chicken (C) and Mouse (M)

Test Substance	Result		Spec.	Setup	Ref.	CellDrum		
							%	μ N
Nifedipine	↓	30±5mmHg	R	In-vivo	[186]	↓	-4,15	-132,8
	↓	15-20mmHg		In-vivo	[143]			
	↓	40% to NE stim.		In-vitro	[138]			
Verapamil	↓	15-29%	H	In Vito	[141]	↓	-1,87	-59,84
Bay-K8644	↑	~130 to Vera/Nife. stim		Organ-bath	[139]	↑	4,4	140,8
	↑	191±6mmHg	R	Organ-Bath	[187]			
	↑	150% to Nife.		In-vitro	[138]			
KCl	↑	350%	R	Organ-bath	[188]	↑	2,6	83,2
	↑	15-20%	C	In-vitro	[189]			
CGRP	↑	20% ∅	R	Organ-bath	[149]	↓	-3	-96
Diazoxide		-	-	-		↓	-3,71	-118,72
Glibenclamide	↓	~60% ti PE stim.		Organ-bath	[174]	↓	-0,66	-21,12
Spermine	↓	~60% to ACh		In-vitro	[190]	↓	-1,81	-57,92
DEA/NO	↑	~60%	M	Organ-bath	[191]	↓	-1,29	-41,28
NE	↑	1,75±0,17mN/mm ²	R	Organ-bath	[145]	↑	4,62	147,84
	↑	4,58+-0,006mN/mm ²	R	In-vitro	[145]			
Acetylcholine	↓	1,75mm ∅		Organ-bath	[192]	↑	2,82	90,24
	↑	~40%	M	Organ-bath	[191]			
	↑	52,1±7,8N/mm ²	R	Organ-bath	[145]			
	↑	0,46±0,1N/mm ²	R	In-vitro	[145]			
AT2	↓	12% ∅	R	Organbath	[73]	↑	4,54	148,28
ET1	↑	3,8±0,2mN/mm ²	R	In-vivo	[193]	↑	5,36	171,52
	↑	23,7±6,7% to KCl stim.	C	Organ-bath	[194]			
Caffeine	↑	3,-15mmHg	H	In-vivo	[195]	↓	-2,99	-95,68
GsMTX-4	-	-	-	-		-	-4,5	-144
Cytochalasin-D	↓	79% to KCl stim.		Organ-bath	[188]	↓	-4,06	-129,92
Sildenafil	↓	3±8%	H	In-vivo	[183]	↓	-0,62	-19,84
	↓	5,3mmHg	H	In-vivo	[196]			

The generation of cellular tone is illustrated by the results [Figure 26], which show an apparent change in tension that correlates with cell number. Furthermore, the soft growth surface of the CellDrums seems to promote the increase and development of cell tone. This is shown in the experiment of mechanical stimulation, where the control [Figure 26] also increases its cell tone in the first days. The effect measured here was recorded after eight days of cultivation so that it can be assumed that this effect is even higher during the growth phase and the subsequent acclimatization of the cells to the new mechanical conditions.

Cell culture media used in this study contained at least 2% FBS. Even though the composition of the FBS used is not documented in detail, it can be assumed that the hormones, proteins and electrolytes contained therein interact with the cells. Based on the results obtained, it can be assumed that even traces of vasoactive mediators like ET1, AT2, NO, catecholamines and fluctuating ion concentrations

will have an impact on the biomechanical properties. In addition, serum proteins such as albumin and prostaglandin synthesizing substances such as indomethacin and corticosterone are expected to contribute to the sample baseline tension[197–199].

The measurement starting from its basal tension has the advantage that the sample can be examined biomechanically without any apparent effects interfering with each other. Nevertheless, the probe can still be FBS-starved to eliminate the influence of growth factors.

The disadvantage of this method is that it creates two unequal maxima. While the maximum contractile force could theoretically go towards infinity, the mechanical preload of the membrane defines the maximum limit of relaxation. Thus, only the cellular relaxation until the initial tension of the membrane is reached can be measured. Taking into account the cellular production of extracellular matrix during cultivation, a new ratio to the total membrane tension is applied. Therefore, the initial membrane tension should not be reached even at maximum cellular relaxation. Thus the different maxima do not pose a problem for the measurement itself, but one should be aware of the measurement constraint of the relaxation maximum.

In order to select the most suitable data acquisition, different measurement methods were examined and published in detail in our recent publication[124].

With regard to the measurement modes, it is evidential that the inflation tests of the LTM and PTM can already measure mechanical cell tension changes of a few N/m^2 , which do not necessarily lead to a change in CellDrum membrane displacement. We noticed this in a direct comparison of the evaluations of RTM and LTM, as the stress deviations in LTM were measurable much earlier than in RTM. Due to the force equilibrium of each CellDrum, the cells must overcome this first. Thus, the cells first generate isotonic stress changes, which can lead to an increase in force without deformation.

Due to this inaccuracy and the lack of necessary data for biomechanical analysis, we refrain from using RTM for comparable studies.

7.2. Hypertension Disease Model Induced by Mechanical Stimulation

Mechanical stimulation was used to simulate arterial hypertension, which is induced by increasing mechanical stress on the circulatory system. The parameter for the SOP was designed for the strongest possible stimulation sequence without provoking cellular detachment or ruptures in the monolayer. The intensity of the stimulation can be defined via three parameters: Time, amplitude and frequency. Apart from the amplitude maximum, the applied deflection can also be modified via the deflection profile of the pressure waves. This characteristic was not considered in this study yet, but technologically already applied within the system.

In direct comparison with vascular physiology, the defined stimulation parameters are not physiological. While the aortic tissue in the human body resists stretching of up to 30%, in the present study, we work with a maximum stretching of 3%[3,122]. Also, cells in a living organism are exposed to cyclic stretching 24 hours a day, whereas in our experiments, they are exposed to stretching only one hour a day in total. Last but not least, the physiological resting heart frequency of an adult is between 60-80bpm, whereas our SOP works at 120bpm. Concerning hypertension, the heartbeat would even decrease with increasing peripheral resistance. Nevertheless, we have decided to induce the additional mechanical load primarily by the increased frequency.

Comparing the parameters chosen in this study with equal studies, cyclical stress and also bi-axial stimulation show recurrent mechanobiological phenomena[Table 20]. In most reviews, the intensity of stimulation is expressed in mmHg of applied pressure, applied force in N (Newton) or strain and

elongation of the stretch. For a precise and comparable quantification of mechanical stimulation, the expression of mechanical strain is best used as it also takes into account the sample geometry.

Table 20 Overview of stress parameters and results of comparable studies. Cell types: huaSMC (human umbilical artery smooth muscle cells); raSMC (rat artery smooth muscle cells); haSMC (human artery smooth muscle cells); huvEC (human umbilic vein smooth muscle cells); baEC(bovine artery smooth muscle cells). FX-2000/3000/4000, are cell stretching devices by the company Flexcell. ST-140, cell stretching device by STREX, enabling to apply uniaxial stress.

System / Stress	Strain	Freq.	Cells	Results	Lit.
Uniaxial	7%	1Hz	huaSMC	SM α -actin \uparrow ; calponin \uparrow ; cellular orientation	[200]
Uniaxial	10%	1Hz	hSMC	P38 \uparrow 3h	[201]
FX 3000	10%	1Hz	raSMC	P21 \uparrow 24h	[202]
Biaxial	4%;	1Hz	hSMC	VEGF; PAI-1;MMP1 \uparrow ; 24h	[203]
Biaxial	1-9%	1Hz	haSMC	P50 \uparrow 24h	[204]
FX 4000	7-20%	1Hz	raSMC	IL-6, p38;JNK \uparrow	[205]
FX 3000	15%	0,5Hz	maSMC	P47phox; MMP2 \uparrow ; 0-24h	[206]
Uniaxial	7-25%	static	haSMC	JNK;p38 \uparrow	[207]
Uniaxial	10-18%	static	haSMC	MMP-2; p4 α 1; JNK; P38 \uparrow	[208]
FX 4000	7-15%	1Hz	raSMC	P38;integrin;p53 \uparrow ; 6h	[209]
Uniaxial	0-25%	1-3Hz	huvEC	Cell orientation \uparrow	[210]
FX 2000	10-20%	1Hz	huvEC	E-modulus, cellular stiffening \uparrow	[211]
ST-140	120%	1Hz	baEC	eNOs phosphorylation; NO \uparrow	[212]
Uniaxial	20-50%	static	huvEC	eNOS \uparrow	[213]
FX 2000	25%	1Hz	huvEC	ET1 \uparrow	[214]
Uniaxial	10%	1Hz	huvEC	ET1 \uparrow	[215]
CellDrum	0-3%	2Hz	haEC	ET1 \uparrow	
CellDrum	0-3%	2Hz	haSMC	SM α -actin; calponin; P21 ; P38; MMP-2; MMP-9; p4H α 1; JNK; Desmin; Caldmodulin; MYH11; CD49; cellular orientation; E-modulus \uparrow ; 5d	

In a direct comparison with studies dealing with mono- or multi-axial mechanical tissue stimulation [Table 20], the strain we obtained is in the lower range to the smallest scale of the produced stress in this study. Thus, the applied elongation of vascular smooth muscle cells ranges between 3-25% [200,207,216] and for endothelial cells, on average 10-25% up to >100% [20].

These values could not be achieved with the CellDrum technology without irreversibly damaging or detaching the cells on the surface. The determination of the parameters was based on our viability tests and various microscopic analyses.

According to the data, the LDH level contained in the media is not significantly increased during the stimulation for eight days. In contrast to the haSMC, the haECs were strongly damaged and detached after seven days of stimulation. This experiment series limited our examination time to five days to ensure cell viability.

In combination with the CMI measurements, we were able to define a particular stimulation interval without cell detachment. A single exposure to mechanical stress over 90min was possible but repetitions do critically harm the cells. Especially from these measurements, we have decided to stimulate the cell for only twice for 30 minutes each, per day.

Another decisive factor in the comparison of stimulation protocols is the type of cell attachment and the resulting force transmission[217]. For cell attachment, the PDMS cultivation area was coated with 1% fibronectin. Depending on the fibronectin concentration used in an *in-vitro* model, the force transmission might differ from physiological equivalents[67,185]. Based on the very thin surface coating and the strong cellular binding, it can be assumed that the stretching parameters of the membrane are transduced one-to-one to the cells. If the corresponding strain parameters were projected onto a cell model on or in a gel matrix, the elasticity of the matrix would have to be considered in the actual cell strain. Due to the usually very elastic matrix structures, large amounts of the applied strain can be compensated by the deformation of the gel.

Due to the chosen stimulation protocol, a significant increase in mechanical tension can be measured up to a maximum of ~19% of the initial tension on day one. Interestingly, the data of all sample groups show an equally increasing mechanical stress over the first three days. Even unstimulated cells increased mechanical tension by ~6%[Figure 37].

The increase of the cellular tension in both groups is explainable due to the sensible mechanical detection of smooth muscle cells[Figure 53]. The cultivation within CellDrums reduces the growth area tension from approximately 3000MPa, which is the physical tension of polystyrene of T-Flasks, down to 100kPa, which was measured from the CellDrum membranes[217,218]. Although the new biomechanical environment of cells whose physiology is similar, this is perceived by the cells as additional stress. Even though we acclimate the cells on CellDrums eight days before, the cells still seemed to adapt and align towards new mechanical conditions. Additionally, the pace of media change during the mechanical stimulation protocol is 400% higher compared to ordinary culture conditions, twice a day. Media changes cause a great mechanical stimulus, in which the membrane reaches back to its initial zero position, having a total height membrane deformation around 1500 μ m. This single but extreme membrane deflection change causes additional mechanical stress, inducing cellular tone, to be adapted over the first three days.

Cytoskeletal adaptations are microscopically visible changes in the cell that adapt to changing mechanical stress states. Studies have shown that both cells and cytoskeleton align with the main mechanical stress directions[219,220]. This orientation increases not only the contraction force of the cell but also the mechanical load capacity. Under constant mechanical load change, this leads to an increased cell tone and a far greater and more coordinated contraction force compared to non-aligned cells. Studies with uniaxial mechanical stimulation clearly show the cell orientation in the main mechanical stress direction as well as the significant increase in contraction force [86,101,221]. Data represented in this study 5.11 show similar characteristics despite the assumption of uniform biaxial tension[117]. We assume that despite the supposed mechanical homogeneity of the membrane, minimal stress gradients lead to cellular alignment. In particular, we think that the changes in length due to strain increase concentrically to the center of the membrane. A high expression level of beta-actin supports the determination of strong morphological changes.

Besides biomechanical properties, the cytoskeleton contains differentiation markers of smooth muscle cells. As described above, the smooth muscle cells are present in two different phenotypes, with individual tasks and therefore generate unique structures to implement them functionally. By analysing these markers, it can be determined whether the cells continue to mature or dedifferentiate as a result of mechanical stimulation. Proteins such as heavy chain myosin, smoothelin, calponin 1 and smooth alpha-actin are indicators of a contractile smooth muscle cell phenotype. The stronger these occur in the cell, the more maturation and differentiation is assumed[58,62,222], which would suggest a more potent contraction force.

The formation of this protein can be initiated by growth factors, but can also be promoted or enhanced by mechanical stimuli[223–225]. This behavior could be shown using qPCR. Both HCM, smoothelin and smooth alpha-actin were significantly higher expressed after five days at the latest. We assume that mechanical stimulation and cultivation on the soft membranes improved cell differentiation towards the contractile phenotype. To be able to make more meaningful statements in this regard, further investigations of these differentiation factors and the comparison between hard and soft growth surfaces are required.

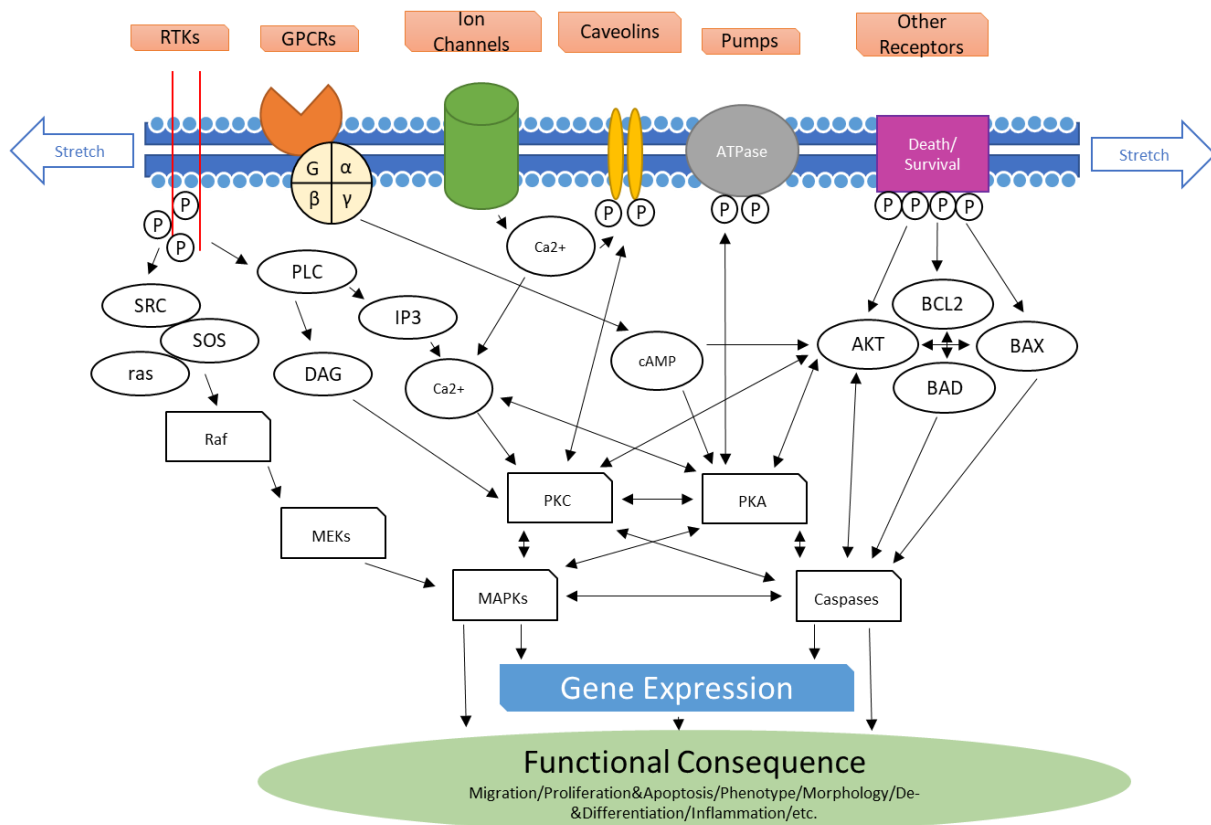


Figure 53 Scheme for mechanically-induced signal conversion in haSMCs. The mechanical stimulus is detected at the cell membrane by mechanosensitive receptors and ion channels and transmitted into the cell interior via molecular transfer. This leads intracellularly, to the activation of various unspecific signaling cascades, by protein phosphorylation and/or alteration of the intracellular ion concentration, which in turn activates further signaling pathways. Finally, the combination of the activated signaling pathways determines the functional response of the cell. These include phenotypic changes, cellular differentiation, migration, proliferation and apoptosis, each affecting the biomechanical properties of the cells. [30](figure adapted).

The contractile phenotype is particularly suitable for the modeling of a contractile vascular cell model. Contrary to the assumption that stronger stimuli improve the differentiation, this effect can change into the opposite. According to the literature, excessive mechanical stress can lead to microcellular damages. This, in turn, leads to the dedifferentiation of the vSMCs, as this initiates the regenerative cascade [Figure 54] in which the cells return to their proliferative phenotypes to repair cell damages[22,213,226]. Especially to estimate the phenotypic change of the cells, we have observed the following genes to estimate the cell differentiation status. According to the qPCR, a strong expression increase of beta-actin can be seen due to the mechanical stimulation, which is a structuring non-contractile cytoskeletal structural proteins and associated sources as a dedifferentiation marker. On the basis of the data, it can be assumed that mechanical stimulation causes the cellular dedifferentiation marker to increase after only a few cycles in order to repair potential cell damage. The LDH measurement of the mechanically stimulated cells, which shows increased LDH concentrations in the medium within the first three days, also speaks in favor of this. It is crucial for the measurements

of this study that cell proliferation was not initiated so that the measurements are not influenced by changing cell numbers. This was supported by the regulation of *CDKN1A*, which indicates inhibition of cell proliferation and keep the actual cell count from the viability tests stable[202,227–229].

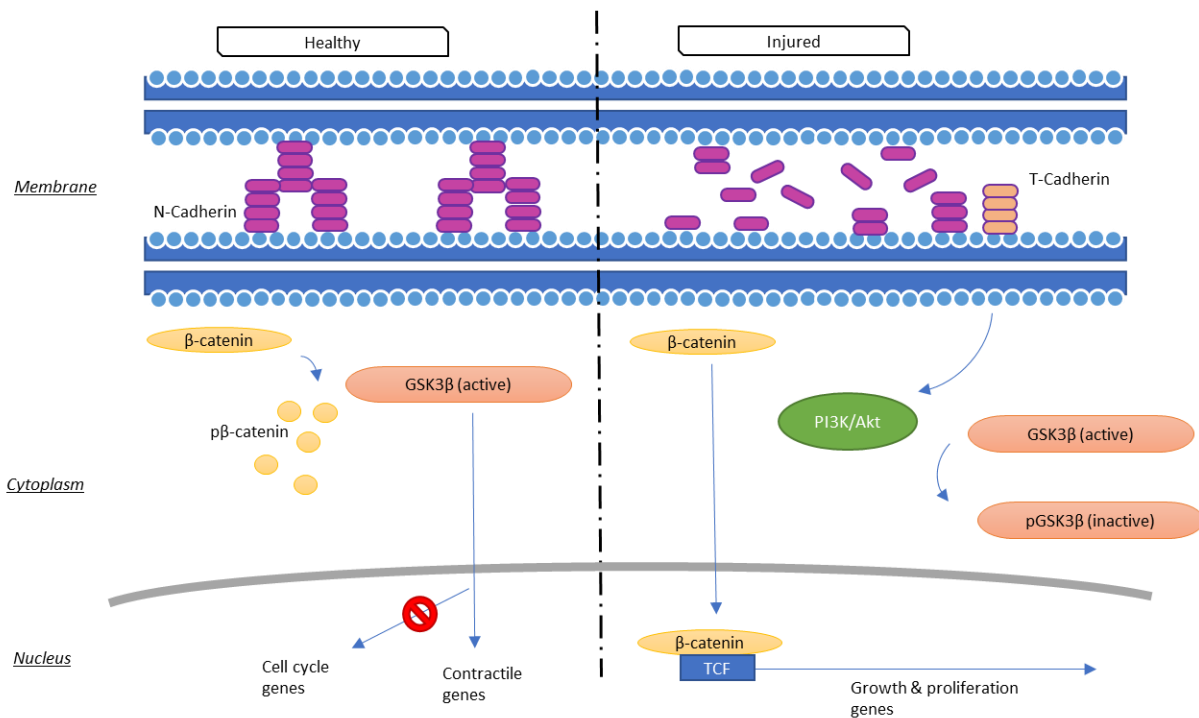


Figure 54 Repair mechanism and phenotypic control of vSMC, by GSK3β, β-Catenin and Cadherine. Elementary for the mitogenic quiescence of the cell is a low cytosolic concentration of β-catenin, which is ensured by the active phosphorylation of the GSK3β complex. Cellular or vascular damages lead to a cleavage of N-cadherin and the degradation of adherent junctions, which reduces the activity of the GSK3β/APC/axin complex. This increases the concentration of β-catenin and leads to a translocation of β-catenin into the cell nucleus. This leads to TCF regulation of the genes responsible for cell growth and proliferation. The damage of the N-cadherins additionally leads to the up-regulation of T-cadherins, which, by activating the PI3K/Akt signaling pathway, completely stops the phosphorylation of GSK3β and supports the following signaling cascade. [230](figure adapted).

The development of hypertension can have many origins, but all of them result in an increase in blood pressure due to the hardening of the vessel wall. This is usually caused for two reasons, either by the cellular solidification or by increased cell proliferation. While the increase in solidity at the cellular level is based on cellular properties such as basic tension, elasticity and mechanical integrity, the increase in tissue is directly related to the dedifferentiation and proliferation of cells.

Based on cellular biomechanics, two contrary indicators of the development of hypertension *in-vitro*. Pathophysiologically, tissue growth and hardening most likely occurs in combination. These mechanisms cannot be differentiated with the physical CellDrum model and would lead to recurrent results. Therefore, our investigations are limited exclusively to the biomechanical solidification of differentiated vSMCs. Under this premise, it is necessary to adapt the mechanical stimulus to avoid cellular dedifferentiation.

The microarray analysis of the whole transcriptome shows significant changes in the overall expression profile after only three days of cyclic mechanical stimulation[Figure 44]. Contrary to expectations, genes that were significantly up- or downregulated after three days were not further amplified by a longer stimulation interval. Instead, the gene profile changed in its entirety. These overall changes suggest that the cells can use different mechanisms to adapt to long-term stress.

We have compared data from databases and epidemiological studies to examine the expression of so-called hypertension signature genes[43,44,167]. The results are scientifically intangible due to the

immense number of indefinable parameters, so we will refrain from including this purely theoretical analysis as a preliminary outcome in this work.

In order to better characterize the biomechanical effect of the mechanical stimulus, we have specifically studied the transcriptional level and specific genes that have served as indicators for a mechanobiological reaction. In general, a stress-induced signature was already apparent in the correlation between the amount of isolated RNA and stimulation duration. A significant impact on the total gene expression could be shown by microarray analysis. The statistics showed at a glance that 118 genes were expressed differently after three days and 1208 genes after five days [Figure 44].

The genes MMP2 and MMP9 were of particular interest because their expression is triggered by mechanical stimulation. MMPs are responsible for the restructuring of the extracellular matrix and thus crucial for the mechanical integrity and stress capacity of the cell. Through the activity of both MMP proteins, it can be assumed that the ECM is mechanically adapted and reconfigured by the cells. It should also be considered that the cells re-modulate the ECM to such an extent that they are ideally able to distribute tensions to the ECM. The importance of the immense influence of these and other non-contractile structures becomes especially evident in the experiments [Figure 34; Figure 35], in which the cellular tension can only be decreased by a few percentages below the initial mechanical stress. With regard to ECM development and restructuring, the expression of P4H α 1 plays an essential role since the expression of the gene is directly related to collagen production [208]. Based on these results, it can be assumed that additional collagen and other ECM components are produced, triggered by the increased mechanical load. These adaptation mechanisms are also described in the literature, which leads to solidification and narrowing of the vascular lumens, in particular, due to increased pressure and vascular stretching [231]. This assumption is supported above all by the results in Figure 37, by the measurable offset of both signals, over time. Furthermore, it is also supported by the results in Figure 42, whereby the mechanical contraction on the active ingredients increases significantly after several days of mechanical stimulation. That the effects are not exclusively due to the development of ECM cannot be shown. Therefore, we assume a cumulative effect of the observed parameters. Nevertheless, the structure and plasticity of the ECM contribute significantly to the cellular force generation [232]. Assuming different firmness of the ECM, cell tensions are facilitated by an increased condensation and stiffness of the ECM and cell tensions by shortening the cells [Figure 55].

Filamin-A is responsible for the direct coupling to the pericellular matrix [233]. The qPCR analysis showed a substantial increase in gene expression after three days of mechanical stimulation [Figure 46]. Filamin-A serves as a cross-linker of the contractile apparatus and the coupling of the cell to the surrounding tissue [234,235]. Although filamin-A is not directly part of the contractile apparatus, it plays a major role in mechanical transduction and cellular strength. In addition, it also appears to have a protective function via beta-1-integrin, which protects the cells from mechanical stress [236].

Also of interest are the genes *P38* and *JNK1*, which are also triggered by various stimuli and especially mechanical stress, promote the transmission of stress signals. The expression of both genes can lead to an excessive sensitization of the cell, which causes the biomechanical homeostasis of the haSMC to become unbalanced. This could play a critical role in the pathogenesis of hypertension and vascular hardening with respect to basal cellular tone and reduction of depolarization potential [237–239].

In addition to structural and morphological cellular adaptation, also the regulation of the receptors and ion channels cannot be excluded [15,60,240,241]. As a result of such an adjustment, the sensitivity of the cell is increased and the ion exchange can be accomplished faster and more intensively.

The expression profile of selected channels and receptors, which are significantly involved in cellular contraction listed in 5.12.2, shows a distinct impact by the mechanical stimulation. In particular, the

androgenic receptor *ADRA1A* and the Ca^{2+} ion channel *CACNA1C* show an increased expression after five days of mechanical stimulation. Both genes' expression level is also slightly elevated in the multiarray analysis but does not exceed the significance level threshold.

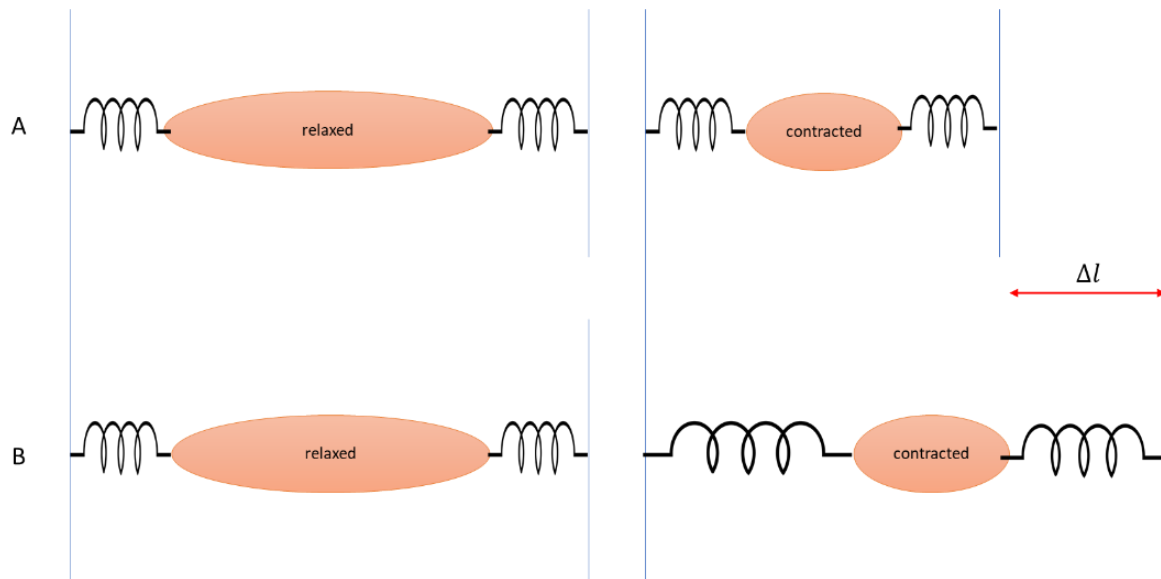


Figure 55 Strongly simplified model for a simplified representation of how different ECM densities can affect the tissue's resulting shortening with identical cellular contraction. $E\text{-modulusECM}(A) > E\text{-modulusECM}(B)$; $\Delta l_{\text{Cell}}(A) = \Delta l_{\text{Cell}}(B)$. Due to the rigid ECM in (A), the entire length of the model is shortened by the cellular contraction. In contrast, the soft ECM in (B) compensated for the shortening of the cell by expanding and thus compensates for the shortening of the entire model.

Functionally, the two results were verified by pharmacological measurements [Figure 28; Figure 32]. The biomechanical effect of NE and Bay-K8644 increases with the number of mechanical stimulation intervals [Figure 42]. However, taking into account the other adaptation and parameters Furthermore, it is also supported by the results in, the sensitization of the cell to the two substances cannot be exclusively attributed to the upregulation of both channels.

From all the data, it can be shown that the biomechanics of the cell model is significantly influenced by the soft growth environment and the additional mechanical stimuli. Both the contractile force of the cells and the basal tension of the monolayer are increased by cellular remodeling of the contractile apparatus, cellular differentiation and enhanced cellular integration. In order to investigate a pathological development of the cell model, specific parameters have to be defined, which will be analyzed under consideration of the mechanobiological events examined in this study.

7.3. Co-Cultivation and Arrangement of haSMC and haEC

Under the objective of designing a functional vascular cell model for CellDrum, the two essential cell types of the vascular system haSMC and haEC were cultivated together. The interaction of EC and SMC regulates both temporary and long-term changes in blood pressure. The cellular combination, interplay and the physiological proximity of the cells make this part of the work an important point, as substance mechanisms and effects, may vary depending on the cellular composition.

The various approaches to implement a three-dimensional structured and direct co-culture were based on models from the literature [Figure 56]. Primarily, the method of Robert A. Brown was used for the ultra-fast production of collagen-based sheets, as it was already successfully used on the CellDrum [125,242]. The production turned out to be complicated and error-prone. The condensation of the

collagen gels reduced the thickness of the sample to a theoretically evaluable thickness around 200µm. At the same time, its strength increased dramatically and no measurable cell force changes were resolvable. The collagen Type-I layer of a few tenths of a millimeter produced by the process seems to require a significantly higher cell count to achieve measurable results. Besides, cellular distribution and vitality can only be estimated using light microscopy and cannot be precisely controlled. In addition, the layer thickness and homogeneity of the collagen gel could not be precisely defined.

Another intensively researched approach dealt with the separation of two monolayers of haSMC and haEC using a sandwich coating of poly-l-lysine and fibronectin[243]. This method was not successful because the lengthy process sharply restricted cell vitality.

A method described by Mark D. Lavender provides for direct cultivation of both cell types separated by a layer of fibronectin and collagen IV [244]. This method seemed to be the most sensible, as the sample rigidity was not significantly more affected by the coating of fibronectin and collagen type IV, compared to the monolayer model. Also, the cultivation of the EC necessarily requires a collagen TypeI/TypeIV coating and the SMC monolayer was already produced in the SOP with the Fibronectin sandwich technique to have a better cell attachment to mechanical stimuli.

Based on the results shown in *Figure 49*, we were able to show that the co-cultivation of both cell types is possible, even if this is initially only temporary. We assume that the lack of the necessary endothelial and fibroblast growth factors will lead to a further haEC detachment over time *Figure 48*. With the help of immunocytochemistry staining, we were able to demonstrate the combined cultivation of haSMC and haEC. However, it was not satisfactorily possible for us to represent the cellular arrangement according to the physiological vascular model.

The time-consuming and challenging quality control of the sample makes the co-culture at present a not yet usable concept for the CellDrum technology. Too many parameters cannot currently be estimated to reproduce the measurement reliably. As long as the control of the sample requires fixation of the cells, we consider the model unsuitable due to the inestimable variables. Nevertheless, this problem can be brought to a successful model based on the obtained data

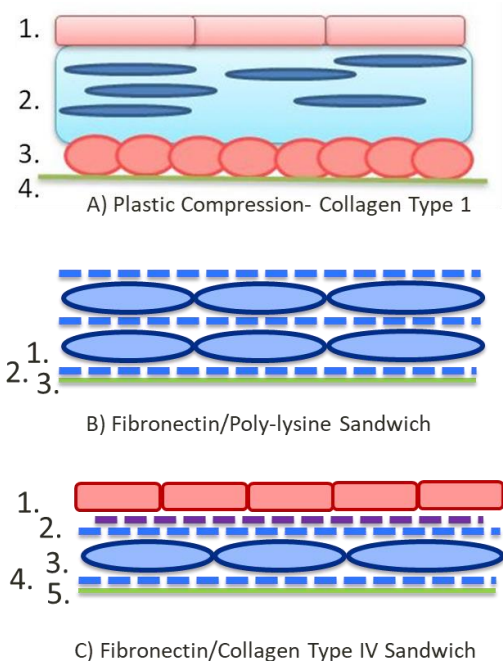


Figure 56 Listing of different tested co-culture models.

A) Co-culture arrangement based on a condensed collagen type I gel (1) haEC (2) Collagen type I gel with haSMC (3)Fibronectin and biofunctionalization (4) CellDrum Membrane

B) Co-culture without gel structure, layered from alternating layers of fibronectin and poly-lysine (1) haSMC with polylysine (2) fibronectin (3) CellDrum Membrane

C) Co-culture arrangement of fibronectin and collagen type IV sandwich (1) haEC (2) Collagen IV and Fibronectin Coating (3) haSMC (4)Fibronectin Coating (5) CellDrum Membrane.

In order to simplify the experimental design and to collect more reliable data, both cell types were evaluated separately. Both models have been described in detail, in which the cellular distribution and

cell tension was analyzed[Figure 26]. The focus of the vasoactive functionality was tested on haSMC. Nevertheless, the effect of haEC on haSMC was estimated by the experimental arrangement of indirect co-cultures, as well.

The results from *Figure 50* have shown that vasoactive substances must already be present in the conditioned medium, which has led to an increase in the haSMC initial tension. As the addition of conditioned medium causes an increased cellular tone, we instead assume that this effect is caused by vasoconstrictive substances like ET1 and or AT2. The production of eNOs cannot be excluded[212,245], but the nitric oxide-induced effect has already been shown to relax smooth muscle cells[Figure 31]. However, the effect was only small and would have been compensated by the presence of the two vaso constructive agents. Besides, eNO is very unstable in a liquid solution and decays within a few seconds, which could have also lead to a possible distortion of the results.

ET1 shows a strong contracting effect on haSMC in *Figure 32*. The secretion of ET1 by endothelial cells is permanent and even accelerated by mechanical stimuli[55,246,247]. We were able to demonstrate this by ELISA as well as that the concentration of ET1 increases depending on the mechanical stimulation. Independent of this, a measurable amount of ET1 is already measurable in the unstimulated sample. The measured ET1 concentration is approximately 0.032nM, which could be responsible for the haSMC tone deviation[214,215].

In the end, we would expect an increase in the basal mechanical tension due to the combined cultivation of both cell types. The effect of the eNOs under culture conditions cannot be estimated at this point due to extremely short half-life in aqueous solution and difficult to estimate quantities [175]. The measured magnitude of the data of NO donors, ET1 and AT2 support the assumption.

7.4. Application for Medical Laboratory Screening

In order to test the potential application of the CellDrum system as a screening and diagnostic tool for clinical research and blood sera screening, sera from the athlete who was exposed to physiological stress were applied to the CellDrum models.

Blood plasma consists of numerous components, which in themselves already influence the tone of the smooth muscles. Besides the plasma proteins globulins and albumins, there are also numerous other biochemical substances, catecholamine, and ions with vasoactive properties. Taking these substances into account, the increase in cellular tone after the addition of the serum control is evident.

Since the exact concentrations of cell culture medium and growth factors are not available from the manufacturers and the test sera have not been further investigated in the laboratory, functional biomechanical changes in composition and concentration dependencies cannot be excluded.

It can be assumed that the ingredients of the growth serum used for the cultivation differ fundamentally from the serum obtained from the test person. Thus, even marginal concentration inhomogeneities can lead to a change in cell tension[248]. Since these changes are relatively small, the primary stimulation by the cell culture medium can be determined. Thus, it can be assumed that the tonus change is increased if the cells have been previously cultivated in serum-free medium and starved conditions[198].

Physical exercise causes the hormone level in the blood serum to rise. Especially the concentration of growth hormones, insulin-like growth factor 1, testosterone, cortisol and catecholamines are increased[48,249]. In particular, catecholamines release leads to a corresponding adjustment of the blood flow by blood vessel relaxation[250]. In contrast to the physiological mechanism of NE, we have

already shown in pharmacological studies that the effect of NE on SMC without endothelium has the opposite effect [251]. From this, we conclude that the increased hormone level, in addition to the increased stress change through the test person's serum, leads to an amplified increase of the cell tone.

The second experimental run was carried out according to precisely the same protocol, except that the volunteer was given a dose of L-citrulline and L-arginine in advance. Both substances are non-essential amino acids and are used in sports nutrition as performance-enhancing supplements. L-citrulline occurs as a by-product of L-arginine's nitric oxide production, resulting in a vasodilating and blood circulation-enhancing effect[252,253]. The combination of these substances leads, on the one hand, to an effective enhancement since the addition of citrulline increases the body's synthesis of arginine and additionally enhances its bioavailability[254,255].

The vasodilating effect of both administered substances also seems to be measurable in the blood serum using the CellDrum model. Taking into account the previously measured increase in tone due to the addition of blood sera, a significant decrease in mechanical tension due to the supplementation is evident.

In the body, the vasodilatory effect is realized via the pathway of endothelial nitric oxide release, which is primarily made possible by the action of vascular endothelium. The strongly measurable SMC relaxation could thus be explained by the increased release of eNOs of the proband during physical stress. However, this would require very high stability of the eNOs, so that it does not disintegrate during sample preparation. On the other hand, citrulline can lead to endothelial-independent relaxation [256] and L-arginine can lead to the production of cGMPs, which increases the sensitivity to eNOs and also has an endothelium-independent relaxing effect on smooth muscle cells [151,257].

The effect of dietary supplements can also be seen in the ECG monitoring of the volunteer[Figure 37]. In direct comparison with the previous run, the intake of the supplements results in a reduction of blood pressure with a slightly increased heart rate.

The dilative effect is comparatively low in contrast to the other substances. Still, it has to be taken into account that the relaxing effect needs to compensate for the contractive effects, which have been shown by the sera only measurements as well. Therefore, a baseline shift must be considered so that it can be assumed that the supplemented blood serum would have a much stronger relaxing effect under better-defined conditions.

7.5. Methodical Discussion

State of the art technology used in this work combines much of the technology and knowledge gained from the last 20 years of CellDrum development. Due to the resulting data, the CellDrum technology has been established as a precise measurement method with versatile types of applications.

Due to geometric adaptation of the CellDrum2017, it leads to demonstrably less cell detachment and a far more stable mechanical signal on repeated measurements. Too small dimensioned tolerances led to a variation of CellDrum membrane residual stress, by repeated analysis and placement into the TTA. The detachment of the cells seems to have been a consequence of the resulting changes in membrane tension. The new dimension of the CellDrums helped to keep the residual stress of the membrane stable unaffiliated from the measurement cycles.

By using PEEK as CellDrum body material, high-temperature resistance, biocompatible thermoplasticity, and the form stability of the CellDrum was highly increased. Thus, the mechanical influence of geometric changes through repeated autoclaving and cleaning of the CellDrum can be

excluded. The high dimensional stability also ensures the consistent biaxial stress distribution of the membranes. Only this allows a uniform cellular stress distribution and prevents the formation of mechanical preferential directions.

By characterizing the membranes concerning their thickness and mechanical properties, it is possible to eliminate further variation, affecting measurement results and integrating the gained knowledge of membrane properties into the manufacturing process.

The characterization of the membrane allows adjusting both the thickness and the mechanical strength to the respective application's physiological parameters. Based on the characterization data obtained from hundreds of manufactured CellDrums, it can be concluded that the layer thickness does not necessarily correlate with the mechanical strength of the membranes. Therefore, the initial membrane tension must be measured before each measurement to enable a standardized measurement.

In addition to the physiological approximation, the membrane characteristics determined for this study also have reasons for their handling. The production process has been optimized so that the membranes can be produced as soft as possible with consistent quality and with as few defect productions as possible. In this way, the membranes can be manufactured with mechanical stress of about 100kPa residual stress. Compared to the rigidity of real vascular tissue, the mechanical properties depend strongly on the vessel segment and particular function. However, coated and cultured CellDrum having residual stress of about 50kPa and are in a tissue-like range in terms of physiological conditions [67–69]. Compared to a disposable cell culture dish made of polystyrene, having mechanical stress around 1000 MPa (DIN 53457), cells experience a >2000-fold change in the ambient tension after passaging. This immense change of the mechanical culture conditions seems to have such a strong influence on the mechanobiology of the cells that this could be an independent part of a follow-up study.

The geometry of the deflected CellDrum membrane is considered a spherical segment to apply the described physical model. Due to the medium's hydrostatic pressure, it can be assumed that the membrane deforms in a parabolic deflection. Taking into account the investigations of J. Trzewik [117] on the stress curve of the CellDrum membrane, the idealized assumption is correct for small deformations. The deformations generated by the PulSElect system are not in the range of considerable small deformations, so the spherical model is no longer applicable. The deformations induced by the PulSElect system can be better described as parabolic deformations. This results in minimal inhomogeneities of membrane stress and globally calculated has a minimally smaller strain on the entire sample than estimated in the idealized model.

In terms of system adaptation, the final iteration of the TTA is fully automated. Its measurement cycles are optimally configured to measure contractive tissue with significant consideration of cell viability. A dramatic reduction of the measurement inflation time from 30 to 12 s ($20\mu\text{L}_{\text{Air}}/\text{s}$) accelerated the measurement and prevented overstretching of the cells, which has often led to cell detachment and monolayer rupture. Measurement shortening made the repetition of measures and subsequent serial measurements possible. However, it should be noted that the interpretation of the acquired data must be inverted. Since the sample is no longer inflated to positive strain, as the measurement ends shortly after the transition from the membrane zero deflection point.

8. Conclusion

The work shows the establishment of a human arterial *in-vitro* model, which allows the analysis of mechanobiological phenomena and the functional testing of vasoactive substances.

The application of vasoactive substances with different mechanisms of action has confirmed that the developed vascular model, consisting of primary arterial smooth muscle cells, represents biomechanical effects physiologically and functionally. Furthermore, the *in-vitro* model allows for resolving these effects as a function of time and concentration. The majority of the tested substances yielded physiologically plausible biomechanical results, leading to mechanical tension alterations of -6% up to +10%, relative to the initial stress (50kPa). However, there seems to be an unexplained problem with the measurement of NO-induced relaxation. This should be further clarified in the following, whether this is a biochemical or purely technical problem.

For the development of a hypertension disease model, the PulSElect system was designed. This, which exposes the vascular models to defined cyclic mechanical stress to induce pathological cell alterations similar to mechanical stress-induced hypertension. In combination with the CellDrum technology, morphological as well as biochemical and transcriptomic cell adaptations could be evaluated and biomechanically correlated. With regard to the increase of cellular tone, cell differentiation markers and cytoskeletal transformations show that cellular differentiation is favored by the mechanical stimulation and the growth environment of the CellDrum. In addition, these results raise further exciting questions concerning time-dependent cellular development, which should be investigated under a newly formulated hypothesis.

Ultimately, the development of a disease model cannot be precisely defined and, therefore, does not allow a clear statement about the model of the presented work. Nevertheless, biomechanical and cellular responses at several cellular levels have been identified that have significantly influenced the samples' properties and may already show possible tendencies of pathological changes.

Two cell culture models were established, and the foundation for a co-culture model was laid, which meet the physical requirements of the CellDrum technology and thus allow reliable biomechanical measurements. The results of the work show that the co-cultivation of haEC and haSMC is possible and that they can also be arranged within CellDrum using the described method. However, due to the highly time and cost-consuming quality control of the three-dimensional co-culture, we cannot speak of an established 3D CellDrum co-culture model yet and retain the right to discuss the biomechanical results at this point. CellDrum technology, as a methodically established measuring procedure, currently provides excellent research potential. Directly related to the work, all that is now required is a fast and precise evaluation procedure to check 3D co-cultures for quality and goodness to perform further biomechanical analyses using haSMC and haEC.

Last but not least, the investigation of blood sera suggests that the CellDrum could be used for pharmacological development and testing as well as a potential screening method for medical and clinical laboratories. The already developed haSMC model should be tested for further clinical investigations, sera from healthy individuals and patients with cardiovascular diseases so that indicators for hypertension patients can already be identified. Moreover, sports medicine studies could be supported by CellDrum generated data. Studies that demonstrate the effects of different training conditions, diets and lifestyles could be functionally proven *in-vitro*.

This research's biological and systematic developments make the CellDrum technology a precise and standardized measurement method for the biomechanical analysis of human vascular cell models. In particular, the introduction of a CellDrum quality management concept allows repeatable and comparable determination of even the smallest cell force deviations (<50 μ N). Due to the precise

characterization and easy handling of the CellDrums, the vascular models would be ideally suited for long-term pharmacological or mechanobiological studies. Even if this work could already extend sample observation from a few minutes to several days, interesting effects from long-term medication and stimulation over months could also be expected.

In the future, hPSC-derived vascular cells derived from hypertension patients could also be used to develop and study individual disease models based on existing or induced genetic defects. These and other modified in vitro models could be further investigated with the developed CellDrum and PulSElect system combined with conventional electrophysiological, molecular biological and fluorescent imaging techniques to answer crucial mechanobiological questions in physiological and pathophysiological developments and to understand their functional and physical implications.

9. References

- 1 Vaupel P, Schaible HG, Mutschler E. Anatomie, Physiologie, Pathophysiologie des Menschen - Kapitel 9 Gefäßsystem und Blutkreislauf. 7. Edit. abavo Wissenschaftliche Verlagsgesellschaft mbH; 2015.
- 2 Bartels R, Bartels H. Stoffaufnahme, Transport und Ausscheidung. In: Jürgens PKD, editor. Physiologie - Lehrbuch der Funktionen des menschlichen Körpers. , 7th ed. Elsevier; 2004; pp 72–233.
- 3 B.H Derrickson, Tatora G. Anatomie und Physiologie. 11. Aufag. Weinheim: Wiley-Blackwell; 2006.
- 4 Robertson AM, Watton PN. Mechanobiology of the Arterial Wall. *Transp Biol Media*. 2013;275–347.
- 5 Tsai AG, Friesenecker B, Cabrales P, Hangai-Hoger N, Intaglietta M. The vascular wall as a regulator of tissue oxygenation. *Curr Opin Nephrol Hypertens*. 2006;15(1):67–71.
- 6 Hsieh H-J, Liu C-A, Huang B, Tseng AH, Wang DL. Shear-induced endothelial mechanotransduction: the interplay between reactive oxygen species (ROS) and nitric oxide (NO) and the pathophysiological implications. *J Biomed Sci*. 2014;21(1):1–15.
- 7 Shweiki D, Itin a, Soffer D, Keshet E. Vascular endothelial growth factor induced by hypoxia may mediate hypoxia-initiated angiogenesis. *Nature*. 1992;359(6398):843–5.
- 8 Ostrow LW, Suchyna TM, Sachs F. Stretch induced endothelin-1 secretion by adult rat astrocytes involves calcium influx via stretch-activated ion channels (SACs). *Biochem Biophys Res Commun*. 2011 Jun;410(1):81–6.
- 9 Castellot JJ, Favreaug L V, Karnovskys MJ, Rosenbergfjgll RD. Inhibition of Vascular Smooth Muscle Cell Growth by Endothelial Cell-derived Heparin - possible role of a platelet endoglycosidase. *J Biol Chem*. 1982;257(19):11256–60.
- 10 Lindner V, Olson NE, Clowes AW, Reidy MA. Inhibition of smooth muscle cell proliferation in injured rat arteries- Interaction of heparin with basic fibroblast growth factor. *JCI*. 1992;90:2044–9.
- 11 Shadwick RE. Mechanical design in arteries. *J Exp Biol*. 1999;202(Pt 23):3305–13.
- 12 Sung YK, Chung L. Connective tissue disease-associated pulmonary arterial hypertension. *Rheum Dis Clin North Am*. 2015 May;41(2):295–313.
- 13 Akagi S, Matsubara H, Nakamura K, Ito H. Modern treatment to reduce pulmonary arterial pressure in pulmonary arterial hypertension. *J Cardiol*. 2018 Jun DOI: 10.1016/J.JJCC.2018.04.014
- 14 Mutschler E, Geisslinger G, Kroemer H k., Ruth P, Schäfer-Korting M. Arzneimittelwirkungen - Lehrbuch der Pharmakologie und Toxikologie. 9th ed. Wissenschaftliche Verlagsgesellschaft mbH Suttgart; 2008.
- 15 Shaw A, Xu Q. Biomechanical Stress-induced Signaling in Smooth Muscle Cells: An Update. *Curr Vasc Pharmacol*. 2005;1(1):41–58.
- 16 Olschewski H. Pulmonale Hypertonie. 2013 Jun;10(S1):53–7.
- 17 Lumb AB, Horncastle E. Pulmonary Physiology. *Pharmacol Physiol Anesth*. 2019 Jan;586–612.
- 18 Lehoux S, Tedgui A. Cellular mechanics and gene expression in blood vessels. *J Biomech*. 2003 May;36(5):631–43.

- 19 Haga JH, Li Y-SJ, Chien S. Molecular basis of the effects of mechanical stretch on vascular smooth muscle cells. *J Biomech.* 2007;40(5):947–60.
- 20 Jufri NF, Mohamedali A, Avolio A, Baker MS. Mechanical stretch : physiological and pathological implications for human vascular endothelial cells. *Vasc Cell.* 2015;1–12.
- 21 Greiner AM, Biela SA, Chen H, Spatz JP, Kemkemer R. Temporal responses of human endothelial and smooth muscle cells exposed to uniaxial cyclic tensile strain. *Exp Biol Med (Maywood).* 2015;1535370215570191.
- 22 Zemel A, De R, Safran SA. Mechanical consequences of cellular force generation. *Curr Opin Solid State Mater Sci.* 2011;15(5):169–76.
- 23 Liu Z, Khalil RA. Evolving mechanisms of vascular smooth muscle contraction highlight key targets in vascular disease. *Biochem Pharmacol.* 2018 Jul;153:91–122.
- 24 Di Salvo J, Raatz Nelson S. Stimulation of G-protein coupled receptors in vascular smooth muscle cells induces tyrosine kinase dependent increases in calcium without tyrosine phosphorylation of phospholipase C γ -1. *FEBS Lett.* 1998 Jan;422(1):85–8.
- 25 Jonas O, Duschl C. Force propagation and force generation in cells. *Cytoskeleton.* 2010;67(9):555–63.
- 26 Wynne BM, Chiao CW, Webb RC. Vascular smooth muscle cell signaling mechanisms for contraction to angiotensin II and endothelin-1. *J Am Soc Hypertens.* 2009;3(2):84–95.
- 27 Webb RC. Smooth muscle contraction and relaxation. *Am J Physiol - Adv Physiol Educ.* 2003;27(1–4):201–6.
- 28 Pollard TD, Earnshaw WC. *Cell Biology.* 2. Edition. Spektrum; 2007.
- 29 Jackson WF. Ion channels and vascular tone. *Hypertens (Dallas, Tex 1979).* 2000;35(1 Pt 2):173–8.
- 30 Li C, Xu Q. Mechanical stress-initiated signal transduction in vascular smooth muscle cells in vitro and in vivo. *Cell Signal.* 2007 May;19(5):881–91.
- 31 Karaki H, Urakawa N, Kutsky P. Potassium-induced contraction in smooth muscle. *Nihon Heikatsukin Gakkai Zasshi.* 1984;20(6):427–44.
- 32 Muscle S, Channels I, Arteries R. Smooth Muscle Ion Channels and Regulation of Vascular Tone in Resistance Arteries and Arterioles. 2018;7(2):485–581.
- 33 Butler MG. Genetics of hypertension • current status. *J Med Liban.* 2010;58(3):175–8.
- 34 M.Fromm, K.Hierholzer. Stoffaufnahme und Ausscheidung. In: Schmidt, Thews, Lang, editors. *Physiologie des Menschen.* , 28th ed. Springer; 2000; p 760.
- 35 G.Löffler, A.Hasilik. *Biochemie und Pathobiochemie.* 7th ed. Springer; 2003.
- 36 Grillo A, Salvi L, Coruzzi P, Salvi P, Parati G. Sodium intake and hypertension. *Nutrients.* 2019;11(9):1–16.
- 37 Maguire JJ, Davenport AP. Endothelin Receptors and Their Antagonists. *Semin Nephrol.* 2015;35(2):125–36.
- 38 Ishikawa S, Miyauchi T, Sakai S, Ushinohama H, Sagawa K, Fusazaki N, et al. Elevated levels of plasma endothelin-1 in young patients with pulmonary hypertension caused by congenital heart disease are decreased after successful surgical repair. *J Thorac Cardiovasc Surg.* 1995 Jul;110(1):271–3.

- 39 Lin Y-J, Kwok C-F, Juan C-C, Hsu Y-P, Shih K-C, Chen C-C, et al. Angiotensin II enhances endothelin-1-induced vasoconstriction through upregulating endothelin type A receptor. *Biochem Biophys Res Commun*. 2014 Aug;451(2):263–9.
- 40 Thomas RM. Endocrine hypertension: An overview on the current etiopathogenesis and management options. *World J Hypertens*. 2015;5(2):14.
- 41 O’Shea PM, Griffin TP, Fitzgibbon M. Hypertension: The role of biochemistry in the diagnosis and management. *Clin Chim Acta*. 2017 Feb;465:131–43.
- 42 Huan T, Esko T, Peters MJ, Pilling LC, Schramm K, Schurmann C, et al. A Meta-analysis of Gene Expression Signatures of Blood Pressure and Hypertension. *PLoS Genet*. 2015;11(3):1–29.
- 43 Jacob JJ, Lindpaintner K, Lincoln SE, Kusumi K, Bunker RK, Mao YP, et al. Genetic mapping of a gene causing hypertension in the stroke-prone spontaneously hypertensive rat. *Cell*. 1991;67(1):213–24.
- 44 Cowley AW. The genetic dissection of essential hypertension. *Nat Rev Genet*. 2006;7(11):829–40.
- 45 Friedman EB, Palevsky HI, Taichman DB. *Pulmonary Vascular Disease*. Elsevier; 2006. DOI: 10.1016/B978-1-4160-2246-6.50011-0
- 46 Humphrey JD, Harrison DG, Figueroa CA, Lacolley P, Laurent S. Central Artery stiffness in hypertension and aging a problem with cause and consequence. *Circ Res*. 2016;118(3):379–81.
- 47 Marini M, Carpi S, Bellini A, Patalano F, Mattoli S. Endothelin-1 induces increased fibronectin expression in human bronchial epithelial cells. *Biochem Biophys Res Commun*. 1996 Mar;220(3):896–9.
- 48 Kraemer WJ, Ratamess NA. Hormonal responses and adaptations to resistance exercise and training. *Sport Med*. 2005;35(4):339–61.
- 49 Marín J, Encabo A, Briones A, García-Cohen E-C, Alonso MJ. Mechanisms involved in the cellular calcium homeostasis in vascular smooth muscle: Calcium pumps. *Life Sci*. 1998 Dec;64(5):279–303.
- 50 Wang W, Watanabe M, Nakamura T, Kudo Y, Ochi R. Properties and expression of Ca²⁺-activated K⁺ channels in H9c2 cells derived from rat ventricle. *Am J Physiol*. 1999 May;276(5 Pt 2):H1559-66.
- 51 Stra M, Direktor S, Doktor G, Gradi TA, Prof I. Einfluss mechanischer Dehnung auf das Wachstum vaskulärer glatter Muskelzellen des Menschen. 1976
- 52 Atala A, Lanza R, Thomson JA, Nerem R, Boerckel JD, Gemmiti C V., et al. *Principles of Regenerative Medicine*. Elsevier; 2011. DOI: 10.1016/B978-0-12-381422-7.10028-8
- 53 Brown TD. Techniques for mechanical stimulation of cells in vitro: a review. *J Biomech*. 2000 Jan;33(1):3–14.
- 54 Qiu J, Zheng Y, Hu J, Liao D, Gregersen H, Deng X, et al. Biomechanical regulation of vascular smooth muscle cell functions: From in vitro to in vivo understanding. *J R Soc Interface*. 2014;11(90). DOI: 10.1098/rsif.2013.0852
- 55 Anwar MA, Shalhoub J, Lim CS, Gohel MS, Davies AH. The effect of pressure-induced mechanical stretch on vascular wall differential gene expression. *J Vasc Res*. 2012;49(6):463–78.
- 56 Korff T, Kimmina S, Martiny-Baron G, Augustin HG. Blood vessel maturation in a 3-dimensional spheroidal coculture model: direct contact with smooth muscle cells regulates endothelial cell quiescence and abrogates VEGF responsiveness. *FASEB J*. 2001 Mar;15(2):447–57.

- 57 Ayoubi S, Sheikh SP, Eskildsen T V. Human induced pluripotent stemcell-derived vascular smooth muscle cells: Differentiation and therapeutic potential. *Cardiovasc Res.* 2017;113(11):1282–93.
- 58 Rensen SSM, Doevendans PAFM, Eys GJJM Van. Regulation and characteristics of vascular smooth muscle cell phenotypic diversity. 2007;15(3):100–8.
- 59 Gomez D, Owens GK. Smooth muscle cell phenotypic switching in atherosclerosis. *Cardiovasc Res.* 2012;95(2):156–64.
- 60 Zhuang J, Yamada KA, Saffitz JE, Kleber AG. Pulsatile stretch remodels cell-to-cell communication in cultured myocytes. *Circ Res.* 2000;87(4):316–22.
- 61 Salameh A, Dhein S. Effects of mechanical forces and stretch on intercellular gap junction coupling. *Biochim Biophys Acta - Biomembr.* 2013;1828(1):147–56.
- 62 Parandakh A, Tafazzoli-Shadpour M, Khani MM. Stepwise morphological changes and cytoskeletal reorganization of human mesenchymal stem cells treated by short-time cyclic uniaxial stretch. *Vitr Cell Dev Biol - Anim.* 2017;53(6):547–53.
- 63 Wanjare M, Agarwal N, Gerecht S. Biomechanical strain induces elastin and collagen production in human pluripotent stem cell-derived vascular smooth muscle cells. *Am J Physiol Cell Physiol.* 2015;309(4):C271-81.
- 64 Dhein S, Schreiber A, Steinbach S, Apel D, Salameh A, Schlegel F, et al. Mechanical control of cell biology. Effects of cyclic mechanical stretch on cardiomyocyte cellular organization. *Prog Biophys Mol Biol.* 2014;115(2–3):93–102.
- 65 Salacinski HJ, Goldner S, Giudiceandrea A, Hamilton G, Seifalian AM, Edwards A, et al. The mechanical behavior of vascular grafts: A review. *J Biomater Appl.* 2001;15(3):241–78.
- 66 Pashneh-Tala S, MacNeil S, Claeysens F. The tissue-engineered vascular graft - Past, present, and future. *Tissue Eng - Part B Rev.* 2016;22(1):68–100.
- 67 Holzapfel GA. Biomechanics of Soft Tissue. *J Biomech.* 2011;1(1):149–54.
- 68 Stålhand J, Klarbring A, Holzapfel GA. The mechanics of arteries including smooth muscle contraction. *J Biomech.* 2006 Jan;39:S326.
- 69 Humphrey JD, Holzapfel GA. Mechanics, mechanobiology, and modeling of human abdominal aorta and aneurysms. *J Biomech.* 2012 Mar;45(5):805–14.
- 70 Sommer G. *Mechanical Properties of Healthy and Diseased Human Arteries.* 2008.
- 71 Skrzypiec-Spring M, Grotthus B, Szelag A, Schulz R. Isolated heart perfusion according to Langendorff-Still viable in the new millennium. *J Pharmacol Toxicol Methods.* 2007;55(2):113–26.
- 72 Rameshrad M, Babaei H, Azarmi Y, Fouladi DF. Rat aorta as a pharmacological tool for in vitro and in vivo studies. *Life Sci.* 2016 Jan;145:190–204.
- 73 Kee H Do, Min SK, Jae HK, Rhim BY, Won SL, Chi DK, et al. Angiotensin II-induced aortic ring constriction is mediated by phosphatidylinositol 3-kinase/L-type calcium channel signaling pathway. *Exp Mol Med.* 2009;41(8):569–76.
- 74 Rocha ML, Bendhack LM. Relaxation evoked by extracellular Ca²⁺ in rat aorta is nerve-independent and involves sarcoplasmic reticulum and L-type Ca²⁺ channel. *Vascul Pharmacol.* 2009;50(3–4):98–103.
- 75 Bellacen K, Lewis EC. Aortic ring assay. *J Vis Exp.* 2009;(33):1–2.
- 76 Mogilner A, Oster G. Force generation by actin polymerization II: The elastic ratchet and tethered filaments. *Biophys J.* 2003;84(3):1591–605.

- 77 Freivalds A. Force measurements by micromanipulation of a single actin filament by glass needles. *Lett to Nat.* 1988;334(7):74–6.
- 78 Gayraud C, Borghi N. FRET-based Molecular Tension Microscopy. *Methods.* 2016;94:33–42.
- 79 Lim CT, Zhou EH, Quek ST. Mechanical models for living cells — a review \$. 2006;39:195–216.
- 80 Kasza KE, Rowat AC, Liu J, Angelini TE, Brangwynne CP, Koenderink GH, et al. The cell as a material DOI: 10.1016/j.ccb.2006.12.002
- 81 Polacheck WJ, Chen CS. Measuring cell-generated forces: A guide to the available tools. *Nat Methods.* 2016;13(5):415–23.
- 82 Addae-Mensah KA, Wikswo JP. Measurement techniques for cellular biomechanics in vitro. *Exp Biol Med.* 2008;233(7):792–809.
- 83 Sugimura K, Lenne PF, Graner F. Measuring forces and stresses in situ in living tissues. *Dev.* 2016;143(2):186–96.
- 84 Xiong Z, Sperelakis N. Regulation of L-type calcium channels of vascular smooth muscle cells. *J Mol Cell Cardiol.* 1995 Jan;27(1):75–91.
- 85 Mollaeian K, Liu Y, Bi S, Wang Y, Ren J, Lu M. Nonlinear Cellular Mechanical Behavior Adaptation to Substrate Mechanics Identified by Atomic Force Microscope. *Int J Mol Sci.* 2018;19(11):3461.
- 86 Zhang Y, Ng SS, Wang Y, Feng H, Chen WN, Chan-Park MB, et al. Collective cell traction force analysis on aligned smooth muscle cell sheet between three-dimensional microwalls. *Interface Focus.* 2014;4(2). DOI: 10.1098/rsfs.2013.0056
- 87 Akhtar R. In vitro characterisation of arterial stiffening: From the macro- to the nano-scale. *Artery Res.* 2014 Mar;8(1):1–8.
- 88 Grosberg A, Nesmith AP, Goss J a., Brigham MD, McCain ML, Parker KK. Muscle on a chip: In vitro contractility assays for smooth and striated muscle. *J Pharmacol Toxicol Methods.* 2012;65:126–35.
- 89 Yang S, Saif T. Micromachined force sensors for the study of cell mechanics. *Rev Sci Instrum.* 2005;76(4):1–8.
- 90 Wang JH-C, Goldschmidt-Clermont P, Yin FC-P. Contractility Affects Stress Fiber Remodeling and Reorientation of Endothelial Cells Subjected to Cyclic Mechanical Stretching. *Ann Biomed Eng.* 2000;28(10):1165–71.
- 91 Matheson LA, Jack Fairbank N, Maksym GN, Paul Santerre J, Labow RS. Characterization of the Flexcell™ Uniflex™ cyclic strain culture system with U937 macrophage-like cells. *Biomaterials.* 2006 Jan;27(2):226–33.
- 92 Quinlan AM, Sierad LN, Capulli AK, Firstenberg LE, Billiar KL. Combining dynamic stretch and tunable stiffness to probe cell mechanobiology in vitro. *PLoS One.* 2011;6(8). DOI: 10.1371/journal.pone.0023272
- 93 Tierversuche in der Forschung : Das 3R-Prinzip und die Aussage- kraft wissenschaftlicher Forschung. Handreichung der Ständigen Senat für tier Exp Forsch der DFG zur Plan und Beschreibung tierexperimenteller Forschungsprojekte. 2019;1. Available from: https://www.dfg.de/download/pdf/dfg_im_profil/geschaeftsstelle/publikationen/handreichung_sk_terversuche.pdf
- 94 Swartz DD, Andreadis ST. Animal models for vascular tissue-engineering. *Curr Opin Biotechnol.* 2013;24(5):916–25.

- 95 Huberts W, Heinen SGH, Zonnebeld N, van den Heuvel DAF, de Vries J-PPM, Tordoir JHM, et al. What is needed to make cardiovascular models suitable for clinical decision support? A viewpoint paper. *J Comput Sci.* 2017 DOI: <https://doi.org/10.1016/j.jocs.2017.07.006>
- 96 Wolf F, Vogt F, Schmitz-Rode T, Jockenhoevel S, Mela P. Bioengineered vascular constructs as living models for in vitro cardiovascular research. *Drug Discov Today.* 2016;21(9):1446–55.
- 97 Boisen L, Drasbek KR, Pedersen AS, Kristensen P. Evaluation of endothelial cell culture as a model system of vascular ageing. *Exp Gerontol.* 2010 Oct;45(10):779–87.
- 98 Davies PF, Truskey GA, Warren HB, Oconnor SE, Eisenhaure BH. Metabolic Cooperation between Vascular Endothelial-Cells and Smooth-Muscle Cells in Co-Culture - Changes in Low-Density Lipoprotein Metabolism. *J Cell Biol.* 1985;101(3):871–9.
- 99 Kretzmer G, Schügerl K. Response of mammalian cells to shear stress. *Appl Microbiol Biotechnol.* 1991;34(5):613–6.
- 100 Ye GJC, Nesmith AP, Parker KK. The role of mechanotransduction on vascular smooth muscle myocytes cytoskeleton and contractile function. *Anat Rec.* 2014;297(9):1758–69.
- 101 Alford PW, Nesmith AP, Seywerd JN, Grosberg A, Parker KK. Vascular smooth muscle contractility depends on cell shape. *Integr Biol.* 2011;3(M):1063.
- 102 Janmey P, Schmidt C. Experimental measurements of intracellular mechanics. In: Mofrad MRK, Roger D.Kamm, editors. *Cytoskeletal Mechnics.* , 1st ed. Cambridge University Press; 2006; pp 18–47.
- 103 Carley WW. Lung microvascular endothelial cells: defining in vitro models. In: Bicknell R, editor. *Endothelial Cell Culture.* , 1st ed. Cambridge University Press; 1996; pp 7–23.
- 104 Buul-Wortelboer MF, Brinkman HJM, Dingemans KP, Groot PGDE, Aken WG Van, Mourik JA Van. Reconstitution of the Vascular Wall In Vitro - A Novel Model to Study Interactionsbetween Endothelial Smooth Muscle Cells. *Exp Res.* 1986;162:151–8.
- 105 Medical O. Coculture of Endothelial Cells and Smooth Muscle Cells in Bilayer and Conditioned Media Models. 1997;178(67):169–78.
- 106 Lavender MD, Zhengyu P, Charles S W, Nklason LE, George A T. A system for the direct co-culture of endothelium on smooth muscle cells. *Biomaterials.* 2005;26:4642–53.
- 107 Mangera A, Chapple CR. Tissue engineering in urethral reconstruction-an update. *Asian J Androl.* 2012 Oct;(May):1–4.
- 108 Thomas L V, Lekshmi V, Nair PD. Tissue engineered vascular grafts--preclinical aspects. *Int J Cardiol.* 2013 Aug;167(4):1091–100.
- 109 Weinberg CB, Bell E. A Blood Vessel Model Constructed from Collagen and Cultured Vascular Cells. 1983;310.
- 110 Kirkpatrick CJ, Fuchs S, Unger RE. Co-culture systems for vascularization--learning from nature. *Adv Drug Deliv Rev.* 2011 Apr;63(4–5):291–9.
- 111 Cheema U, Brown R a. Rapid Fabrication of Living Tissue Models by Collagen Plastic Compression: Understanding Three-Dimensional Cell Matrix Repair In Vitro. *Adv wound care.* 2013 May;2(4):176–84.
- 112 Wu H-C, Wang T-W, Kang P-L, Tsuang Y-H, Sun J-S, Lin F-H. Coculture of endothelial and smooth muscle cells on a collagen membrane in the development of a small-diameter vascular graft. *Biomaterials.* 2007 Mar;28(7):1385–92.

- 113 McClure MJ, Sell SA, Simpson DG, Walpoth BH, Bowlin GL. A three-layered electrospun matrix to mimic native arterial architecture using polycaprolactone, elastin, and collagen: a preliminary study. *Acta Biomater.* 2010 Jul;6(7):2422–33.
- 114 Artmann GM, Hescheler J, Meruvu H, Kizildag S, Temiz-Artmann A. Biological, Physical and Technical Basics of Cell Engineering. In: Digel I, editor. , 1st ed. 2018. DOI: 10.1007/978-981-10-7904-7
- 115 Trzewik J, Ates M, Artmann GM. A novel method to quantify mechanical tension in cell monolayers. *European Cells and Materials.* 2002. DOI: 10.1515/bmte.2002.47.s1a.379
- 116 Artmann GM, Chien S. *Bioengineering in Cell and Tissue Research.* 1st ed. Springer; 2008.
- 117 Trzewik J. *Experimental analysis of biaxial mechanical tension in cell monolayers and cultured three-dimensional tissues.* 2007
- 118 Goßmann M, Frotscher R, Linder P, Neumann S, Bayer R, Epple M, et al. Mechano-pharmacological characterization of cardiomyocytes derived from human induced pluripotent stem cells. *Cell Physiol Biochem.* 2016;1182–98.
- 119 Linder P, Trzewik J, Ruffer M, Artmann GM, Digel I, Kurz R, et al. Contractile tension and beating rates of self-exciting monolayers and 3D-tissue constructs of neonatal rat cardiomyocytes. *Med Biol Eng Comput.* 2010 DOI: 10.1007/s11517-009-0552-y
- 120 Gossmann M, Palm T, Kolossov E, Artmann AT. Human iPSC-derived Cardiac Myocyte-Fibroblast 3D Co-Cultures: A Predictive In Vitro Model to Assess Drug-induced Contractile and Metabolic Liabilities
- 121 R.Bayer, A.Artmann, I.Diegel, F.Falkenstein, T.Creuz, G.Artmann, et al. Mechano-pharmacological testing of L-type Ca²⁺ channel modulators via human vascular CellDrum model. *Cell Physiol Biochem.* 2019
- 122 Bayer R, Creutz T, Artmann G, Artmann AT, Hescheler J. The CellDrum and PulSElect system : Tools to evaluate mechanical and pharmacological effects on arterial cells. *BMT 2018 - Poster.* 2018 DOI: 10.13140/RG.2.2.14824.32002
- 123 Creuz T. Cyclic mechanical stimulation effects on cell cytoskeleton in 2D and 3D culture models via new cellDrum PulSElect using optimal parameters. 2017
- 124 Bayer R, Artmann AT, Digel I, Falkenstein J, Artmann G, Creutz T, et al. Mechano-pharmacological testing of L-type Ca²⁺ channel modulators via human vascular CellDrum model. *Cell Physiol Biochem.* 2020;(54):371–83.
- 125 Goßmann M. *Entwicklung eines autokontraktiven Herzmuskelmodells zur funktionalen Medikamenten- und Toxinforschung.* 2015
- 126 Klinkhammer J. *Prozessoptimierung der spektrometrischen Schichtdickenbestimmung zur Qualitätssicherung der CellDrum-Membran.* 2016
- 127 Bayer R. *Optimization of CellDrum Biofunctionalization.* 2012
- 128 Artmann GM, Bayer R, Goßmann M, Linder P. CellDrum electrode arrangement for measuring mechanical stress - WO 2017/121890 A1. WIPO/PCT. 2016 DOI: WO 2017/121890 A1
- 129 Bayer R. *Development of a multi-channel Tissue Tension Analyzer, based on capacitive proximity sensor.* 2014
- 130 Miki Y, Ono K, Hata S, Suzuki T, Kumamoto H, Sasano H. The advantages of co-culture over mono cell culture in simulating in vivo environment. *J Steroid Biochem Mol Biol.* 2012 Sep;131(3–5):68–75.

- 131 Herbert J -M, Maffrand J -P. Heparin interactions with cultured human vascular endothelial and smooth muscle cells: Incidence on vascular smooth muscle cell proliferation. *J Cell Physiol.* 1989;138(2):424–32.
- 132 Reilly CF, Fritze LMS, Rosenberc RD. Heparin Inhibition of Smooth Muscle Cell Proliferation: A Cellular Site of Action. *J Cell Physiol.* 1986;129.
- 133 Schweigerer L, Neufeld G, Friedmant J, Abrahamt JA, Fiddest JC, Gospodarowicz D. Capillary endothelial cells express basic fibroblast growth factor, a mitogen that promotes their own growth. *Nature.* 1986;325:12–4.
- 134 Lindner V, Olson NE, Clowes AW, Reidy MA. Inhibition of smooth muscle cell proliferation in injured rat arteries. Interaction of heparin with basic fibroblast growth factor. *J Clin Invest.* 1992;90(5):2044–9.
- 135 C??be Suarez S, Pieren M, Cariolato L, Arn S, Hoffmann U, Bogucki A, et al. A VEGF-A splice variant defective for heparan sulfate and neuropilin-1 binding shows attenuated signaling through VEGFR-2. *Cell Mol Life Sci.* 2006;63(17):2067–77.
- 136 Berk BC, Brock TA, Webb RC, Taubman MB, Atkinson WJ, Gimbrone MA, et al. Epidermal growth factor, a vascular smooth muscle mitogen, induces rat aortic contraction. *J Clin Invest.* 1985;75(3):1083–6.
- 137 Gopalakrishnan V, Park LE, Triggle CR. The effect of the calcium channel agonist, Bay K-8644 on human vascular smooth muscle. *Eur J Pharmacol.* 1985;113(3):447–51.
- 138 Alonso MJ, Rico I, Salaices M, Marin J. Effects of the Ca agonists Bay K 8644 and CGP 28392 on vascular smooth muscle tone. *Gen Pharmacol.* 1989;20(6):827–31.
- 139 Salaices M, Alonso MJ, Rico I, Fern MS, Marin J. Vasoconstrictor effect of the Ca²⁺ agonist Bay K 8644 on human cerebral arteries. 1989;490:133–40.
- 140 Jin J, Shen X, Tai Y, Li S, Liu M, Zhen C, et al. Arterial relaxation is coupled to inhibition of mitochondrial fission in arterial smooth muscle cells: comparison of vasorelaxant effects of verapamil and phentolamine. *Acta Pharm Sin B.* 2017 May;7(3):319–25.
- 141 Stadler P, Leonardi L, Riesen W, Ziegler W, Marone C, Beretta-Piccoli C. Cardiovascular effects of verapamil in essential hypertension. *Clin Pharmacol Ther.* 1987;42(5):485–92.
- 142 Takahara A, Nozaki S, Ishiguro A, Okamura K, Cao X, Aimoto M, et al. Selectivity of Ca²⁺ channel blockers for dilator actions on the isolated lower esophageal sphincter and aorta from rats. *J Pharmacol Sci.* 2018 May;137(1):98–100.
- 143 Morettini A, Poggesi L, Paoli G, Galanti G, Masotti G. Antihypertensive Action of Nifedipine: Effects on Arteries and Veins. *J Clin Pharmacol.* 2013;25(1):27–35.
- 144 Xiao XH, Rand MJ. Mechanisms of vasoconstrictor responses to KCl in rat isolated perfused tail arteries: interaction with the α 2-adrenoceptor agonist UK14304. *Eur J Pharmacol.* 1991;196(2):133–6.
- 145 Oishi K, Itoh Y, Isshiki Y, Kai C, Takeda Y, Yamaura K, et al. Agonist-induced isometric contraction of smooth muscle cell-populated collagen gel fiber. *Am J Physiol Cell Physiol.* 2000;279(5):C1432–42.
- 146 Nelson MT, Huang Y, Brayden JE, Hescheler J, Standen NB. Arterial dilations in response to calcitonin gene-related peptide involve activation of K⁺channels. *Nature.* 1990;344(6268):770–3.
- 147 Becker B, Morel N, Vanbellin ghen AM, Lebrun P. Blockade of calcium entry in smooth muscle cells by the antidepressant imipramine. *Biochem Pharmacol.* 2004;68(5):833–42.

- 148 Hashitani H, Lang RJ, Mitsui R, Mabuchi Y, Suzuki H. Distinct effects of CGRP on typical and atypical smooth muscle cells involved in generating Abbreviations : 2009;(June):2030–45.
- 149 Kitazono T, Heistad DD, Faraci FM. Role of ATP-sensitive K⁺ channels in CGRP-induced dilatation of basilar artery in vivo. *Am J Physiol.* 1993;265(2 Pt 2):H581-5.
- 150 Miller MR, Megson IL. Recent developments in nitric oxide donor drugs. *Br J Pharmacol.* 2007;151(3):305–21.
- 151 Krawutschke C, Koesling D, Russwurm M. Cyclic GMP in vascular relaxation: Export is of similar importance as degradation. *Arterioscler Thromb Vasc Biol.* 2015;35(9):2011–9.
- 152 Jaiswal N, Lambrecht G, Mutschler E, Tacke R, Malik KU. Pharmacological characterization of the vascular muscarinic receptors mediating relaxation and contraction in rabbit aorta. *J Pharmacol Exp Ther.* 1991;258(3):842–50.
- 153 Touyz RM, Alves-Lopes R, Rios FJ, Camargo LL, Anagnostopoulou A, Arner A, et al. Vascular smooth muscle contraction in hypertension. *Cardiovasc Res.* 2018;114(4):529–39.
- 154 Of E, On A, Smooth THE, Cell M, Main I, Artery C, et al. From the Department of Pharmacology , Faculty of Medicine , . 1979;119–33.
- 155 Brozovich F V, Nicholson CJ, Degen C V, Gao YZ, Aggarwal M, Morgan KG. Mechanisms of Vascular Smooth Muscle Contraction and the Basis for Pharmacologic Treatment of Smooth Muscle Disorders. *Pharmacol Rev.* 2016;68(2):476–532.
- 156 Echeverri D, Montes FR, Cabrera M, Galán A, Prieto A. Caffeine’s Vascular Mechanisms of Action. *Int J Vasc Med.* 2010;2010:1–10.
- 157 Cooper J a. Effects of cytochalasin and phalloidin on actin. *J Cell Biol.* 1987 Oct;105(4):1473–8.
- 158 Suchyna TM. Piezo channels and GsMTx4: Two milestones in our understanding of excitatory mechanosensitive channels and their role in pathology. 2018;130:244–53.
- 159 Gnanasambandam R, Ghatak C, Yasman A, Nishizawa K, Sachs F, Ladokhin AS, et al. GsMTx4: Mechanism of Inhibiting Mechanosensitive Ion Channels. *Biophys J.* 2017;112(1):31–45.
- 160 Bayer R, A.Artmann, G.Artmann, L.Käfer. Quantifying the order of cell internal fibrous structures – The Cell Morphologie Index. 9th International Conference of Cell and Stem Cell Engineering. 2014.
- 161 Firat IS. Quantifying the cytoskeletal reassembly of mechanical biaxial stimulated different aged cells using cell morphology index. 2017
- 162 Schmidt MS. Optimizing the detection of structural elements of the cytoskeleton in eukariotic cells. 2018
- 163 Sinkovec R. Charakterisierung der biomechanischen Reaktivität von mechanisch stimulierter haSMC auf vasoaktive Substanzen
- 164 Olschewski A, Berghausen EM, Eichstaedt CA, Fleischmann BK, Grünig E, Grünig G, et al. Pathobiology, pathology and genetics of pulmonary hypertension: Update from the Cologne Consensus Conference 2018. *Int J Cardiol.* 2018 Sep DOI: 10.1016/J.IJCARD.2018.09.070
- 165 Marian AJ. Genetic markers: Genes involved in human hypertension. *J Cardiovasc Risk.* 1997;4(5):341–5.
- 166 Gao Y, Qi GX, Jia ZM, Sun YX. Prediction of marker genes associated with hypertension by bioinformatics analyses. *Int J Mol Med.* 2017;40(1):137–45.
- 167 Ehret GB, Caulfield MJ. Genes for blood pressure: An opportunity to understand hypertension. *Eur Heart J.* 2013;34(13):951–61.

- 168 Burdyga T V, Wray S. On the mechanisms whereby temperature affects excitation-contraction coupling in smooth muscle. *J Gen Physiol.* 2002;119(1):93–104.
- 169 Katz AM, Hager WD, Messineo FC, Pappano AJ. Cellular Actions and Pharmacology of the Calcium Channel Blocking Drugs. *Am J Med.* 1984;77(2):2–10.
- 170 Amberg GC, Navedo MF. Calcium Dynamics in Vascular Smooth Muscle. *Microcirculation.* 2013;20(4):281–9.
- 171 Curtis TM, Scholfield CN. Nifedipine blocks Ca²⁺ store refilling through a pathway not involving L-type Ca²⁺ channels in rabbit arteriolar smooth muscle. *J Physiol.* 2001;532(3):609–23.
- 172 McDonald TF, Pelzer S, Trautwein W, Pelzer DJ. Regulation and modulation of calcium channels in cardiac, skeletal, and smooth muscle cells. *Physiol Rev.* 1994;74(2):365–507.
- 173 Antoine M, Berkenboom G, Fang Z, Fontaine J, Herchuelz A, Lebrun P. Mechanical and ionic response of rat aorta to diazoxide. 1992;216:299–306.
- 174 Kim B, Lee K, Chinannai KS, Ham I, Bu Y, Kim H, et al. Endothelium-independent vasorelaxant effect of ligusticum jeholense root and rhizoma on rat thoracic aorta. *Molecules.* 2015;20(6):10721–33.
- 175 Kelm M. Nitric oxide metabolism and breakdown. *Biochim Biophys Acta - Bioenerg.* 1999;1411(2–3):273–89.
- 176 Sampson LJ, Plane F, Garland CJ. Involvement of cyclic GMP and potassium channels in relaxation evoked by the nitric oxide donor, diethylamine NONOate, in the rat small isolated mesenteric artery. *Naunyn Schmiedebergs Arch Pharmacol.* 2001;364(3):220–5.
- 177 Walker SE, Choudhury J, Law S, Iazzetta J. Stability of ibuprofen solutions in normal saline or 5% dextrose in water. *Can J Hosp Pharm.* 2011;64(5):354–61.
- 178 Angus JA, Cocks TM, McPherson GA, Broughton A. The acetylcholine paradox: A constrictor of human small coronary arteries even in the presence of endothelium. *Clin Exp Pharmacol Physiol.* 1991 DOI: 10.1111/j.1440-1681.1991.tb01373.x
- 179 Wagner KA, Yacono PW, Golan DE, Tashjian AH. Mechanism of spontaneous intracellular calcium fluctuations in single GH 4 C 1 rat pituitary cells. *Biochem J.* 1993;292(1):175–82.
- 180 Chang GJ, Lin TP, Ko YS, Lin MS. Endothelium-dependent and -independent vasorelaxation induced by CIJ-3-2F, a novel benzyl-furoquinoline with antiarrhythmic action, in rat aorta. *Life Sci.* 2010;86(23–24):869–79.
- 181 Chilman Bae, Sachs F, Gottlieb PA. The mechanosensitive ion channel Piezo1 is inhibited by the peptide GsMTx4. *Biochemistry.* 2012;23(1):1–7.
- 182 Li H, Xu J, Shen ZS, Wang GM, Tang M, Du XR, et al. The neuropeptide GsMTx4 inhibits a mechanosensitive BK channel through the voltage-dependent modification specific to mechano-gating. *J Biol Chem.* 2019;294(31):11892–909.
- 183 Dishy V, Sofowora G, Harris PA, Kandcer M, Zhan F, Wood AJJ, et al. The effect of sildenafil on nitric oxide-mediated vasodilation in healthy men. *Clin Pharmacol Ther.* 2001;70(3):270–9.
- 184 Oger S, Behr-Roussel D, Gorny D, Lebret T, Validire P, Cathelineau X, et al. Signalling pathways involved in sildenafil-induced relaxation of human bladder dome smooth muscle. *Br J Pharmacol.* 2010;160(5):1135–43.
- 185 Wagenseil JE, Mecham RP. Vascular Extracellular Matrix and Arterial Mechanics. *Physiol Rev.* 2009;89(3):957–89.

- 186 Fleckenstein A, Frey M, Fleckenstein-gron G. Antihypertensive and Arterial Anticalcinotic Effects of Calcium Antagonis. 1983;57:1D-10D.
- 187 Watts SW, Finta KM, Lloyd MC, Storm DS, Webb RC. Enhanced vascular responsiveness to bay k 8644 in mineralocorticoid- and n-nitro arginine-induced hypertension. *Blood Press.* 1994;3(5):340–8.
- 188 Roy S, Thacher T, Silacci P, Stergiopoulos N. Arterial biomechanics after destruction of cytoskeleton by Cytochalasin D. *J Biomech.* 2009;42(15):2562–8.
- 189 Anabuki J, Hori M, Hayakawa K, Akahane S, Ozaki H, Karaki H. Muscarinic stimulation does not induce rhoA/ROCK-mediated Ca²⁺ sensitization of the contractile element in chicken gizzard smooth muscle. *Pflugers Arch Eur J Physiol.* 2000;441(2–3):189–99.
- 190 Myung SC, Oh SY, Kim K Do, Kim SC, Lee MY. Effects of spermine on the relaxation response of rat detrusor smooth muscles. *Eur J Pharmacol.* 2007;573(1–3):196–200.
- 191 Alonso F, Boittin FX, Bény JL, Haefliger JA. Loss of connexin40 is associated with decreased endothelium-dependent relaxations and eNOS levels in the mouse aorta. *Am J Physiol - Hear Circ Physiol.* 2010;299(5). DOI: 10.1152/ajpheart.00029.2010
- 192 Ludmer PL, Selwyn AP, Shook TL, Wayne RR, Mudge GH, Alexander RW, et al. Paradoxical vasoconstriction by acetylcholine in atherosclerotic coronary arteries. *N Engl J Med.* 1986;315(17):1046–51.
- 193 Iglarz M, Lévy BI, Henrion D. Chronic endothelin-1-induced changes in vascular reactivity in rat resistance arteries and aorta. *Eur J Pharmacol.* 1998 Oct;359(1):69–75.
- 194 Rincón R, Hernández A, Orozco C. In vitro effect of endothelin-1 and nifedipine on pulmonary vascular contraction of pulmonary hypertensive and non-pulmonary hypertensive chickens. *J Appl Anim Res.* 2016;2119(January). DOI: 10.1080/09712119.2015.1125355
- 195 Mort JR, Kruse HR. Timing of blood pressure measurement related to caffeine consumption. *Ann Pharmacother.* 2008;42(1):105–10.
- 196 Vardi Y, Klein L, Nassar S, Sprecher E, Gruenwald I. Effects of sildenafil citrate (viagra) on blood pressure in normotensive and hypertensive men. *Urology.* 2002;59(5):747–52.
- 197 Leeman M, Choi J, Hansson S, Storm MU, Nilsson L. Proteins and antibodies in serum, plasma, and whole blood—size characterization using asymmetrical flow field-flow fractionation (AF4). *Anal Bioanal Chem.* 2018;410(20):4867–73.
- 198 Bina RB., Hill N, Brem AS. Effect of serum on vascular smooth muscle function. *Life Sci.* 1998;62(13):1195–201.
- 199 Cr M. Mg, K, Ca, Ti, V, Cr, Fe, Ni, Cu, Zn, Ga, Ge. *Handb Stable Isot Anal Tech.* 2009;743–879.
- 200 Bono N, Pezzoli D, Levesque L, Loy C, Candiani G, Fiore GB, et al. Unraveling the role of mechanical stimulation on smooth muscle cells: A comparative study between 2D and 3D models. *Biotechnol Bioeng.* 2016;113(10):2254–63.
- 201 Zhu JH, Chen CL, Flavahan S, Harr J, Su B, Flavahan NA. Cyclic stretch stimulates vascular smooth muscle cell alignment by redoxdependent activation of Notch3. *Am J Physiol - Hear Circ Physiol.* 2011;300(5):1770–80.
- 202 Chapman GB, Durante W, Hellums JD, Schafer AI. Physiological cyclic stretch causes cell cycle arrest in cultured vascular smooth muscle cells. *Am J Physiol - Hear Circ Physiol.* 2000;278(3 47-3):748–54.
- 203 Yajun Feng, Jeong-Hee Yang, Hayden Huang, Scott P. Kennedy, Thomas G. Turi, John F. Thompson, Peter Libby RTL. Transcriptional Profile of Mechanically Induced Genes in Human Vascular Smooth Muscle Cells. *Circ Res.* 1999;1118–23.

- 204 Schulze PC, De Keulenaer GW, Kassik KA, Takahashi T, Chen Z, Simon DI, et al. Biomechanically Induced Gene *ie*x-1 Inhibits Vascular Smooth Muscle Cell Proliferation and Neointima Formation. *Circ Res.* 2003;93(12):1210–7.
- 205 Zampetaki A, Zhang Z, Hu Y, Xu Q. Biomechanical stress induces IL-6 expression in smooth muscle cells via Ras/Rac1-p38 MAPK-NF- κ B signaling pathways. *Am J Physiol - Hear Circ Physiol.* 2005;288(6 57-6):2946–54.
- 206 Grote K, Flach I, Luchtefeld M, Akin E, Holland SM, Drexler H, et al. Mechanical stretch enhances mRNA expression and proenzyme release of matrix metalloproteinase-2 (MMP-2) via NAD(P)H oxidase-derived reactive oxygen species. *Circ Res.* 2003;92(11):1–7.
- 207 Haga JH, Li Y-SJ, Chien S. Molecular basis of the effects of mechanical stretch on vascular smooth muscle cells. *J Biomech.* 2007 Jan;40(5):947–60.
- 208 Li M, Wang L, Ge C, Wang H, Zhang M. Mechanical stretch promotes matrix metalloproteinase-2 and prolyl-4-hydroxylase α 1 production in human aortic smooth muscle cells via Akt-p38 MAPK-JNK signaling. *Int J Biochem Cell Biol.* 2015 DOI: 10.1016/j.biocel.2015.02.009
- 209 Wernig F, Mayr M, Xu Q. Mechanical stretch-induced apoptosis in smooth muscle cells is mediated by β 1-integrin signaling pathways. *Hypertension.* 2003;41(4):903–11.
- 210 Haghighipour N, Tafazzoli-Shadpour M, Shokrgozar MA, Amini S. Effects of cyclic stretch waveform on endothelial cell morphology using fractal analysis. *Artif Organs.* 2010;34(6):481–90.
- 211 Hatami J, Tafazzoli-Shadpour M, Haghighipour N, Shokrgozar MA, Janmaleki M. Influence of Cyclic Stretch on Mechanical Properties of Endothelial Cells. *Exp Mech.* 2013;53(8):1291–8.
- 212 Takeda H, Komori K, Nishikimi N, Nimura Y, Sokabe M, Naruse K. Bi-phasic activation of eNOS in response to uni-axial cyclic stretch is mediated by differential mechanisms in BAECs. *Life Sci.* 2006;79(3):233–9.
- 213 Hu B, Dobson J, El Haj AJ. Control of smooth muscle α -actin (SMA) up-regulation in HBMSCs using remote magnetic particle mechano-activation. *Nanomedicine.* 2014 Jan;10(1):45–55.
- 214 Cheng TH, Shih NL, Chen SY, Loh SH, Cheng PY, Tsai CS, et al. Reactive oxygen species mediate cyclic strain-induced endothelin-1 gene expression via Ras/Raf/extracellular signal-regulated kinase pathway in endothelial cells. *J Mol Cell Cardiol.* 2001;33(10):1805–14.
- 215 Toda M, Yamamoto K, Shimizu N, Obi S, Kumagaya S, Igarashi T, et al. Differential gene responses in endothelial cells exposed to a combination of shear stress and cyclic stretch. *J Biotechnol.* 2008;133(2):239–44.
- 216 Bieler FH, Ott CE, Thompson MS, Seidel R, Ahrens S, Epari DR, et al. Biaxial cell stimulation: A mechanical validation. *J Biomech.* 2009 Aug;42(11):1692–6.
- 217 Discher DE, Janmey P, Wang Y. Tissue Cells Feel and Respond to the Stiffness of Their Substrate. *Science (80-).* 2005;310(5751):1139–43.
- 218 Lacolley P, Regnault V, Segers P, Laurent S. Vascular Smooth Muscle Cells and Arterial Stiffening: Relevance in Development, Aging, and Disease. *Physiol Rev.* 2017;97(4):1555–617.
- 219 Jang J-Y, Lee SW, Park SH, Shin JW, Mun C, Kim S-H, et al. Combined effects of surface morphology and mechanical straining magnitudes on the differentiation of mesenchymal stem cells without using biochemical reagents. *J Biomed Biotechnol.* 2011;2011:860652.
- 220 Shim J, Grosberg A, Nawroth JC, Kit Parker K, Bertoldi K. Modeling of cardiac muscle thin films: Pre-stretch, passive and active behavior. *J Biomech.* 2012;45:832–41.

- 221 Stricker J, Falzone T, Gardel ML. Mechanics of the F-actin cytoskeleton. *J Biomech.* 2010 Jan;43(1):9–14.
- 222 Van Der Loop FTL, Schaart G, Timmer EDJ, Ramaekers FCS, Van Eys GJJM. Smoothelin, a novel cytoskeletal protein specific for smooth muscle cells. *J Cell Biol.* 1996;134(2):401–11.
- 223 Pannu H, Tran-Fadulu V, Papke CL, Scherer S, Liu Y, Presley C, et al. MYH11 mutations result in a distinct vascular pathology driven by insulin-like growth factor 1 and angiotensin II. *Hum Mol Genet.* 2007;16(20):2453–62.
- 224 Haga JH, Li Y-SJ, Chien S. Molecular basis of the effects of mechanical stretch on vascular smooth muscle cells. *J Biomech.* 2007 Jan;40(5):947–60.
- 225 Chalovich JM. Actin mediated regulation of muscle contraction. *Pharmacol Ther.* 1992;55(2):95–148.
- 226 Clevers H. Modeling Development and Disease with Organoids. *Cell.* 2016;165(7):1586–97.
- 227 Shah H, Rawal Mahajan S. Photoaging: New insights into its stimulators, complications, biochemical changes and therapeutic interventions. *Biomed Aging Pathol.* 2013 Jul;3(3):161–9.
- 228 Pathway KBA, Kim JM, Yoon M, Kim J, Kim SS, Kang I, et al. Phosphatidylinositol 3-Kinase Regulates Differentiation of H9c2 Cardiomyoblasts Mainly through the Protein. 1999;367(1):67–73.
- 229 Matsushita H, Monshlta R, Klda I, Hayashi S, Tomlta N, Yamamoto K, et al. Inhibition of Growth of Human Vascular Smooth Muscle Cells by Overexpression of p21 Gene Through Induction of Apoptosis. *Hypertension.* 1998;31:493–8.
- 230 Frismantiene A, Philippova M, Erne P, Resink TJ. Smooth muscle cell-driven vascular diseases and molecular mechanisms of VSMC plasticity. *Cell Signal.* 2018 Dec;52:48–64.
- 231 Renna NF, Garcia R, Ramirez J, Miatello RM. Vascular Repair and Remodeling: A Review. *Physiol Pathol Angiogenes - Signal Mech Target Ther.* 2017 DOI: 10.5772/67485
- 232 Yunoki S, Ikoma T, Tanaka J. Development of collagen condensation method to improve mechanical strength of tissue engineering scaffolds. *Mater Charact.* 2010;61(9):907–11.
- 233 Hong Z, Reeves KJ, Sun Z, Li Z, Brown NJ, Meininger GA. Vascular smooth muscle cell stiffness and adhesion to collagen I modified by vasoactive agonists. *PLoS One.* 2015;10(3):1–12.
- 234 Stossel TP, Condeelis J, Cooley L, Hartwig JH, Schleicher M, Shapiro SS. FILAMINS AS INTEGRATORS OF CELL MECHANICS AND SIGNALLING. 2001;2(February):138–45.
- 235 Mezawa M, Pinto VI, Kazembe MP, Lee WS, McCulloch CA. Filamin A regulates the organization and remodeling of the pericellular collagen matrix. *FASEB J.* 2016;30(10):3613–27.
- 236 D’Addario M, Arora PD, Fan J, Ganss B, Ellen RP, McCulloch CAG. Cytoprotection against Mechanical Forces Delivered through β 1 Integrins Requires Induction of Filamin A. *J Biol Chem.* 2001;276(34):31969–77.
- 237 Lifton RP. Molecular Genetics of Human Blood Pressure Variation. *Science (80-).* 1996;272(Science (80- .)):676–80.
- 238 Wang L, Cheng F, Hu J, Wang H, Tan N, Li S, et al. Pathway-based gene-gene interaction network modelling to predict potential biomarkers of essential hypertension. *BioSystems.* 2018;172(July):18–25.
- 239 Patel RS, Masi S, Taddei S. Understanding the role of genetics in hypertension. *Eur Heart J.* 2017;38(29):2309–12.

- 240 David J. Triggle, Murali Gopalakrishnan, David Rampe WZ. Voltage-gated ion channels as drug targets. 29th ed. 2006.
- 241 Ghosh D, M.F.Navedo. Calcium Channels in Vascular Smooth Muscle. *Vascular Pharmacology: Smooth Muscle*. , 78th ed. University of California, Davis, CA, United States: Elsevier Science & Technology; 2017; pp 49–74.
- 242 Brown L, Koerner T, Horton JH, Oleschuk RD. Fabrication and characterization of poly(methylmethacrylate) microfluidic devices bonded using surface modifications and solvents. *Lab Chip*. 2006 Jan;6(1):66–73.
- 243 Gand A, Tabuteau M, Chat C, Ladam G, Atmani H, Van Tassel PR, et al. Fibronectin-based multilayer thin films. *Colloids Surfaces B Biointerfaces*. 2017;156:313–9.
- 244 Lavender MD, Pang Z, Wallace CS, Niklason LE, Truskey G a. A system for the direct co-culture of endothelium on smooth muscle cells. *Biomaterials*. 2005 Aug;26(22):4642–53.
- 245 Hu Z, Xiong Y, Han X, Geng C, Jiang B, Huo Y, et al. Acute Mechanical Stretch Promotes eNOS Activation in Venous Endothelial Cells Mainly via PKA and Akt Pathways. *PLoS One*. 2013;8(8). DOI: 10.1371/journal.pone.0071359
- 246 Morawietz H, Talanow R, Szibor M, Rueckschloss U, Schubert A, Bartling B, et al. Regulation of the endothelin system by shear stress in human endothelial cells. *J Physiol*. 2000;525(3):761–70.
- 247 Wang DL, Wung B -S, Peng Y -C, Wang JJ. Mechanical strain increases endothelin-1 gene expression via protein kinase C pathway in human endothelial cells. *J Cell Physiol*. 1995;163(2):400–6.
- 248 Ainslie K, Shi ZD, Garanich JS, Tarbell JM. Rat aortic smooth muscle cells contract in response to serum and its components in a calcium independent manner. *Ann Biomed Eng*. 2004;32(12):1667–75.
- 249 Meckel Y, Nemet D, Bar-Sela S, Radom-Aizik S, Cooper DM, Sagiv M, et al. Hormonal and inflammatory responses to different types of sprint interval training. *J Strength Cond Res*. 2011;25(8):2161–9.
- 250 Leistungsphysiologie MS-. *Molekulare Sport- und Leistungsphysiologie*. 2018. DOI: 10.1007/978-3-7091-1591-6
- 251 Davies PF, Tripathi SC. Mechanical stress mechanisms and the cell. An endothelial paradigm. *Circ Res*. 2012;72(2):239–45.
- 252 Wijnands KA, Meesters DM van BK et al. Citrulline Supplementation Improves Organ Perfusion and Arginine Availability under Conditions with Enhanced Arginase Activity. *Nutrients*. 2015;7(07):5217–38.
- 253 Figueroa A, Alvarez-Alvarado S, Jaime SJ KR. L-Citrulline supplementation attenuates blood pressure, wave reflection and arterial stiffness responses to metaboreflex and cold stress in overweight men. *Br J Nutr*. 2016;116(02):279–85.
- 254 Suzuki T, Morita M, Hayashi T KA. The effects on plasma L-arginine levels of combined oral L-citrulline and L-arginine supplementation in healthy males. *Biosci Biotechnol Biochem*. 2017;81(02):372–5.
- 255 Gröber U. L-Citrullin verbessert Bioverfügbarkeit an L-Arginin. *Zs.fOrthomolMed*. 2019;17(02):4.
- 256 Ruiz E, Tejerina T. Relaxant effects of L-citrulline in rabbit vascular smooth muscle. *Br J Pharmacol*. 1998;125(1):186–92.

257 Gold ME, Wood KS, Byrns RE. L-Arginine-dependent vascular smooth muscle relaxation and cGMP formation. *Am Physiol Soc.* 1990;259(6):1813–21.

10. Appendix

10.1. List of Abbreviations

μC	Microcontroller	LDH	L-Lactatdehydrogenase
ACE	Angiotensin-Converting Enzyme	LMA	Levenberg-Marquardt Algorithm
ADP	Adinosindiphosphate	LTM	Long Term Mode
AT2	Angiotensin 2	MEA	Multielectrode Array
ATP	Adinosintriphosphate	MHC	Myosin Heavy Chain
bFGF	Basic Fibroblast Growth Factor	MLC	Myosin Light Chain
Ca2+	Calcium Ion	MLCK	Myosin Light Chain Kinase
cAMP	Adenosine Monophosphate	Na+	Sodium-Ion
CBC	Cross Bridge Cycle	NaCl	Sodium chloride
cDNA	complementary DNA	NE	Norepinephrine
cGMP	cyclic Guanosine Monophosphate	O2	Oxygen
CGRP	Calcitonin gene-related peptide	PBS	Phosphate-buffered saline
CMI	Cell Morphology Index	PCB	Printed Circuit Board
CMMC	Center For Molecular Medicine Cologne	PDE-5	Phosphodiesterase-5
CO2	Carbon Dioxide	PDMS	Polydimethylsiloxane
CVD	Cardiovascular Disease	PEEK	Polyetheretherketone
DAG		PIP2	Phosphatidylinositol-4,5-bisphosphate
DAPI	4',6-diamidino-2-phenylindole	PMMA	Polymethylmethacrylate
DEA/NO	Diethylamine NONOate	PTM	Particular Time Mode
DMEM	Dulbecco's modified Eagle's medium	RNA	Ribonucleic acid
DMSO	Dimethyl Sulfoxide	RNase	Ribonuclease
EC	Endothelial Cells	RTM	Real-Time Mode
ECM	Extra Cellular Matrix	qPCR	Quantitative Polymerase Chain Reaktion
EDTA	Ethylenediaminetetraacetic	SEM	Standard Error of Mean
eNO	Endothelial Nitric Oxide	SMC	Smooth Muscle Cells
ER	Endoplasmatic Reticulum	SMD	Surface Mounted Device
ET1	Endothelin 1		Smooth Muscle Cell Differentiation Serum
FBS	Fetal Bovine Serum	SMGS	Smooth Muscle Cells Growth Serum
GCS		SOP	Standard Operation Procedure
GND	Ground	TTA	Tissue Tension Analyzer
GUI	Graphic User Interface	TTL	Transistor to Transistor Logic
haEC	human aortic endothelial cells	vSMC	Vascular Smooth Muscle Cells
haSMC	human aortic smooth muscle cells	WHO	World health organization
hEGF	Human Endothelial Growth Factor	KCL	Potassium Chloride
IDE	Integrated Development Environment	LDH	L-Lactatdehydrogenase
IP3	Inositol trisphosphate	LMA	Levenberg-Marquardt Algorithm
K+	Potassium Ion		

10.2. List of Figures

<i>Figure 1 Schematic structure of an artery with the designation of the individual functional layers (Adventitia, Media & Intima) and the related connecting layers.</i>	<i>9</i>
<i>Figure 2 Schematic</i>	<i>10</i>
<i>Figure 3 Contraction and relaxation mechanism of a smooth muscle cell as a schematic overview. The left half of the picture describes the contraction by electrical tension (1), receptor (2) and strain (3) dependent Ca^{2+} channels as well as by receptor-controlled (4) release of Ca^{2+} ions from the sarcoplasmic reticulum (SR). Muscle relaxing mechanisms are shown in the right half of the figure. Decrease of the cytosolic Ca^{2+} nucleotide by Ca^{2+}-ATPase(5,6) and $3Na^+/Ca^{2+}$ exchange (7) as well as the effect of the cyclic nucleotide cAMP (8) and cGMP (9). Molecular contraction mechanism in the center of the image, CAM calmodulin, PLC phospholipase C, AC adenylyl cyclase, G G protein, IP_3 inositol triphosphate, ANP atriopeptin, GC guanylylcyclase[1] (figure adapted).</i>	<i>11</i>
<i>Figure 4 Overview and progress of different causes of high blood pressure[1] (figure adapted)</i>	<i>13</i>
<i>Figure 5 Overview of all systems and programs developed for this work. Orange Box: Adaptation of CellDrum and measurement methods for quality management. Blue Box: Measuring system for the biomechanical analysis of the CellDrums and software for data acquisition, evaluation and sensor calibration. Green Box: Technical development for mechanical stimulation of CellDrum samples. Red Box: Software for the quantification of cytoskeletal distribution.</i>	<i>20</i>
<i>Figure 6 A) Sliced computer-aided design scheme of a CellDrum with membrane and cell culture media. The CellDrum offers a $2cm^2$ cultivation area, consisting of an ultra-flexible polydimethylsiloxane (PDMS) membrane. Due to surface functionalization, cells can attach to the membrane [124] B) Photo of CellDrum 2017.</i>	<i>20</i>
<i>Figure 7 A) Illustration of the measuring principle for photometric layer thickness measurement. VIS light penetrates the CellDrum membrane and generates an interference pattern, which indicates the layer thickness by the refractive index, internal reflection and material parameters. B) Recorded interference pattern[126] C) Formula for determining the coating thickness using the wavelength interference.....</i>	<i>21</i>
<i>Figure 8 A) Picture of the Tissue Tension Analyzer with a detailed schematic arrangement of the measurement socket - 1) CellDrum; 2) Cells attached to the CellDrum membrane with cell culture media (500μl) on top; 3) GND electrode; 4) Counter electrode; 5) Electrical shielding; 6) Measurement socket; 7) Deflection sensor; 8) Pressure sensor; 9) Syringe pump; 10) Processing unit; 11) Peripheral computer and data storage[121,124]. B) Photographs of the TTA test base; above: Cover open with two CellDrums and view of the cylinder electrodes; bottom: Closed with cover and protective cap.....</i>	<i>22</i>
<i>Figure 9 TTA motherboard for data acquisition and control of the system via computer. On the top left, in light blue, you can see the microvalves, which are pneumatically connected to the PMMA pressure distributor in the center. The pressure in the closed system is measured by an SMD pressure sensor on the bottom right. Power supply and voltage regulators can be seen on the bottom left. The slots of the individual measuring chambers can be seen at the top right. Directly below the motherboard is the microcontroller to establish communication with the computer. Underneath it is a mechanical relay that ensures the complete decoupling of the individual sensors.</i>	<i>24</i>
<i>Figure 10 A) Bottom view of the measurement socket. Proximity sensors connected to the base, 0V electrode and pressure connection. B) TTA sealing cap bottom view with 0V gold electrodes for contacting the cell culture medium with LC-resonant circuit.</i>	<i>24</i>

Figure 11 Schematic diagram of the measuring electrode arrangement. All components are connected to one of the separated oscillating circuits. The capacitance change of the system takes place between the red CellDrum membrane and the blue active cylinder surface[129]. 25

Figure 12 Interface of the measurement software. (A) Configuration of serial communication between TTA and computer. (B) Real-time monitoring of data acquisition. (C) Controlpanel to select sample chamber and control valves. (D) Timeout control and indicator enables automated pressure equilibration between the measurements. (E) Datafile configuration and save options. 26

Figure 13 Interface of the analysis software. In (A) all data of the selected file path are listed. The file selected in (A) is opened in (B) where the data can be trimmed. The default settings for the analysis range is the time interval 0.5s-11.5s. The data is cut out and displayed in (C). Both data series are merged and the deflection over the pressure course is displayed in white. (D) also represents the best non-linear adaptation in red. The resulting data is presented in (E) and can be buffered in (F) using ADD. 27

Figure 14 Key figure for the CellDrum physical model with CellDrum fitted Barlow's formula to derive the cellular tension from recorded pressure deflection curves. r) Radius of the CellDrum (16mm). h) Indicates the deflection of the CellDrum membrane to the baseline (in μm). R) Radius of the theoretical hemisphere. The formula is used to derive the tension from the recorded pressure deflection curves. σ) Calculated axial stress (N/m^2). p) measured pressure (in Pa). s) CellDrum membrane thickness (in μm).[124] 28

Figure 15 The starting point of the mathematical model is the Barlow formula, which allows calculating the stress distribution in thin-walled boilers. For the calculation of the mechanical stress within the CellDrum membrane the calculation of the tangential stress σ_T is necessary. The formula for calculating a hemisphere is shown below the drawing 28

Figure 16 A) haSMC in cultivated on slides. Fixed and stained smooth muscle cell-alpha-actin. B) haEC grown on slides. Fixed and CD31 antibody stained. 30

Figure 17 Drawing of the conditioned co-culture. Conditioning was carried out inside the CellDrums with 150.000 haSMCs and 200.000 haECs a.) Cells were cultivated in separate cell culture vessels with the cytospecific media. b) After 24h the medium of the haSMCs is removed and then replaced by the medium of the haEC. 31

Figure 18 Graphic illustration of the planned three-dimensional co-culture model consisting of smooth muscle cells and endothelial cells. 1) CellDrum membrane 2) Fibronectin coating 3) haSMC monolayer 4) Fibronectin coating 5th) collagen type IV coating 6) haEC monolayer 33

Figure 19 Representative live/dead staining of haSMC monolayer on CellDrum. For functional testing, cell lesions were induced by excessive mechanical stress. Intact cells are displayed in green and damaged cells in red fluorescence[124]. 33

Figure 20 Overview of the vasoactive mechanisms of action of all substances used in this study. cAMP(cyclic adenosine monophosphate); cGMP (cyclic guanosine monophosphat); DAG (1,2-Diacylglycerol); ER (endoplasmatic reticulum); GC-S (Guaninacyclase-S); G-Protein; GTP (guanintriphosphate); IP3 (Inositol-1,4,5-triphosphate); M2,M3 (Muscarinreceptor 2,3); PDE-5 (phosphodiesterase type 5); PIP2 (phosphate idyilonositol-4,5-biphosphate); PKG (Proteinkinase G); PLC (Phospholipase C). 37

Figure 21 A) PulSElect sample sockets for the mechanical stimulation of twelve CellDrums. A printed component made of clear resin with a FormLabs 2 3D printer B) Compilation of all components of the PulSElect system C) Sketch of the individual components of the PulSElect system and arrangement in operation. The green box indicates the incubator, including all parts which can be placed in the incubator during mechanical stimulation D) Calibration of the PulSElect system. The deflection is plotted against the increasing pressure applied to the system. The pressure is measured directly below the CellDrums, which is displayed in the second Y-axis[123]E) Software for creating user-defined pressure waves. The waveform can be generated from two Gaussian functions using the controllers. The data is then transposed into the appropriate data format to be compiled on the microcontroller. F) Real-time recording of the waveform created in Figure 21 E. The measurement was recorded using laser-assisted TTA at a sample rate of 1kHz[122].	39
Figure 22 Real-time recording of the mech stimulation SOP signal. The measurements were recorded by laser-assisted TTA with a sampling rate of 1kHz.	40
Figure 23 Flowchart of the stimulation SOP represented on a daily cycle.	40
Figure 24 Explanation of the CMI analysis. Comparison of example models (left), similar cell examples (middle) and the resulting CMI value. Linear ordered structures result in a higher CMI value, whereas chaotic structures result in a CMI value close to zero.	41
Figure 25 RTM measurement of haSMC cells treated with 100nM Bay K8644 over time. The data points represent the movement of the CellDrum membrane in μm [124].	46
Figure 26 Cell number dependent rise of mechanical tension. Each bar represents the mean value of three individual samples. The error bars show the SEM. All measurements show the change in mechanical stress compared to non-populated CellDrum, both with smooth muscle cells and endothelial cells.	46
Figure 27 Temperature-dependent cell tonus measurement over time. The points represent the mean value of 6 individually measured CellDrums, each loaded with a previously chilled medium. The error bars represent the SEM.	46
Figure 28 Time courses of L-Type Ca^{2+} channel modulators CellDrum investigation via LTM (N=6 mean \pm 1 SEM). The change in the mechanical stress caused by the test substance is expressed as the relative difference of the mechanical stress (%) to the initial value. A) Application of 10nM nifedipine B) Analysis of the biomechanical effect of 50nM verapamil C) Biomechanical effect over time by S-Bayk8644[124]	47
Figure 29 Time courses of substances acting on K^+ channels, CellDrum investigation via LTM (N=6 mean \pm 1 SEM). The change in the mechanical stress caused by the test substance is expressed as the relative difference of the mechanical stress (%) to the initial value. A) 50mM KCl B) 5,2 μM CGRP C) 1 μM Diazoxide D)5 μM Glibenclamide.	48
Figure 30 Analysis of the single and combined biomechanical effect of CGRP and glibenclamide on haSMC over time. CellDrum investigation via LTM (N=6 mean \pm 1 SEM). The change in the mechanical stress caused by the test substance expressed as the relative difference of the mechanical stress (%) to the initial value. All substances were measured on separate CellDrum samples. The sample of the measurement series glibenclamide+CGRP was first pretreated with glibenclamide for 30 minutes. The measurement was started when the CGRP was added to illustrate the competitive substance effect.	49
Figure 31 Time courses of NO-Donators. CellDrum investigation via LTM (N=6 mean \pm 1 SEM). The change in the mechanical stress caused by the test substance is expressed as the relative difference of the mechanical stress (%) to the initial value. A) 5mM Spermine NO-complex KCl B) 1mM DEA/NO	50

Figure 32 Time courses of measurement of various hormonal vasoactive agents. CellDrum investigation via LTM (N=6 mean \pm 1 SEM). The change in the mechanical stress caused by the test substance is expressed as the relative difference of the mechanical stress (%) to the initial value. A) 1 μ M Norepinephrine B) 1 μ M Acetylcholin C) 100 nM Angiotensin II D) 100nM Endothelin I 51

Figure 33 Time courses of vasoactive agents with various mechanisms of effect. CellDrum investigation via LTM (N=6 mean \pm 1 SEM). The change in the mechanical stress caused by the test substance is expressed as the relative difference of the mechanical stress (%) to the initial value. A) 1 μ M Sildenafil 52

Figure 34 Time courses of vasoactive agents with various mechanisms of effect. CellDrum investigation via LTM (N=6 mean \pm 1 SEM). The change in the mechanical stress caused by the test substance is expressed as the relative difference of the mechanical stress (%) to the initial value. A) 10 μ M Caffeine B) 250nM GsMTx-4 Spider Venom C) 100 nM Cytochalasin D 53

Figure 35 Analysis of the biomechanical effect of serial application of cytochalasin D and norepinephrine over time. CellDrum investigation via LTM (N=6 mean \pm 1 SEM). The change in the mechanical stress caused by the test substance expressed as the relative difference of the mechanical stress (%) to the initial value. Both substances were added in series to the same sample to show the effect of the substance mixture. A) Addition of 1 μ M norepinephrine followed by 100nM cytochalasin D. B) Stimulation of 100nM cytochalasin D followed by 1 μ M norepinephrine 54

Figure 36 Dose-response model of all tested agents in the concentrations of 0.1nM, 1nM, 10nM, 100nM and 1 μ M. Y-Axis indicates the deviation in mechanical stress relative to control in % to the initial stress. The X-Axis represents the substance concentration on a log scale. Every data point represents five (n=5) measurements taken from three individual samples(N=6). The error bars indicate the SEM [124](figure adapted) 55

Figure 37 Showing the biomechanical changes of haSMC induced by mechanical stimulation over five days. CellDrum investigation via PTM. Every data point represents the mean value of five independent measured specimens and the error bars represent the SEM (N=6 mean n=5 \pm 1 SEM). The time course data represent the stimulated specimen compared to the unstimulated specimen..... 56

Figure 38 Monitoring of cell vitality and cell count of haSMC throughout mechanical stimulation according to SOP for six days. A) Quantification of cell count and viability by automatic cell counter and trypan blue staining (N=6; n=2 \pm SEM) B) Viability test by LDH assay and photometric analysis Comparison of stimulated and unstimulated samples (N=6; n=2 \pm SEM). 56

Figure 39 Monitoring of cell vitality and cell count of haEC throughout mechanical stimulation according to SOP for six days. A) Quantification of cell count and viability by automatic cell counter and trypan blue staining (N=6; n=2 \pm SEM) B) Viability test by LDH assay and photometric analysis Comparison of stimulated and unstimulated samples (N=6; n=2 \pm SEM). 57

Figure 40 Representative images of live/dead stainings, showing dead cells that have not detached from the CellDrum membrane. The parameters of the training were adjusted so that no more damaged cells could be detected. 57

Figure 41 CMI evaluation for the quantification of cytoskeletal f-actin alignment by mechanical stimulation on CellDrums. Each data set was stimulated and unstimulated with three individual CellDrums for the stimulation intervals 0min, 30min, 60min, 90min (N=3; n=30 ±SEM). The intensity parameters correspond to the parameters of the SOP (f=2Hz, P=-40Pa). Below representative images of the corresponding stimulation protocols of haSMC, fixed and stained with Alexaflour Phalloidin 488. 58

Figure 42 Showing how mechanical stimulation affects the biomechanical response of haSMC to vasoactive agents. Every substance was tested by six individual CellDrums, which were measured after mechanical stimulation after 0 days, three days and five days via PTM and the error bars represent the SEM (N=6 mean n=5 ± 1 SEM)[163](figure adapted)..... 59

Figure 43 Endothelin secretion measured via ET1 ELISA Kit over the time of 5 days. Every dataset represents the pooled values of three individual samples with two technical replicates of stimulated and unstimulated Cells(N=3 mean n=2 ± 1 SEM). The used CellDrum model consisted of each 200.000 haEC monolayer. 60

Figure 44 A+B) Comparison of gene expression profile due to mechanical stimulation according to stimulation SOP after three and five days. Genes have been highlighted at a significant (P<0.05) change in expression level (foldchanges >2 ; <-2). C+D)Comparison of gene expression profile due to mechanical stimulation according to stimulation SOP after three and five days. Venn diagram to visualize the diversity of regulated genes. Data were evaluated by microarray analysis (Affymetrix) and TAC4.0 Software 61

Figure 45 A+B) Comparison of gene expression of pooled genes from different epidemiological studies, which could be related as signature genes for the pathogenesis of hypertension, after three and five days of mechanical stimulation [43,164–167]. Genes have been highlighted without consideration of significant fold change (Fold >0<; p>0<). The arrangement of the data points suggests that the majority of signature genes were not significantly affected by mechanical manipulation. C) Heatmap of pooled signature genes. Data were evaluated by microarray analysis (Affymetrix) and TAC4.0 Software. 62

Figure 46 Evaluation of qPCR data A) of genes related to changes in cytoskeletal structures B) of genes directly related to the contractile apparatus C) of mechanosensitive genes, which also respond to cell signaling and mechanical stress adaptation. Each data set describes the pooled data of three individual haSMC samples, each with three technical replicates. The error bars show the SEM. Direct comparison of gene expression after three and five days of mechanical stimulation concerning the unstimulated control..... 63

Figure 47 Evaluation of the qPCR data A) androgenic receptors B) of different calcium channels C) of strain-dependent calcium channels D) of potassium channels in a direct comparison of gene expression after three and five days of mechanical stimulation with the unstimulated control. Each data set describes the pooled data of three individual samples with three technical replicates each. The error bars show the SEM. 64

Figure 48 Reviews the cell number and cell viability due to exposure to standard media and co-culture media. The X-axis represents the time course in days, Y-axis 1 represents the total cell number and Y-axis 2 represents the cell viability in percentage. The displayed data show the mean values from three individual biological samples and two technical replicates, and the error bars show the standard deviation. A) Proliferation curve of haSMC with initial growth supplement. On day eight, the medium for cell differentiation was added. B) Proliferation curve of haEC with M200 medium and low serum growth supplement. C+D) Cultivation of haSMC and haEC in final co-culture medium. The initial cell count was adjusted according to the defined cell models.. 65

Figure 49 Strategic microscopic investigation of haSMC and haEC single and co-cultures in monolayer and three-dimensional arrangement. A) Phase-contrast image of differentiated haSMC on polystyrene slides cultivated with co-culture medium. B) Phase-contrast image of haEC grown on polystyrene slides in co-culture medium. C) Smooth muscle cell alpha-actin antibody staining of haSMC cultivated in co-culture medium. D) CD-31 antibody staining of haEC in co-culture medium. E) Phase-contrast image of a direct co-culture of haSMC and haEC in monolayer. Cell ratio 1:1, cultivated on polystyrene slide in co-culture medium. F) Co-culture of haSMC and haEC cultivated on polystyrene and stained with antibodies CD31 and smooth muscle cell alpha action. G+H) co-culture of two monolayers consisting of haSMC and haEC arranged three-dimensionally on top of each other in CellDrums. They were cultivated in the co-culture medium. Endothelium stained with CellTracker Deep red and smooth muscle cells with CellTracker green..... 66

Figure 50 Time courses observation of biomechanical effect induces conditioned medium. CellDrum investigation via LTM (N=6 mean \pm 1 SEM). The change in the mechanical stress caused by the test Media expressed as the relative difference of the mechanical stress (%) to the initial value. The control measurement was performed using M231 medium. The control measurement M200 was carried out with fresh M200 medium. Conditioned M200 was conditioned for 24h on CellDrums with 200.000haEC before application..... 67

Figure 51 Analysis of the biomechanical effect of blood sera obtained from fresh blood collected from different scenarios over time. CellDrum investigation via LTM (N=6 mean \pm 1 SEM). The change in the mechanical stress caused by the test substance is expressed as the relative difference of the mechanical stress (%) to the initial value..... 68

Figure 52 ECG patient monitoring during the two ECG measurements. The curve Pre shows the ECG course of the first run without taking the sports supplements, whereas Post shows the ECG course after taking the supplements. It can be seen that the heart rate increases in the second run while the blood pressure is lower compared to the first run. 68

Figure 53 Scheme for mechanically-induced signal conversion in haSMCs. The mechanical stimulus is detected at the cell membrane by mechanosensitive receptors and ion channels and transmitted into the cell interior via molecular transfer. This leads intracellularly, to the activation of various unspecific signaling cascades, by protein phosphorylation and/or alteration of the intracellular ion concentration, which in turn activates further signaling pathways. Finally, the combination of the activated signaling pathways determines the functional response of the cell. These include phenotypic changes, cellular differentiation, migration, proliferation and apoptosis, each affecting the biomechanical properties of the cells. [30](figure adapted). 77

Figure 54 Repair mechanism and phenotypic control of vSMC, by GSK3 β , β -Catenin and Cadherine. Elementary for the mitogenic quiescence of the cell is a low cytosolic concentration of β -catenin, which is ensured by the active phosphorylation of the GSK3 β complex. Cellular or vascular damages lead to a cleavage of N-cadherin and the degradation of adherent junctions, which reduces the activity of the GSK3 β /APC/axin complex. This increases the concentration of β -catenin and leads to a translocation of β -catenin into the cell nucleus. This leads to TCF regulation of the genes responsible for cell growth and proliferation. The damage of the N-cadherins additionally leads to the up-regulation of T-cadherins, which, by activating the PI3K/Akt signaling pathway, completely stops the phosphorylation of GSK3 β and supports the following signaling cascade. [228](figure adapted). 78

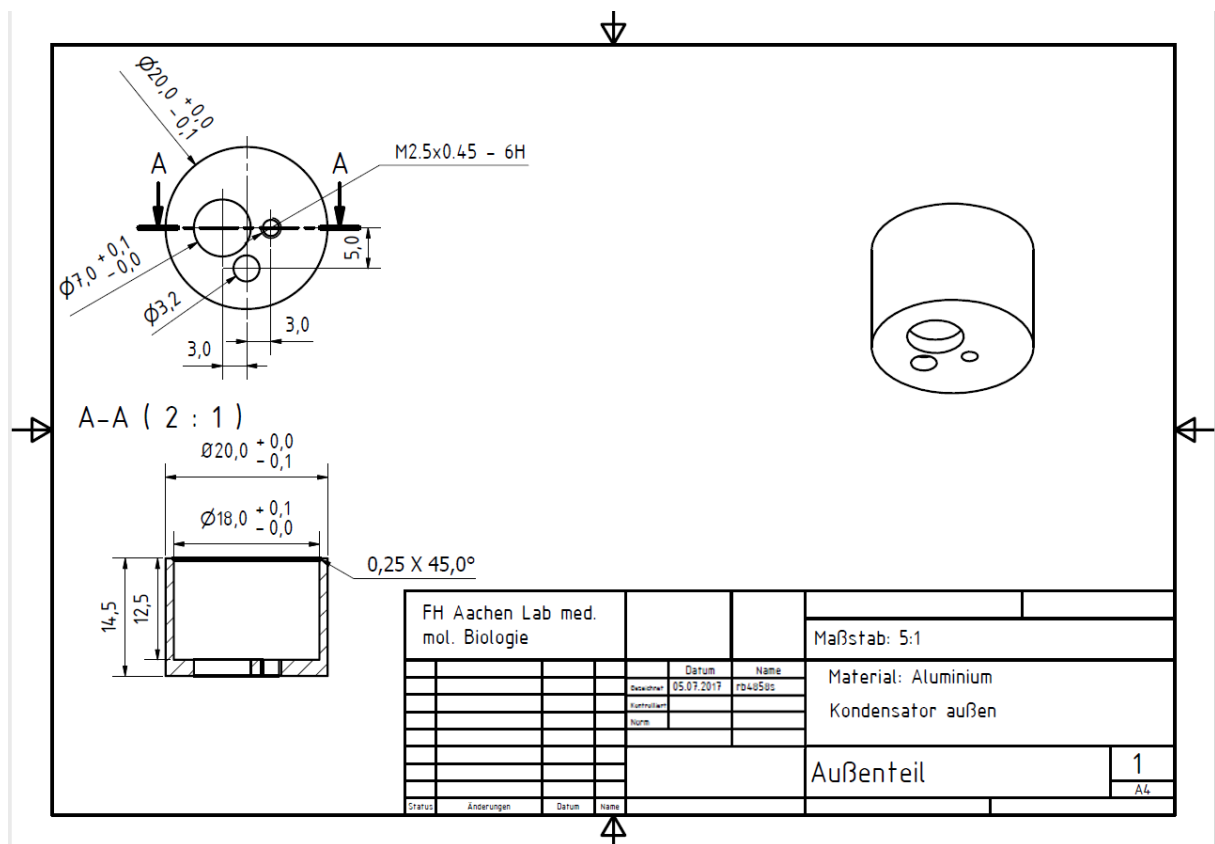
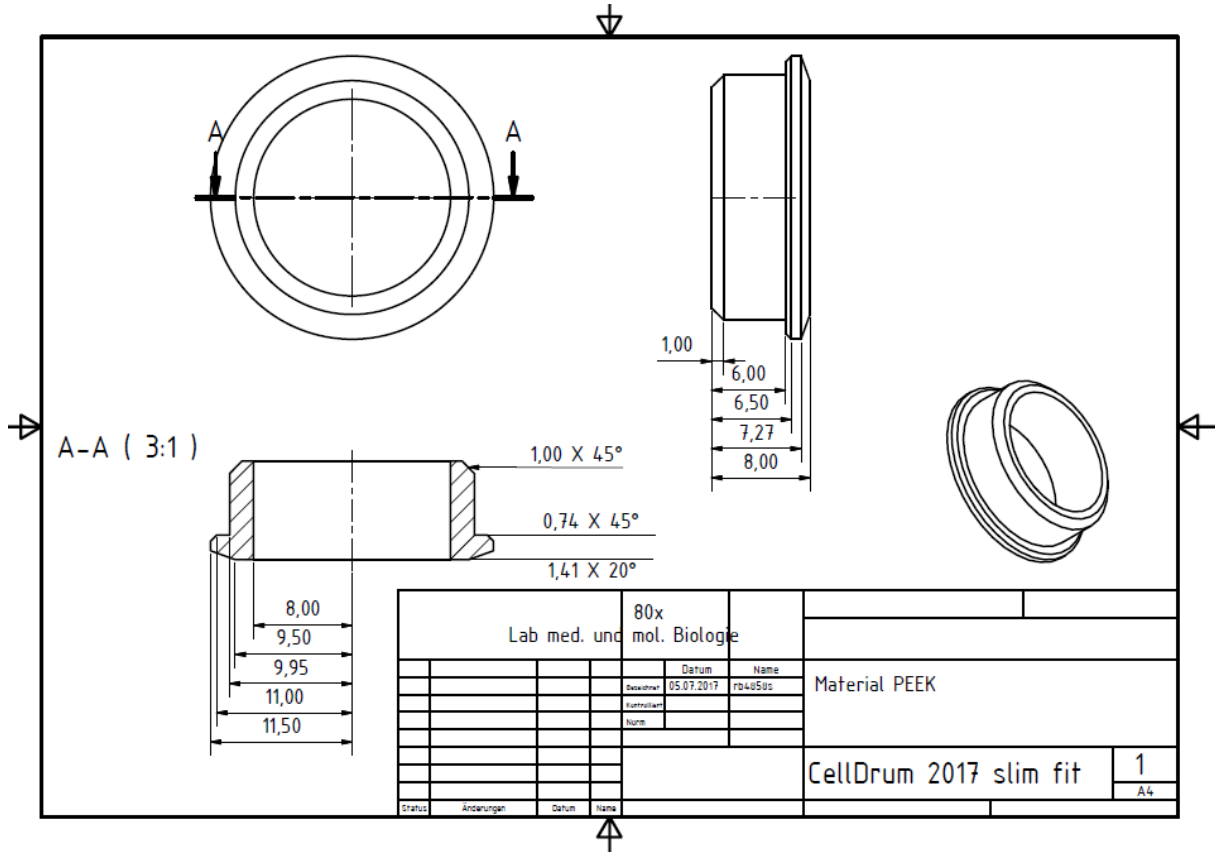
Figure 55 Strongly simplified model for a simplified representation of how different ECM densities can affect the tissue's resulting shortening with identical cellular contraction. $E\text{-modulusECM}(A) > E\text{-modulusECM}(B)$; $\Delta l_{\text{Zell}}(A) = \Delta l_{\text{Zell}}(B)$. Due to the rigid ECM in (A), the entire length of the model is shortened by the cellular contraction. In contrast, the soft ECM in (B) compensated for the shortening of the cell by expanding and thus compensates for the shortening of the entire model. 80

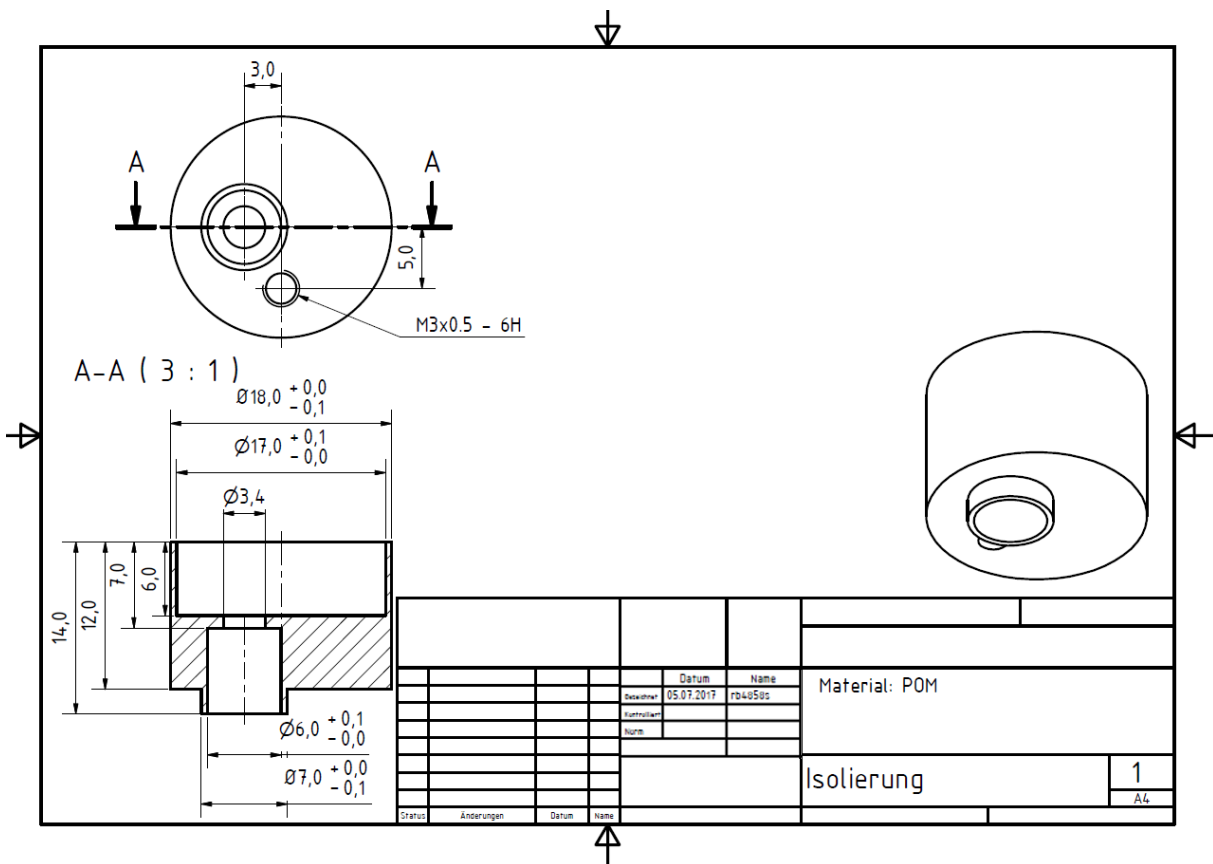
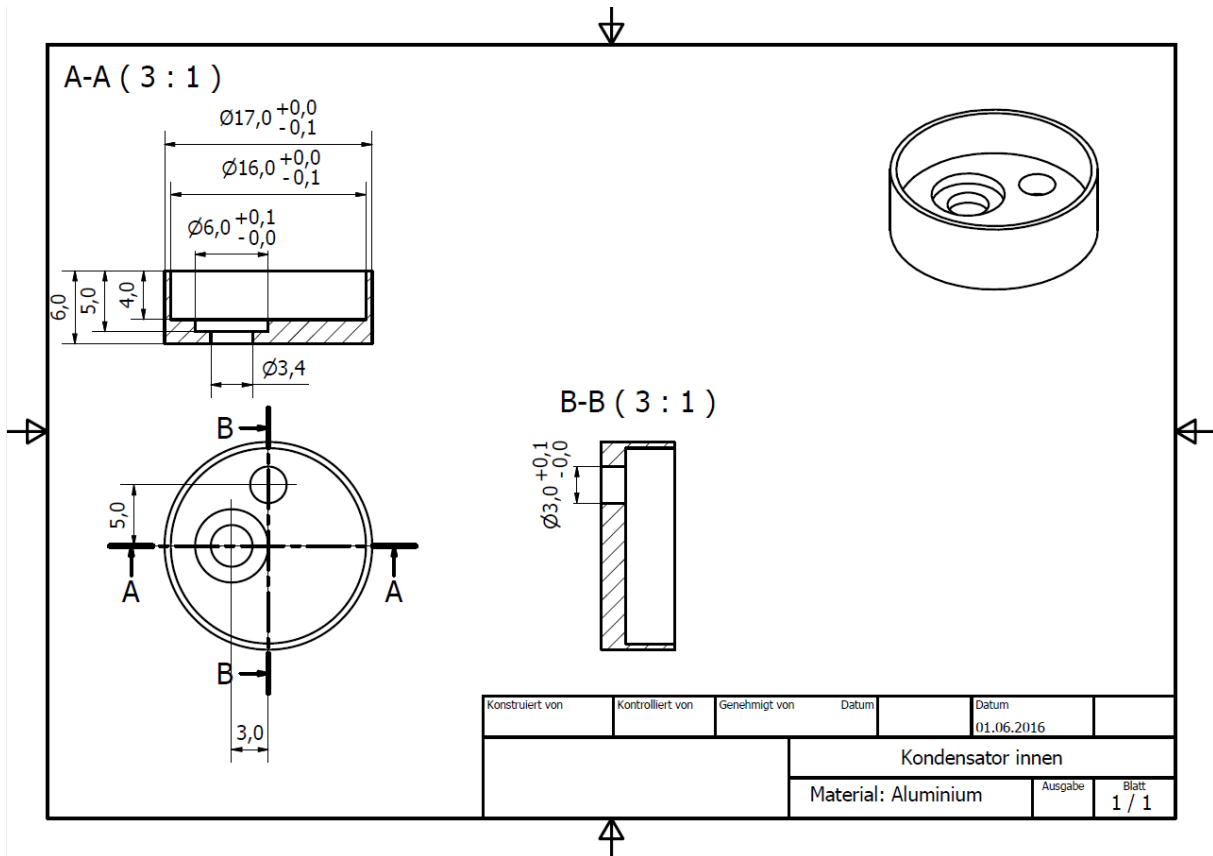
Figure 56 Listing of different tested co-culture models..... 81

10.3. List of Tables

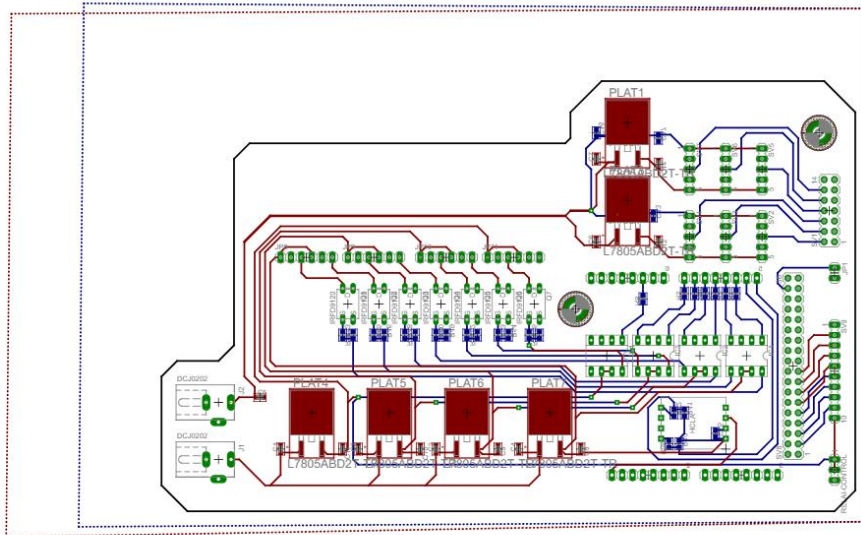
Table 1 High Hypertension categorization according to the level of blood pressure [1]	12
Table 2 Chemicals.....	18
Table 3 Systems & Devices.....	19
Table 4 Overview of media additives and growth factors	32
Table 5 Overview of media additives and growth factors effects on haSMCs and haECs respectively	32
Table 6 L-Type Ca ²⁺ -channel modulators	35
Table 7 K ⁺ channel modulators	35
Table 8 Nitric oxide donators.....	36
Table 9 Biological vasoconstrictors and catecholamines.....	36
Table 10 PDE5 inhibitor.....	36
Table 11 List of stimulants and toxins.....	36
Table 12 Housekeeping Gene	42
Table 13 Genes which are associated with changes in the cytoskeleton.	43
Table 14 List of mechanosensitive genes that contribute to biomechanical adaptation and cellular signal transduction.....	43
Table 15 Selection of genes that are directly related to the contractile force of the cell via the contractile mechanism.....	43
Table 16 Selection of different genes which are related to the expression of receptors and ion channels responsible for cell contraction.	44
Table 17 Components of SsoAdvanced universal SYBR Green supermix.....	45
Table 18 Biorad I-Cycler Settings.....	45
Table 19 Comparison of the data acquired by us with comparable studies. Subject species: Rat (R); Human (H); Chicken (C) and Mouse (M).....	73
Table 20 Overview of stress parameters and results of comparable studies. Cell types: huaSMC (human umbilical artery smooth muscle cells); raSMC (rat artery smooth muscle cells); haSMC (human artery smooth muscle cells); huvEC (human umbilic vein smooth muscle cells); baEC(bovine artery smooth muscle cells). FX-2000/3000/4000, are cell stretching devices by the company Flexcell. ST-140, cell stretching device by STREX, enabling to apply uniaxial stress.	75

10.4. Constructions

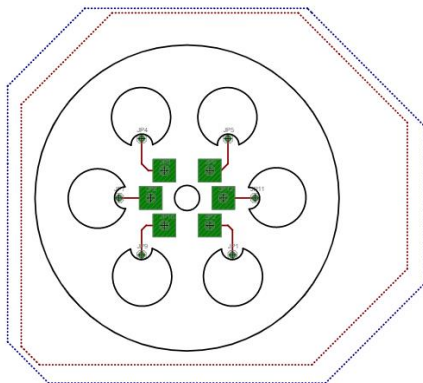




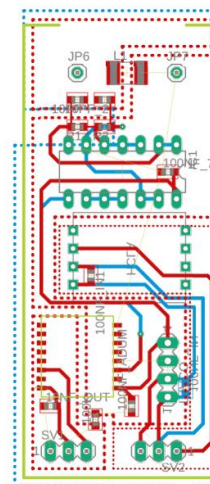
TTA Motherboard



Sensor Cap



Senor



10.6. Coding

```

#include <DueTimer.h>
#include <Wire.h>
#include <DueTC.h>
unsigned int count0;
byte dat[4];
byte v[]={2,14,15,16,17,18,19};
byte s[]={41,43,45,47,49,51,53};
String inputString = "";
boolean stringComplete = false;
void setup(){
  for (int i=0; i<7; i++){
    pinMode(v[i],OUTPUT);
    digitalWrite(v[i],LOW);
    pinMode(s[i],OUTPUT);
    digitalWrite(s[i],HIGH);
    analogReadResolution(16);
    Serial.begin(115200);
    REG_TCO_WPMR = 0x54494D00;
    REG_TC1_WPMR = 0x54494D00;
    REG_PMC_PCER0 =
    0b111110000000000000000000100000000;
    REG_PMC_PCER1 =
    0b000000000000000000000000100101111;
    REG_TCO_CMRO =
    0b000000000000000000001001001000000101;
    REG_TCO_BMR =
    0b000000000000000000000000000000000;
    REG_TCO_CCRO =
    0b0000000000000000000000000000000001;
    Timer3.attachInterrupt(senden);
    Timer3.start(1000);
  }
  void loop(){
    if (stringComplete) {Ventil();}
  }
  void senden(){
    count0 = REG_TCO_CV0;
    REG_TCO_CCRO =
    0b0000000000000000000000000000000100;
    int Druck = analogRead(A0);
    dat[0] = byte(lowByte(count0));
    dat[1] = byte(highByte(count0));
    dat[2] = byte(lowByte(Druck));
    dat[3] = byte(highByte(Druck));
    Serial.write(dat,4);
    Serial.println();
  }
  void Ventil() {
    if (stringComplete) {
      Serial.println(inputString);
      if (inputString.startsWith("v")) {
        int i = inputString.substring(1).toInt();
        digitalWrite(v[i], HIGH);
      }
      if (inputString.startsWith("V")) {
        int i = inputString.substring(1).toInt();
        digitalWrite(v[i], LOW);
      }
      if (inputString.startsWith("s")) {
        int i = inputString.substring(1).toInt();
        digitalWrite(s[i],HIGH);
      }
      if (inputString.startsWith("S")) {
        int i = inputString.substring(1).toInt();
        digitalWrite(s[i],LOW);
      }
      if (inputString.startsWith("stop")) {
        while (1) {}
      }
      inputString="";
      stringComplete=false;
    }
  }
  void serialEvent() {
    while (Serial.available()) {
      char inChar = (char)Serial.read();
      if (inChar == '\n') {
        stringComplete = true;
      }
      else {
        inputString += inChar;
      }
    }
  }
}

```

Affidavit

Ich versichere, dass ich die von mir vorgelegte Dissertation selbstständig angefertigt, die benutzten Quellen und Hilfsmittel vollständig angegeben und die Stellen der Arbeit -einschließlich Tabellen, Karten und Abbildungen -, die anderen Werken im Wortlaut oder dem Sinn nach entnommen sind, in jedem Einzelfall als Entlehnung kenntlich gemacht habe; dass diese Dissertation noch keiner anderen Fakultät oder Universität zur Prüfung vorgelegen hat; dass sie - abgesehen von unten angegebenen Teilpublikationen -noch nicht veröffentlicht worden ist sowie, dass ich eine solche Veröffentlichung vor Abschluss des Promotionsverfahrens nicht vornehmen werde. Die Bestimmungen dieser Promotionsordnung sind mir bekannt. Die von mir vorgelegte Dissertation ist von Prof. Hescheler & Prof.T.Artmann betreut worden.

Übersicht der Publikationen:

- Bayer R, Artmann AT, Digel I, Falkenstein J, Artmann G, Creutz T, et al. Mechano-pharmacological testing of L-type Ca²⁺ channel modulators via human vascular CellDrum model. Cell Physiol Biochem. 2020;(54):371–83

Ich versichere, dass ich alle Angaben wahrheitsgemäß nach bestem Wissen und Gewissen gemacht habe und verpflichte mich, jedmögliche, die obigen Angaben betreffenden Veränderungen, dem Promotionsausschuss unverzüglich mitzuteilen.

Jülich, 26.02.2021

A handwritten signature in black ink, consisting of stylized, overlapping letters, positioned above a horizontal dotted line.